



# AERMOD Model Formulation and Evaluation



EPA-454/B-21-003  
April 2021

## AERMOD Model Formulation and Evaluation

U.S. Environmental Protection Agency  
Office of Air Quality Planning and Standards  
Air Quality Assessment Division  
Research Triangle Park, NC

## **Notice**

The original document, AERMOD: Description of Model Formulation, was published in September 2004, with the EPA document number EPA-454/R-03-004. This version of the document has several revisions, including a new title (AERMOD Model Formulation and Evaluation), the new model formulations added to the model since the original publication in 2004, a model evaluation based on version 21112 of AERMOD and AERMET, and minor changes to the formatting and supplemental content to make it appropriate according to current EPA document publication standards.

This report has been reviewed by the Office of Air Quality Planning and Standards, U.S. Environmental Protection Agency, and has been approved for publication. Mention of trade names or commercial products does not constitute endorsement or recommendation for use.

## **Acknowledgments**

This project was made possible through the continued support of Mr. Joe Tikvart, of EPA's Office of Air Quality Planning and Standards (OAQPS), and Mr. Frank Schiermeier, of NOAA's Atmospheric Sciences Modeling Division. The authors are particularly grateful to Dr. Gary Briggs, and Mr. John Irwin, of NOAA's Atmospheric Sciences Modeling Division, for their thorough and constructive review of an earlier version of this document. Finally, we would like to thank the many scientists who participated in peer reviews and beta testing.

This report was originally compiled primarily by Alan J. Cimorelli, Steven G. Perry, Akula Venkatram, Jeffrey C. Weil, Robert J. Paine, Robert B. Wilson, Russell F. Lee, Warren D. Peters, Roger W. Brode, James O. Paumier, and James Thurman

## Table of Contents

Section	Page
Notice.....	ii
Acknowledgments.....	iii
Table of Contents.....	iv
Figures.....	vii
Tables.....	viii
1. Introduction.....	1
1.1 Background.....	1
1.2 The AERMIC focus: a replacement for the ISC3 model.....	3
1.3 Model development process .....	4
1.4 Purpose of the document.....	6
2. Model overview .....	7
3. Meteorological preprocessor (AERMET).....	11
3.1 Energy balance in the PBL .....	11
3.1.1 Net radiation.....	12
3.1.2 Transition between the CBL and SBL .....	13
3.2 Derived parameters in the CBL .....	14
3.2.1 Friction velocity ( $u_*$ ) and Monin Obukhov length ( $L$ ) in the CBL.....	14
3.2.2 Convective velocity scale ( $w_*$ ).....	15
3.3 Derived parameters in the SBL.....	16
3.3.1 Original friction velocity ( $u_*$ ) in the SBL .....	16
3.3.2 Adjusted friction velocity ( $u_*$ ) in the SBL .....	19
3.3.3 Sensible heat flux ( $H$ ) in the SBL .....	20
3.3.4 Monin-Obukhov length ( $L$ ) in the SBL .....	21
3.4 Mixing height.....	21
3.4.1 Convective mixing height ( $z_{ic}$ ).....	21
3.4.2 Mechanical mixing height ( $z_{im}$ ).....	22

3.5 Adjustment for the low wind speed/stable conditions in AERMET.....	24
4. Vertical structure of the PBL - AERMOD'S meteorological interface.....	25
4.1 General profiling equations.....	26
4.1.1 Wind speed profiling.....	26
4.1.2 Wind direction profiles .....	28
4.1.3 Profiles of the potential temperature gradient.....	28
4.1.4 Potential temperature profiling .....	31
4.1.5 Vertical turbulence calculated.....	32
4.1.6 Lateral turbulence calculated by the interface .....	35
4.2 Vertical inhomogeneity in the boundary layer as treated by the interface .....	39
5. The AMS/EPA regulatory Model: AERMOD.....	44
5.1 General structure of AERMOD including terrain.....	46
5.2 Concentration predictions in the CBL .....	51
5.2.1 Direct Source contribution to concentration calculations in the CBL .....	60
5.2.2 Indirect Source contribution to concentration calculations in the CBL.....	62
5.2.3 Penetrated source contribution to concentration calculations in the CBL .....	63
5.3 Concentrations in the SBL .....	63
5.4 Treatment of lateral plume meander .....	65
5.5 Estimation of dispersion coefficients.....	67
5.5.1 Dispersion from ambient turbulence.....	69
5.5.2 Buoyancy induced dispersion (BID) component of $\sigma_y$ and $\sigma_z$ .....	74
5.5.3 Treatment of building downwash .....	74
5.6 Plume rise calculations in AERMOD.....	76
5.6.1 Plume rise in the CBL.....	76
5.6.2 Plume rise in the SBL .....	78
5.7 Source characterization.....	79
5.8 Plume volume molar ration method (PVMRM) .....	81
5.8.1 Definition of plume volume.....	81
5.8.2 Minimum ozone concentration for stable conditions.....	86
5.9 Adjustments for the urban boundary layer.....	86

6. List of symbols.....	92
Appendix A. Input / output needs and data usage .....	97
Appendix B. Model evaluation results.....	106
Appendix C. Evaluation of modified urban option.....	147
References .....	154

## Figures

Figure	Page
Figure 1. Data flow in the AERMOD modeling system.....	9
Figure 2. Wind speed profile, for both the CBL and SBL, in the region below $7z_0$ .....	27
Figure 3. Wind speed profiling, for both the CBL and SBL, in the region above $7z_0$ .....	28
Figure 4. Profile of potential temperature gradient for the SBL.....	31
Figure 5. Convective portion of the vertical turbulence in the CBL .....	33
Figure 6. Mechanical portion of the vertical turbulence in the CBL .....	34
Figure 7. Profile of vertical turbulence in the SBL.....	35
Figure 8. Family of lateral mechanical turbulence profiles over a range of mechanical mixing heights .....	38
Figure 9. AERMOD's Treatment of the Inhomogeneous Boundary Layer.....	40
Figure 10. AERMOD two state approach. The total concentration predicted by AERMOD is the weighted sum of the two extreme possible plume states.....	47
Figure 11. Treatment of Terrain in AERMOD. Construction of the weighting factor used in calculating total concentration.....	50
Figure 12. Instantaneous and corresponding ensemble-averaged plume in the CBL.....	53
Figure 13. AERMOD's three plume treatment of the CBL.....	54
Figure 14. AERMOD's pdf approach for plume dispersion in the CBL.....	57
Figure 15. Probability density function of the vertical velocity. While the Gaussian curve is unskewed, the bi-Gaussian curve has a skewness of $S=1$ .....	58
Figure 16. Lateral spread ( $F_y$ ) as a function of non-dimensional distance ( $X$ ). The data is taken from the Prairie Grass experiment (Barad, 1958) .....	70
Figure 17. AERMOD's construction of a continuous meteorological profile by interpolating between observations. ....	104

## Tables

Table	Page
Table 1. AERMOD evaluation databases used for comparisons of AERMOD 15181 and AERMOD 16216.....	107
Table 2. Hourly, 3-hour, and 24-hour RHC for turbulence cases. Best performing model compared to observed RHC are highlighted in gray. ....	134
Table 3. Hourly, 3-hour, and 24-hour RHC for non-turbulence cases. Best performing model compared to observed RHC are highlighted in gray. ....	135
Table 4. Composite Performance Measure (CPM) for turbulence cases. Scenarios with lowest CPM's for each study location are highlighted in gray. ....	136
Table 5. Composite Performance Measure (CPM) for non-turbulence databases. Scenarios with lowest CPM's for each study location are highlighted in gray. ....	136
Table 6. Martins Creek Model Comparison Measure (MCM) results. Confidence intervals highlighted in gray are significant at that percent. ....	139
Table 7. Lovett Model Comparison Measure (MCM) results. Confidence intervals highlighted in gray are significant at that percent. ....	140
Table 8. Westvaco Model Comparison Measure (MCM) results. Confidence intervals highlighted in gray are significant at that percent. ....	141
Table 9. Kincaid Model Comparison Measure (MCM) results. Confidence intervals highlighted in gray are significant at that percent. ....	142
Table 10. Bowline Model Comparison Measure (MCM) results. Confidence intervals highlighted in gray are significant at that percent. ....	143
Table 11. Baldwin Model Comparison Measure (MCM) results. Confidence intervals highlighted in gray are significant at that percent. ....	144
Table 12. Clifty Creek Model Comparison Measure (MCM) results. Confidence intervals highlighted in gray are significant at that percent. ....	145

## 1. Introduction

### 1.1 Background

In 1991, the American Meteorological Society (AMS) and the U.S. Environmental Protection Agency (EPA) initiated a formal collaboration with the designed goal of introducing current planetary boundary layer (PBL) concepts into regulatory dispersion models. A working group (AMS/EPA **R**egulatory **M**odel **I**mprovement **C**ommittee, **AERMIC**) comprised of AMS and EPA scientists was formed for this collaborative effort.

In most air quality applications, one is concerned with dispersion in the PBL, the turbulent air layer next to the earth's surface that is controlled by the surface heating and friction and the overlying stratification. The PBL typically ranges from a few hundred meters in depth at night to 1 - 2 km during the day. Major developments in understanding the PBL began in the 1970s through numerical modeling, field observations, and laboratory simulations; see Wyngaard (1988) for a summary. For the convective boundary layer (CBL), a milestone was Deardorff's (1972) numerical simulations which revealed the CBL's vertical structure and important turbulence scales. Major insights into dispersion followed from laboratory experiments, numerical simulations, and field observations (e.g., see Briggs (1988), Lamb (1982) and Weil (1988a) for reviews). For the stable boundary layer (SBL), advancements occurred more slowly. However, a sound theoretical/experimental framework for surface layer dispersion and approaches for elevated sources emerged by the mid-1980s (e.g., see Briggs (1988) and Venkatram (1988)).

During the mid-1980s, researchers began to apply this information to simple dispersion models for applications. This consisted of eddy-diffusion techniques for surface releases, statistical theory and PBL scaling for dispersion parameter estimation, a new probability density function (pdf) approach for the CBL, simple techniques for obtaining meteorological variables (e.g., surface heat flux) needed for turbulence parameterizations, etc. Much of this work was reviewed and promoted in workshops (Weil 1985), revised texts (Pasquill and Smith 1983), and in short courses and monographs (Nieuwstadt and van Dop 1982; Venkatram and Wyngaard 1988). By the mid-1980s, new applied dispersion models based on this technology had been

developed including PPSP (Weil and Brower 1984), OML (Berkowicz et al. 1986), HPDM (Hanna and Paine 1989), TUPOS (Turner et al. 1986), CTDMPPLUS (Perry et al. 1989); later, ADMS developed in the United Kingdom (see Carruthers et al. (1992)) was added as well as SCIPUFF (Sykes et al. 1996). AERMIC members were involved in the development of three of these models - PPSP, CTDMPPLUS and HPDM.

By the mid-to-late 1980s, a substantial scientific base on the PBL and new dispersion approaches existed for revamping regulatory dispersion models. In a review of existing or proposed regulatory models developed prior to 1984, Smith (1984) reported that the techniques were many years behind the state-of-the-art and yielded predictions that did not agree well with observations. Similar findings were reported by Hayes and Moore (1986), who summarized 15 model evaluation studies. The need for a comprehensive overhaul of EPA's basic regulatory models was clearly recognized. This need, including a summary of background information and recommendations, was the focus of an AMS/EPA Workshop on Updating Applied Diffusion Models held 24-27 January 1984 in Clearwater, Florida (see Weil (1985) and other review papers in the November 1985 issue of the Journal of Climate and Applied Meteorology).

In February 1991, the U.S. EPA, in conjunction with the AMS, held a workshop for state and EPA regional meteorologists on the parameterization of PBL turbulence and state-of-the-art dispersion modeling. One of the outcomes of the workshop was the formation of AERMIC. As noted above, the expressed purpose of the AERMIC activity was to build upon the earlier model developments and to provide a state-of-the-art dispersion model for regulatory applications. The early efforts of the AERMIC group are described by Weil (1992). In going through the design process and in considering the nature of present regulatory models, AERMIC's goal expanded from its early form. In addition to improved parameterization of PBL turbulence, other problems such as plume interaction with terrain, surface releases, building downwash and urban dispersion were recognized as needing attention.

The new model developed by AERMIC is aimed at short-range dispersion from stationary industrial sources, the same scenario handled by the EPA Industrial Source Complex Model, ISC3 (U.S. Environmental Protection Agency, 1995). This work clearly has benefitted from the model development activities of the 1980s, especially in the parameterization of mean

winds and PBL turbulence, dispersion in the CBL, and the treatment of plume/terrain interactions. Techniques used in the new model for PBL parameterizations and CBL dispersion are similar to those used in earlier models. Turbulence characterization in the CBL adopts "convective scaling", as suggested by Deardorff (1972), as is included in most of the models mentioned above (e.g., PPSP, OML, and HPDM). Algorithms used in these earlier models were considered along with variants and improvements to them. In addition, the developers of OML met with AERMIC to discuss their experiences. Thus, much credit for the AERMIC model development is to be given to the pioneering efforts of the 1980s.

## **1.2 The AERMIC focus: a replacement for the ISC3 model**

AERMIC's initial focus has been on the regulatory models that are designed for estimating near-field impacts from a variety of industrial source types. EPA's regulatory platform for near-field modeling, during the past 25 years has, with few exceptions, remained fundamentally unchanged. During this period, ISC3 was the workhorse regulatory model (used in the construction of most State Implementation Plans, new source permits, risk assessments and exposure analysis for toxic air pollutants) with code structure that is conducive to change. Therefore, AERMIC selected the EPA's ISC3 Model for a major overhaul. AERMIC's objective was to develop a complete replacement for ISC3 by: 1) adopting ISC3's input/output computer architecture; 2) updating, where practical, antiquated ISC3 model algorithms with newly developed or current state-of-the-art modeling techniques; and 3) insuring that the source and atmospheric processes presently modeled by ISC3 will continue to be handled by the AERMIC Model (AERMOD), albeit in an improved manner.

The AERMOD modeling system consists of two pre-processors and the dispersion model. The AERMIC meteorological preprocessor (AERMET) provides AERMOD with the meteorological information it needs to characterize the PBL. The AERMIC terrain pre-processor (AERMAP) both characterizes the terrain and generates receptor grids for the dispersion model (AERMOD).

AERMET uses meteorological data and surface characteristics to calculate boundary layer parameters (e.g. mixing height, friction velocity, etc.) needed by AERMOD. This data,

whether measured off-site or on-site, must be representative of the meteorology in the modeling domain. AERMAP uses gridded terrain data for the modeling area to calculate a representative terrain-influence height associated with each receptor location. The gridded data is supplied to AERMAP in the format of the Digital Elevation Model (DEM) data (USGS 1994). The terrain preprocessor can also be used to compute elevations for both discrete receptors and receptor grids.

In developing AERMOD, AERMIC adopted design criteria to yield a model with desirable regulatory attributes. It was felt that the model should: 1) provide reasonable concentration estimates under a wide variety of conditions with minimal discontinuities; 2) be user friendly and require reasonable input data and computer resources as is the case with the ISC3 model; 3) capture the essential physical processes while remaining fundamentally simple; and, 4) accommodate modifications with ease as the science evolves.

Relative to ISC3, AERMOD currently contains new or improved algorithms for: 1) dispersion in both the convective and stable boundary layers; 2) plume rise and buoyancy; 3) plume penetration into elevated inversions; 4) computation of vertical profiles of wind, turbulence, and temperature; 5) the urban nighttime boundary layer; 6) the treatment of receptors on all types of terrain from the surface up to and above the plume height; 7) the treatment of building wake effects; 8) an improved approach for characterizing the fundamental boundary layer parameters; and 9) the treatment of plume meander.

### **1.3 Model development process**

A seven-step model development process, followed by AERMIC, resulted in the promulgation of AERMOD, a regulatory replacement for the ISC3 model. The process followed was: 1) initial model formulation; 2) developmental evaluation; 3) internal peer review and beta testing; 4) revised model formulation; 5) performance evaluation and sensitivity testing; 6) external peer review; and 7) submission to EPA's Office of Air Quality Planning and Standards (OAQPS) for consideration as a regulatory model.

The initial formulations of AERMOD are summarized in Perry et al. (1994) and Cimorelli et al. (1996). Once formulated, the model was tested (developmental evaluation) against a variety of field measurements in order to identify areas needing improvement. The developmental evaluation provided a basis for selecting formulation options.

This developmental evaluation was conducted using five data bases. Three consisted of event-based tracer releases, while the other two each contain up to a full year of continuous SO<sub>2</sub> measurements. These data bases cover elevated and surface releases, complex and simple terrain, and rural and urban boundary layers. A description of the early developmental evaluation is presented in Lee et al. (1995) and in a later report by Lee et al. (1998). Additionally, a comprehensive peer review (U.S. Environmental Protection Agency, 2002) was conducted. Many revisions to the original formulation have resulted from this evaluation and comments received during the peer review, beta testing, and the public forum at EPA's Sixth Conference on Air Quality Modeling (in 1995). Lee et al. (1998) describe the developmental evaluation repeated with the current model (i.e., revisions based on the developmental evaluation and peer review).

In addition, AERMOD underwent a comprehensive performance evaluation (Brode 2002) designed to assess how well AERMOD's concentration estimates compare against a variety of independent data bases and to assess the adequacy of the model for use in regulatory decision making. That is, how well does the model predict concentrations at the high end of the concentration distribution? AERMOD was evaluated against five independent data bases (two in simple terrain and three in complex terrain), each containing one full year of continuous SO<sub>2</sub> measurements. Additionally, AERMOD's performance was compared against the performance of four other applied, regulatory models: ISC3 (U.S. Environmental Protection Agency, 1995), CTDMPPLUS (Perry 1992), RTDM (Paine and Egan 1987), and HPDM (Hanna and Paine 1989; Hanna and Chang 1993). The performance of these models against AERMOD has been compared using the procedures in EPA's "Protocol for Determining the Best Performing Model" (U.S. Environmental Protection Agency, 1992).

On 21 April 2000 EPA proposed<sup>1</sup> that AERMOD be adopted as a replacement to ISC3 in appendix A of the Guideline on Air Quality Models (Code of Federal Regulations 1997). As such, upon final action, AERMOD would become EPA's preferred regulatory model for both simple and complex terrain. Furthermore, on 19 May 2000 EPA announced<sup>2</sup> its intention to hold the Seventh Conference on Air Quality Modeling on 28-29 June 2000. The purpose of this conference was to receive comments on the April 2000 proposal. At the Seventh Conference, results of the performance evaluation and peer review were presented, and public comments were received. Based on these comments AERMOD was revised to incorporate the PRIME algorithms for building downwash, to remove the dependency on modeling domain in AERMOD's complex terrain formulation, and a variety of other less significant issues. A description of the fully revised model is presented here and in Cimorelli et al. (2004) and Perry et al. (2003). Performance of the final version of AERMOD is documented in Perry et al. (2003) and Brode (2002).

#### **1.4 Purpose of the document**

The purpose of this document is to provide a comprehensive, detailed description of the technical formulation of AERMOD and its preprocessors. This document is intended to provide many of the details that are not included in the published journal articles (Cimorelli et al. 2004; Perry et al. 2003).

---

<sup>1</sup>40 CFR Part 51 pages 21506-21546

<sup>2</sup>Federal Register on May 19, 2000 (Volume 65, Number 98)

## 2. Model overview

This section provides a general overview of the most important features of AERMOD. AERMOD serves as a complete replacement for ISC3. Thus, the AERMOD model described here is applicable to rural and urban areas, flat and complex terrain, surface and elevated releases, and multiple sources (including, point, area and volume sources). Every effort has been made to avoid model formulation discontinuities wherein large changes in calculated concentrations result from small changes in input parameters.

AERMOD is a steady-state plume model. In the stable boundary layer (SBL), it assumes the concentration distribution to be Gaussian in both the vertical and horizontal. In the convective boundary layer (CBL), the horizontal distribution is also assumed to be Gaussian, but the vertical distribution is described with a bi-Gaussian probability density function (pdf). This behavior of the concentration distributions in the CBL was demonstrated by Willis and Deardorff (1981) and Briggs (1993). Additionally, in the CBL, AERMOD treats “plume lofting,” whereby a portion of plume mass, released from a buoyant source, rises to and remains near the top of the boundary layer before becoming mixed into the CBL. AERMOD also tracks any plume mass that penetrates into the elevated stable layer, and then allows it to re-enter the boundary layer when and if appropriate. For sources in both the CBL and the SBL AERMOD treats the enhancement of lateral dispersion resulting from plume meander.

Using a relatively simple approach, AERMOD incorporates current concepts about flow and dispersion in complex terrain. Where appropriate, the plume is modeled as either impacting and/or following the terrain. This approach has been designed to be physically realistic and simple to implement, while avoiding the need to distinguish among simple, intermediate and complex terrain, as required by other regulatory models. As a result, AERMOD removes the need for defining complex terrain regimes. All terrain is handled in a consistent and continuous manner while considering the dividing streamline concept (Snyder et al. 1985) in stably stratified conditions.

One of the major improvements that AERMOD brings to applied dispersion modeling is its ability to characterize the PBL through both surface and mixed layer scaling. AERMOD

constructs vertical profiles of required meteorological variables based on measurements and extrapolations of those measurements using similarity (scaling) relationships. Vertical profiles of wind speed, wind direction, turbulence, temperature, and temperature gradient are estimated using all available meteorological observations. AERMOD is designed to run with a minimum of observed meteorological parameters. As a replacement for the ISC3 model, AERMOD can operate using data of a type that is readily available from National Weather Service (NWS) stations. AERMOD requires only a single surface measurement of wind speed (measured between  $7z_o$  and 100m - where  $z_o$  is the surface roughness height), wind direction and ambient temperature. Like ISC3, AERMOD also needs observed cloud cover. However, if cloud cover is not available (e.g. from an on-site monitoring program) two vertical measurements of temperature (typically at 2 and 10 meters), and a measurement of solar radiation can be substituted. A full morning upper air sounding (rawinsonde) is required in order to calculate the convective mixing height throughout the day. Surface characteristics (surface roughness, Bowen ratio, and albedo) are also needed in order to construct similarity profiles of the relevant PBL parameters.

Unlike existing regulatory models, AERMOD accounts for the vertical inhomogeneity of the PBL in its dispersion calculations. This is accomplished by "averaging" the parameters of the actual PBL into "effective" parameters of an equivalent homogeneous PBL.

Figure 1 shows the flow and processing of information in AERMOD. The modeling system consists of one main program (AERMOD) and two pre-processors (AERMET and AERMAP). The major purpose of AERMET is to calculate boundary layer parameters for use by AERMOD. The meteorological INTERFACE, internal to AERMOD, uses these parameters to generate profiles of the needed meteorological variables. In addition, AERMET passes all meteorological observations to AERMOD.

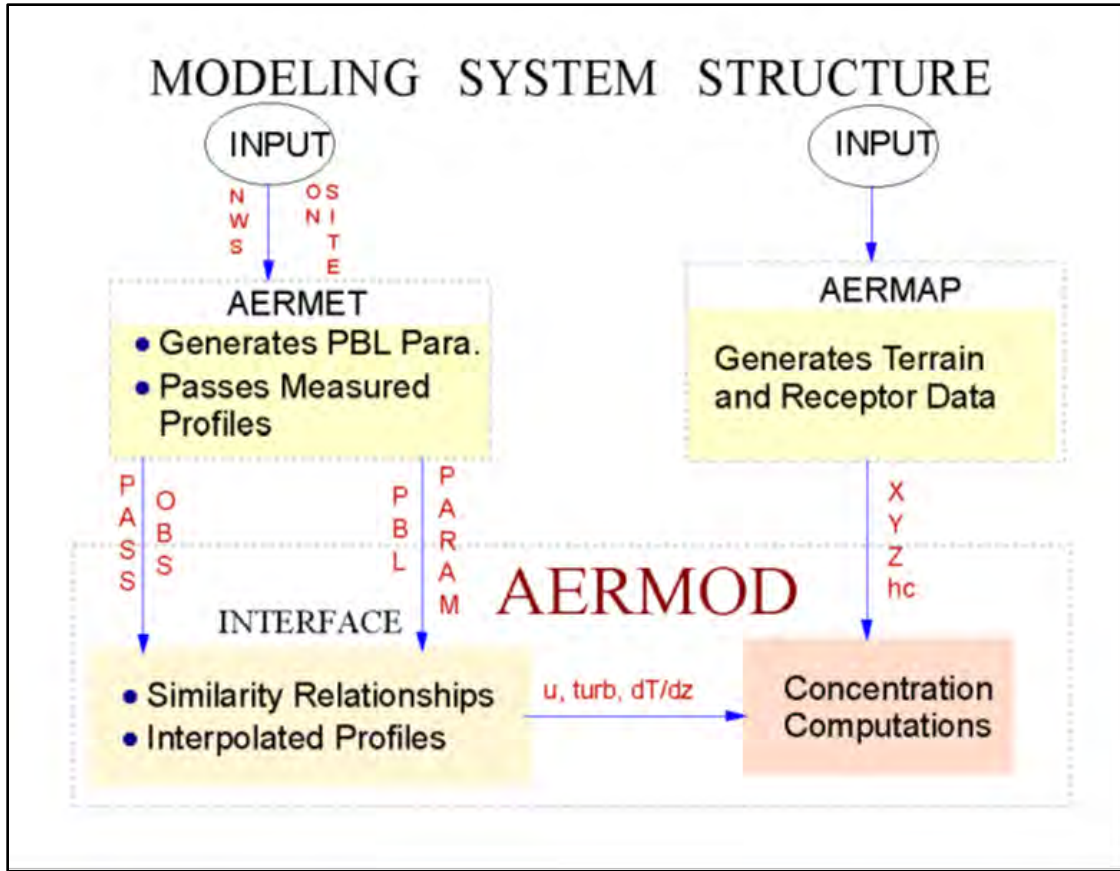


Figure 1. Data flow in the AERMOD modeling system

Surface characteristics in the form of albedo, surface roughness, and Bowen ratio, plus standard meteorological observations (wind speed, wind direction, temperature, and cloud cover), are input to AERMET. AERMET then calculates the PBL parameters: friction velocity ( $u_*$ ), Monin-Obukhov length ( $L$ ), convective velocity scale ( $w_*$ ), temperature scale ( $\theta_*$ ), mixing height ( $z_i$ ), and surface heat flux ( $H$ ). These parameters are then passed to the INTERFACE (which is within AERMOD) where similarity expressions (in conjunction with measurements) are used to calculate vertical profiles of wind speed ( $u$ ), lateral and vertical turbulent fluctuations ( $\sigma_v$ ,  $\sigma_w$ ), potential temperature gradient ( $d\theta/dz$ ), and potential temperature ( $\theta$ ).

The AERMIC terrain pre-processor AERMAP uses gridded terrain data to calculate a representative terrain-influence height ( $h_c$ ), also referred to as the terrain height scale. The terrain height scale  $h_c$ , which is uniquely defined for each receptor location, is used to calculate the dividing streamline height. The gridded data needed by AERMAP is selected from Digital

Elevation Model (DEM) data. AERMAP is also used to create receptor grids. The elevation for each specified receptor is automatically assigned through AERMAP. For each receptor, AERMAP passes the following information to AERMOD: the receptor's location ( $x_r$ ,  $y_r$ ), its height above mean sea level ( $z_r$ ), and the receptor specific terrain height scale ( $h_c$ ).

A comprehensive description of the basic formulation of the AERMOD dispersion model, including the INTERFACE, AERMET, and AERMAP, is presented in this document. Included are: 1) a complete description of the AERMET algorithms that provide quantitative hourly PBL parameters; 2) the general form of the concentration equation with adjustments for terrain; 3) plume rise and dispersion algorithms appropriate for both the convective and stable boundary layers; 4) handling of boundary layer inhomogeneity; 5) algorithms for developing vertical profiles of the necessary meteorological parameters; 6) a treatment of the nighttime urban boundary layer; 7) treatment of building downwash (incorporation of PRIME); and 8) enhancement of lateral dispersion due to plume meander. The model described here represents the 16261 versions of AERMOD, AERMET and AERMAP. In addition, all of the symbols used for the many parameters and variables that are referred to in this document are defined, with their appropriate units, in the section titled "List of Symbols."

### 3. Meteorological preprocessor (AERMET)

The basic purpose of AERMET is to use meteorological measurements, representative of the modeling domain, to compute certain boundary layer parameters used to estimate profiles of wind, turbulence and temperature. These profiles are estimated by the AERMOD interface, which is described in Section 4.

While the structure of AERMET is based upon an existing regulatory model preprocessor, the Meteorological Processor for Regulatory Models (MPRM) (Irwin et al. 1988), the actual processing of the meteorological data is similar to that done for the CTDMPLUS (Perry 1992) and HPDM (Hanna and Paine 1989; Hanna and Chang 1993) models. The growth and structure of the atmospheric boundary layer is driven by the fluxes of heat and momentum which in turn depend upon surface effects. The depth of this layer and the dispersion of pollutants within it are influenced on a local scale by surface characteristics such as surface roughness, reflectivity (albedo), and the availability of surface moisture. The surface parameters provided by AERMET are the Monin-Obukhov Length ( $L$ ), surface friction velocity ( $u_*$ ), surface roughness length ( $z_o$ ), surface heat flux ( $H$ ), and the convective scaling velocity ( $w_*$ ). AERMET also provides estimates of the convective and mechanical mixed layer heights,  $z_{ic}$  and  $z_{im}$ , respectively. AERMET defines the stability of the PBL by the sign of  $H$  (convective for  $H > 0$  and stable for  $H < 0$ ). Although AERMOD is capable of estimating meteorological profiles with data from as little as one measurement height, it will use as much data as the user can provide for defining the vertical structure of the boundary layer. In addition to PBL parameters, AERMET passes all measurements of wind, temperature, and turbulence in a form AERMOD needs.

#### 3.1 Energy balance in the PBL

The fluxes of heat and momentum drive the growth and structure of the PBL. To properly characterize the PBL, one first needs a good estimate of the surface sensible heat flux ( $H$ ) which depends on the net radiation ( $R_n$ ) and surface characteristics such as the available surface moisture (described in the form of the Bowen ratio ( $B_o$ )). In the CBL, a simple energy

balance approach, as in Oke (1978), is used to derive the expression, used in AERMET, to calculate the sensible heat flux,  $H$ . We begin with the following simple characterization of the energy balance in the PBL:

$$H + \lambda E + G = R_n \quad (1)$$

where  $H$  is the sensible heat flux,  $\lambda E$  is the latent heat flux,  $G$  is the soil heat flux, and  $R_n$  is the net radiation. To arrive at an estimate of  $H$  simple parameterizations are made for the soil and latent heat flux terms; that is  $G=0.1 R_n$  and  $\lambda E = H / B_o$ , respectively. Substituting these expressions into eq. (1) the expression for surface heat flux becomes

$$H = \frac{0.9 R_n}{(1 + 1/B_o)} \quad (2)$$

### 3.1.1 Net radiation

If measured values for  $R_n$  are not available, the net radiation is estimated from the insolation and the thermal radiation balance at the ground following the method of Holtslag and van Ulden (1983) as

$$\frac{R_n = (1 - r\{\varphi\}) R + c_1 T_{ref}^6 - \sigma_{SB} T_{ref}^4 - c_2 n}{1 + c_3}, \quad (3)$$

where  $c_1 = 5.31 \times 10^{-13} \text{ W m}^{-2} \text{ K}^{-4}$ ,  $c_2 = 60 \text{ W m}^{-2}$ ,  $c_3 = 0.12$ ,  $\sigma_{SB}$  is the Stefan Boltzman constant ( $5.67 \times 10^{-8} \text{ W m}^{-2} \text{ K}^{-4}$ ),  $T_{ref}$  is the ambient air temperature at the reference height for temperature, and  $R_n$  is the net radiation. The albedo is calculated as

$$\{\varphi\} = r' + (1 - r') \exp(a\varphi + b),$$

where  $a = -0.1$ ,  $b = -0.5(1-r')$ , and  $r' = r\{\varphi-90^\circ\}$ . Note, braces,  $\{\}$ , are used throughout this report to denote the functional form of variables.

Solar radiation,  $R$ , corrected for cloud cover, is taken from Kasten and Czeplak (1980) as

$$R = R_o (1 - 0.75n^{3.4}), \quad (4)$$

where  $n$  is the fractional cloud cover and  $R_o$  is the clear sky insolation, which is calculated as  $R_o = 990(\sin \varphi - 30)$ , and  $\varphi = (\varphi\{t_p\} + \varphi\{t\})/2$  is the solar elevation ( $t_p$  and  $t$  are the previous and present hours, respectively(1975). Note that when observations of cloud cover are unavailable a value of 0.5 is assumed in eq. (3) and measurements of solar radiation are required.

### 3.1.2 Transition between the CBL and SBL

When the PBL transitions from convective to stable conditions the heat flux changes sign from a positive to a negative value. At the point of transition, the heat flux must therefore vanish, implying that the net radiation is equal to zero. By setting  $R_o$  equal to zero in eq. (3), and solving for  $\sin \varphi$ , the critical solar elevation angle,  $\varphi_{crit}$ , corresponding to the transition point between the CBL and the SBL can be determined from

$$\sin(\varphi_{crit}) = \frac{1}{990} \left[ \frac{-c_1 T^6 + \sigma_{SB} T^4 - c_2 n}{(1 - r\{\varphi\})(1 - 0.75n^{3.4})} + 30 \right]. \quad (5)$$

Therefore, AERMET defines the point of transition between the CBL and SBL (day to night) as the point in time when the solar elevation angle  $\varphi = \varphi_{crit}$ . On average, for clear and partly cloudy conditions, the transition from stable to convective conditions occurs when  $\varphi$  reaches approximately  $13^\circ$ ; for overcast conditions  $\varphi_{crit}$  increases to about  $23^\circ$  (Holtslag and van Ulden 1983).

However, if solar radiation measurements are available AERMET determines  $\varphi_{crit}$  from an estimate of cloud cover rather than the actual observations themselves. In eq. (5) the cloud cover ( $n$ ) is replaced with an equivalent cloud cover ( $n_{eq}$ ) that is calculated from eq. (4) such that

$$n_{eq} = \left(1 - R/R_o/0.75\right)^{1/3.4}$$

## 3.2 Derived parameters in the CBL

### 3.2.1 Friction velocity ( $u_*$ ) and Monin Obukhov length ( $L$ ) in the CBL

In the CBL, AERMET computes the surface friction velocity,  $u_*$ , and the Monin-Obukhov length,  $L$ , using the value of  $H$  estimated from eq. (2). Since the friction velocity and the Monin Obukhov length depend on each other, an iterative method, similar to that used in CTDMPPLUS (Perry 1992), is used. AERMOD initializes  $u_*$  and  $L$  by assuming neutral conditions (i.e.,  $L=\infty$ ). The final estimate of  $u_*$  and  $L$  is made once convergence is reached through iterative calculations (i.e., there is less than a 1% change between successive iterations). The expression for  $u_*$  (e.g., Panofsky and Dutton (1984)) is

$$u_* = \frac{k u_{ref}}{\ln(z_{ref}/z_0) - \Psi_m\{z_{ref}/L\} + \Psi_m\{z_0/L\}}, \quad (6)$$

where  $k$  is the von Karman constant ( $= 0.4$ ),  $u_{ref}$  is the wind speed at reference height,  $z_{ref}$  is the reference measurement height for wind in the surface layer, and  $z_0$  is the roughness length. The stability terms ( $\Psi_m$ 's) in eq. (6) are computed as follows:

$$\Psi_m\left\{\frac{z_{ref}}{L}\right\} = 2 \ln\left(\frac{1 + \mu}{2}\right) + \ln\left(\frac{1 + \mu^2}{2}\right) - 2 \tan^{-1} \mu + \pi/2 \quad (7)$$

$$\Psi_m\left\{\frac{z_0}{L}\right\} = 2 \ln\left(\frac{1 + \mu_0}{2}\right) + \ln\left(\frac{1 + \mu_0^2}{2}\right) - 2 \tan^{-1} \mu_0 + \pi/2$$

where  $\mu = (1 - 16z_{ref}/L)^{1/4}$  and  $\mu_0 = (1 - 16z_0/L)^{1/4}$ .

The initial step in the iteration is to solve eq. (6) for  $u_*$  assuming that  $\psi_m = 0$  (neutral limit) and setting  $u = u_{ref}$ . Having an initial estimate of  $u_*$ ,  $L$  is calculated from the following definition (e.g., see Wyngaard (1988)):

$$L = \frac{\rho c_p T_{ref} u_*^3}{k g H} \quad (8)$$

where  $g$  is the acceleration of gravity,  $c_p$  is the specific heat of air at constant pressure,  $\rho$  is the density of air, and  $T_{ref}$  is the ambient temperature representative of the surface layer. Then  $u_*$  and  $L$  are iteratively recalculated using eqs. (6), (7), and (8) until the value of  $L$  changes by less than 1%.

The reference heights for wind speed and temperature that are used in determining the friction velocity and Monin-Obukhov length are optimally chosen to be representative of the surface layer in which the similarity theory has been formulated and tested with experimental data. Typically, a 10 m height for winds and a temperature within the range of 2 to 10 m is chosen. However, for excessively rough sites (such as urban areas where  $z_o$  can be in excess of 1 m), AERMET has a safeguard to accept wind speed reference data that range vertically between  $7z_o$  and 100 m. Below  $7z_o$  (roughly, the height of obstacles or vegetation), measurements are unlikely to be representative of the general area. A similar restriction for temperature measurements is imposed, except that temperature measurements as low as  $z_o$  are permitted. Above 100 m, the wind and temperature measurements are likely to be above the surface layer, especially during stable conditions. Therefore, AERMET imposes an upper limit of 100 meters for reference wind speed and temperature measurements for the purpose of computing the similarity theory friction velocity and Monin-Obukhov length each hour. Of course, other US EPA guidance for acceptable meteorological siting should be consulted in addition to keeping the AERMET restrictions in mind.

### 3.2.2 Convective velocity scale ( $w_*$ )

AERMOD utilizes the convective velocity scale to characterize the convective portion of the turbulence in the CBL. Field observations, laboratory experiments, and numerical modeling studies show that the large turbulent eddies in the CBL have velocities proportional to the convective velocity scale ( $w_*$ ) (Wyngaard 1988). Thus, in order to estimate turbulence in the

CBL, an estimate of  $w_*$  is needed. AERMET calculates the convective velocity scale from its definition as:

$$w_* = \left( \frac{g H z_{ic}}{\rho c_p T_{ref}} \right)^{1/3}, \quad (9)$$

where  $z_{ic}$  is the convective mixing height (see Section 3.4).

### 3.3 Derived parameters in the SBL

In this section the parameters used to characterize the SBL are discussed along with their estimation methods. During stable conditions the energy budget term associated with the ground heating component is highly site-specific. During the day, this component is only about 10% of the total net radiation, while at night its value is comparable to that of the net radiation (Oke, 1978). Therefore, errors in the ground heating term can generally be tolerated during the daytime, but not at night. To avoid using a nocturnal energy balance approach that relies upon an accurate estimate of ground heating, AERMIC has adopted a much simpler semi-empirical approach for computing  $u_*$  and  $L$ .

#### 3.3.1 Original friction velocity ( $u_*$ ) in the SBL

The computation of  $u_*$  depends on the empirical observation that the temperature scale,  $\theta_*$  defined as

$$\theta_* = -H/\rho c_p u_*, \quad (10)$$

varies little during the night. Following the logic of Venkatram (1980), we combine the definition of  $L$  eq. (8) with eq. (10) to express the Monin-Obukhov length in the SBL as

$$L = \frac{T_{ref}}{k g \theta_*} u_*^2 \quad (11)$$

From (Panofsky and Dutton 1984) the wind speed profile in stable conditions takes the form

$$u = \frac{u_*}{k} \left[ \ln \left( \frac{z}{z_0} \right) + \frac{\beta_m z_{ref}}{L} \right], \quad (12)$$

where  $\beta_m = 5$  and  $z_{ref}$  is the wind speed reference measurement height. Substituting eq. (11) into eq. (12) and defining the drag coefficient,  $C_D$ , as  $k / \ln(z_{ref}/z_0)$  (Garratt 1992), results in

$$\frac{u}{u_*} = \frac{1}{C_D} + \frac{\beta_m z_{ref} g \theta_*}{T_{ref} u_*^2}. \quad (13)$$

Multiplying eq. (13) by  $C_D u_*^2$  and rearranging yields a quadratic of the form

$$u_*^2 - C_D u u_* + C_D u_0^2 = 0 \quad (14)$$

where  $u_0^2 = \beta_m z_{ref} g \theta_* / T_{ref}$ . As is used in HPDM (Hanna and Chang 1993) and CTDMPLUS (Perry 1992) this quadratic has a real solution of the form

$$u_* = \frac{C_D u_{ref}}{2} \left[ 1 + \left( 1 - \left( \frac{2 u_0}{C_D^{\frac{1}{2}} u_{ref}} \right)^2 \right)^{1/2} \right] \quad (15)$$

Equation (15) produces real-valued solutions only when the wind speed is greater than or equal to the critical value  $u_{cr} = [4 \beta_m z_{ref} g \theta_* / T_{ref} C_D]^{1/2}$ . For the wind speed less than the critical value,  $u_*$  and  $\theta_*$  are parameterized using the following linear expression:

$$u_* = u_* \{u = u_{cr}\} \left( \frac{u}{u_{cr}} \right) \quad \text{for } u < u_{cr}$$

$$\theta_* = \theta_* \left( \frac{u}{u_{cr}} \right) \quad \text{for } u < u_{cr}$$

These expressions approximate the  $u_*$  versus  $\theta_*$  dependence found by van Ulden and Holtslag (1983).

In order to calculate  $u_*$  from eq. (15), an estimate of  $\theta_*$  is needed. If representative cloud cover observations are available, the temperature scale in the SBL is taken from the empirical form of van Ulden and Holtslag (1985) as

$$\theta_* = 0.09 (1 - 0.5 n^2), \quad (16)$$

where  $n$  is the fractional cloud cover.

If cloud cover measurements are not available, AERMET can estimate  $\theta_*$  from measurements of temperature at two levels and wind speed at one level. This technique, known as the Bulk Richardson approach, starts with the similarity expression for potential temperature (Panofsky and Dutton 1984), that is,

$$\theta\{z\} - \theta_0 = \frac{\theta_*}{k} \left( \ln \frac{z}{z_0} + \beta_m \frac{z}{L} \right), \quad (17)$$

where  $\beta_m \approx 5$  and  $k (= 0.4)$  is the von Karman constant. Applying eq. (17) to the two levels of temperature measurements and rearranging terms yields

$$\theta_* = \frac{k(\theta_2 - \theta_1)}{\left[ \left( \ln \frac{z_2}{z_1} \right) + \beta_m \frac{(z_2 - z_1)}{L} \right]}. \quad (18)$$

Since both  $u_*$  (eq.(12)) and  $\theta_*$  (eq. (18)) depend on  $L$ , and  $L$  (eq. (11)) in turn depends on  $u_*$  and  $\theta_*$ , an iterative approach is needed to estimate  $u_*$ . First  $u_*$  and  $\theta_*$  are found by assuming an initial value for  $L$  and iterating among the expressions for  $u_*$ ,  $\theta_*$  (eq. (18)) and  $L$  (eq. (11)) until convergence is reached. The expression used for  $u_*$  in the iteration, is taken from (Holtslag 1984) and depends on atmospheric stability. For situations in which  $z/L < 0.5$  is estimated using eq. (12), otherwise (for more stable cases)  $u_*$  is calculated as follows:

$$u_* = \frac{ku}{\left[ \ln \frac{z}{z_o} + 7 \ln \frac{z}{L} + \frac{4.25}{(z/L)} - \frac{0.5}{(z/L)^2} + \frac{\beta_m}{2} - 1.648 \right]}. \quad (19)$$

### 3.3.2 Adjusted friction velocity ( $u_*$ ) in the SBL

Beginning with the 2017 updated regulatory version of the model (version 16216), a second approach for calculating the  $u_*$  value based on Qian and Venkatram (2011) was added. Under this formulation,  $u_*$  is computed as a function of the drag coefficient for neutral conditions ( $C_{DN}$ ),

$$C_{DN} = \frac{k^2}{\left( \ln \left( \frac{z_r - d_h}{z_0} \right) \right)^2}$$

where  $z_r$  is the measurement height and  $d_h$  the zero-plane displacement (see Eq. 20 in Qian and Venkatram (2011)). Using  $C_{DN}$ ,  $u_*$  can be calculated based on eq. 26 from Qian and Venkatram (2011),

$$u_* = \frac{C_{DN}U}{2} \left( \frac{1 + \exp \left( -\frac{r^2}{2} \right)}{1 - \exp \left( -\frac{2}{r} \right)} \right),$$

with

$$r = \frac{2u_0}{U(C_{DN})^{1/4}}$$

and

$$u_0 = \left[ \left( \frac{\beta_g(z_r - d_h - z_0) T_0}{T_0} \right)^{1/2} \right]$$

The minimum limit of the  $u_*$  value here can be computed as

$$u_{*,min} = \frac{U_{Cr} C_{DN}^{1/2}}{4}$$

with

$$U_{Cr} = \frac{2u_0}{C_{DN}^{1/4}}.$$

The final  $u_*$  value is then the maximum of  $u_{*,min}$  and the  $u_*$ . Using this value of  $u_*$ ,  $\theta_*$  is computed based on eq. (18).

As with the original method, if cloud cover measurements are not available, AERMET can estimate  $\theta_*$  from measurements of temperature at two levels and wind speed at one level. This technique, known as the Bulk Richardson approach; however, when using the adjusted  $u_*$  formulation, the computation is based on Luhar and Rayner (2009). When the  $z_{ref}$  (reference height for the wind speed) is greater than  $0.7*L$  (the Monin-Obukhov Length), then  $u_*$  is calculated based on the initial estimate of  $L$  derived from the two-level temperature measurements,

$$u_* = \frac{ku}{\alpha \left[ \zeta^\beta (1 + \gamma \zeta^{(1-\beta)}) - \zeta_0^\beta (1 + \gamma \zeta_0^{(1-\beta)}) \right]}$$

where  $\alpha = 4$ ,  $\beta = 0.5$  and  $\gamma = 0.3$  and

$$\zeta = \frac{z_0}{L}.$$

Using this value of  $u_*$ ,  $\theta_*$  is computed based on eq. (18).

### 3.3.3 Sensible heat flux ( $H$ ) in the SBL

Having computed  $u_*$  and  $\theta_*$  for stable conditions, AERMET calculates the surface heat flux from eq. (10) as

$$H = -\rho c_p u_* \theta_* . \quad (20)$$

AERMET limits the amount of heat that can be lost by the underlying surface to  $64 \text{ W m}^{-2}$ . This value is based on a restriction that Hanna (1986) placed on the product of  $\theta_*$  and  $u_*$ . That is, for typical conditions, Hanna found that

$$[\theta_* u_*]_{max} = 0.05 \text{ ms}^{-1} \text{ K} . \quad (21)$$

When the heat flux, calculated from eq. (20), is such that  $\theta_* u_* > 0.05 \text{ m s}^{-1} \text{ K}$ , AERMET recalculates  $u_*$  by substituting  $0.05/u_*$  into eq. (15) for  $\theta_*$  ( $u_o$  in eq. (15) is a function of  $\theta_*$ ).

#### 3.3.4 Monin-Obukhov length ( $L$ ) in the SBL

Using the sensible heat flux of eq. (20) and  $u_*$  from eq. (15), the Monin-Obukhov Length, for the SBL, is calculated from eq. (8).

### **3.4 Mixing height**

The mixing height ( $z_i$ ) in the CBL depends on both mechanical and convective processes and is assumed to be the larger of a mechanical mixing height ( $z_{im}$ ) and a convective mixing height ( $z_{ic}$ ). Whereas, in the SBL, the mixing height results exclusively from mechanical (or shear induced) turbulence and therefore is identically equal to  $z_{im}$ . The same expression for calculating  $z_{im}$  is used in both the CBL and the SBL. The following two sections describe the procedures used to estimate  $z_{ic}$  and  $z_{im}$ , respectively.

#### 3.4.1 Convective mixing height ( $z_{ic}$ )

The height of the CBL is needed to estimate the profiles of important PBL variables and to calculate pollutant concentrations. If measurements of the convective boundary layer height are available, they are selected and used by the model. If measurements are not available,  $z_{ic}$  is calculated with a simple one-dimensional energy balance model (Carson 1973), as modified by Weil and Brower (1983). This model uses the early morning potential temperature sounding (prior to sunrise), and the time varying surface heat flux to calculate the time evolution of the convective boundary layer as

$$z_{ic}\theta\{z_{ic}\} - \int_0^{z_{ic}} \theta\{z\}dz = (1 + 2A) \int_0^t \frac{H\{t'\}}{\rho c_p} dt, \quad (22)$$

where  $\theta$  is the potential temperature,  $A$  is set equal to 0.2 from Deardorff (1980), and  $t$  is the hour

after sunrise. Weil and Brower found good agreement between predictions and observations of  $z_{ic}$ , using this approach.

### 3.4.2 Mechanical mixing height ( $z_{im}$ )

In the early morning when the convective mixed layer is small, the full depth of the PBL may be controlled by mechanical turbulence. AERMET estimates the heights of the PBL during convective conditions as the maximum of the estimated (or measured if available) convective boundary layer height ( $z_{ic}$ ) and the estimated (or measured) mechanical mixing height. AERMET uses this procedure to ensure that in the early morning, when  $z_{ic}$  is very small, but considerable mechanical mixing may exist, the height of the PBL is not underestimated. When measurements of the mechanical mixed layer are not available,  $z_{im}$  is calculated by assuming that it approaches the equilibrium height given by Zilitinkevich (1972) as

$$z_{ie} = 0.4 \left( u_* L / f \right)^{0.5}, \quad (23)$$

where  $z_{ie}$  is the equilibrium mechanical mixing height and  $f$  is the Coriolis parameter.

Venkatram (1980) has shown that, in mid-latitudes, eq. (23) can be empirically represented as

$$z_{ie} = 2400 u_*^{3/2}, \quad (24)$$

where  $z_{ie}$  (calculated from eq. (24)) is the unsmoothed mechanical mixed layer height. When measurements of the mechanical mixed layer height are available, they are used in lieu of  $z_{ie}$ .

To avoid estimating sudden and unrealistic drops in the depth of the shear-induced, turbulent layer, the time evolution of the mechanical mixed layer height (whether measured or estimated) is computed by relaxing the solution toward the equilibrium value appropriate for the current hour. Following the approach of Venkatram (1982)

$$\frac{dz_{im}}{dt} = \frac{(z_{ie} - z_{im})}{\tau}. \quad (25)$$

The time scale,  $\tau$ , governs the rate of change in height of the layer and is taken to be proportional to the ratio of the turbulent mixed layer depth and the surface friction velocity (i.e.  $\tau = z_{im} / \beta_\tau u_*$ ). AERMOD uses a constant  $\beta_\tau$  value of 2. For example, if  $u_*$  is of order  $0.2 \text{ m s}^{-1}$ , and  $z_{im}$  is of order 500 m, the time scale is of the order of 1250 s, which is related to the time it takes for the mechanical mixed layer height to approach its equilibrium value. Notice that when  $z_{im} < z_{ie}$ , the mechanical mixed layer height increases to approach its current equilibrium value; conversely, when  $z_{im} > z_{ie}$ , the mechanical mixed layer height decreases towards its equilibrium value.

Because the friction velocity changes with time, the current smoothed value of  $z_{im}\{t+\Delta t\}$  is obtained by numerically integrating eq. (25) such that

$$z_{im}\{t + \Delta t\} = z_{im}\{t\}(e^{-\Delta t/\tau}) + z_{ie}\{t + \Delta t\}[1 - (e^{-\Delta t/\tau})] . \quad (26)$$

where  $z_{im}\{t\}$  is the previous hour's smoothed value. For computing the time scale in eq. (26),  $z_{im}$  is taken from the previous hour's estimate and  $u_*$  from the current hour. In this way, the time scale (and thus relaxation time) will be short if the equilibrium mixing height grows rapidly but will be long if it decreases rapidly.

Although eqs. (24) and (26) are designed for application in the SBL, they are used in the CBL to ensure a proper estimate of the PBL height during the short transitional period at the beginning of the day when mechanical turbulence generally dominates. The procedure, used by AERMET, guarantees the use of the convective mixing height once adequate convection has been established even though the mechanical mixing height is calculated during all convective conditions. Since AERMET uses eq. (26) to estimate the height of the mixed layer in the SBL, discontinuities in  $z_i$  from nighttime to daytime are avoided.

In AERMOD, the mixing height  $z_i$ , has an expanded role in comparison to how it is used in ISC3. In AERMOD the mixing height is used as an elevated reflecting/penetrating surface,

an important scaling height, and enters in the  $w_*$  determination found in eq. (9). The mixing height  $z_i$  for the convective and stable boundary layers is therefore defined as follows:

$$\begin{aligned} z_i &= \text{MAX}[z_{ic} ; z_{im}] && \text{for } L < 0 \text{ (CBL)} \\ z_i &= z_{im} && \text{For } L > 0 \text{ (SBL)} \end{aligned} \tag{27}$$

The sign of  $L$  is used by AERMET; if  $L < 0$  then the PBL is considered to be convective (CBL) otherwise it is stable (SBL). then the PBL is considered to be convective (CBL) otherwise it is stable (SBL).

### 3.5 Adjustment for the low wind speed/stable conditions in AERMET

An option has been incorporated in AERMET to address issues associated with model overpredictions under low wind/stable conditions. The ADJ\_U\* option is available in AERMET by specifying ADJ\_U\* on the METHOD STABLEBL keyword in the Stage 3 AERMET input file.

The ADJ\_U\* option can be specified with or without the Bulk Richardson Number option in AERMET, which utilizes delta-T measurements. The Bulk Richardson Number option in AERMET is selected by specifying BULKRN on a separate METHOD STABLEBL keyword in the Stage 3 AERMET input file. The formulation for the ADJ\_U\* option without the BULKRN option is based on Equation 26 of Qian and Venkatram (2011). The formulation for the ADJ\_U\* option with the BULKRN option is based on Equations 22, 23, and 25 of Luhar and Rayner (2009), with a critical value of  $z/L$  of 0.7.

#### 4. Vertical structure of the PBL - AERMOD'S meteorological interface

The AERMOD interface, a set of routines within AERMOD, uses similarity relationships with the boundary layer parameters, the measured meteorological data, and other site-specific information provided by AERMET to compute vertical profiles of: 1) wind direction, 2) wind speed, 3) temperature, 4) vertical potential temperature gradient, 5) vertical turbulence ( $\sigma_w$ ), and 6) lateral turbulence ( $\sigma_v$ ).

For any one of these six variables (or parameters), the interface (in constructing the profile) compares each height at which a meteorological variable must be calculated with the heights at which observations were made and if it is below the lowest measurement or above the highest measurement (or in some cases data is available at only one height), the interface computes an appropriate value from selected PBL similarity profiling relationships. If data are available both above and below a given height, an interpolation is performed which is based on both the measured data and the shape of the computed profile (see Section A.1). Thus, the approach used for profiling simultaneously takes advantage of the information contained in both the measurements and similarity parameterizations. As will be discussed, at least one level of measured wind speed, wind direction, and temperature is required. However, turbulence profiles can be parameterized without any direct turbulence measurements.

The following sections provide a comprehensive description of AERMOD's profiling equations and how these estimated profiles are used to extract pertinent layer-averaged meteorology for AERMOD's transport and dispersion calculations. Also, example profiles (one typical of the CBL and one typical of the SBL) for the various parameters have been constructed for illustration. The CBL case assumes that  $z_i = 1000$  m,  $L = -10$  m and  $z_o = 0.1$  m (i.e.,  $z_o = 0.0001 z_i$  and  $L = -0.01 z_i$ ). The SBL case assumes that  $z_i = 100$  m,  $L = 10$  m and  $z_o = 0.1$  m (i.e.,  $z_o = 0.001 z_i$  and  $L = 0.1 z_i$ ).

## 4.1 General profiling equations

### 4.1.1 Wind speed profiling

The AERMOD profile equation for wind speed, has the familiar logarithmic form:

$$\begin{aligned}
 u &= u\{7z_o\} \left[ \frac{z}{7z_o} \right] & \text{for } z < 7z_o \\
 u &= \frac{u_*}{k} \left[ \ln\left(\frac{z}{z_o}\right) - \Psi_m\left\{\frac{z}{L}\right\} + \Psi_m\left\{\frac{z_o}{L}\right\} \right] & \text{for } 7z_o \leq z \leq z_i \\
 u &= u\{z_i\} & \text{for } z > z_i
 \end{aligned} \tag{28}$$

At least one wind speed measurement, that is representative of the surface layer, is required for each simulation with AERMOD. Since the logarithmic form does not adequately describe the profile below the height of obstacles or vegetation, eq. (28) allows for a linear decrease in wind speed from its value at  $7z_o$ .

For the CBL, the  $\Psi_m$ s are evaluated using eq. (7) with  $z_{ref}$  replaced by  $z$ , and during stable conditions they are calculated from van Ulden & Holtslag (1985) as

$$\begin{aligned}
 \Psi_m\left\{\frac{z}{L}\right\} &= -17 \left[ 1 - \exp\left(-0.29\frac{z}{L}\right) \right] \\
 \Psi_m\left\{\frac{z_o}{L}\right\} &= -17 \left[ 1 - \exp\left(-0.29\frac{z_o}{L}\right) \right].
 \end{aligned} \tag{29}$$

For small  $z/L$  ( $\ll 1$ ) and with a series expansion of the exponential term, the first equation in (29) reduces to the form given in eq. (12), i.e.,  $\psi_m = \beta_m z/L$  with  $\beta_m = 5$ . However, for large  $z/L$  ( $> 1$ ) and heights as great as 200 m in the SBL, the  $\psi_m$  given by eq. (29) is found to fit wind observations much better than the  $\psi_m$  given by eq. (12) (van Ulden and Holtslag 1985). Using the example case parameter values, Figure 2 and Figure 3 were constructed to illustrate the form of the wind profiles used by AERMOD in the layers above and below  $7z_o$ .

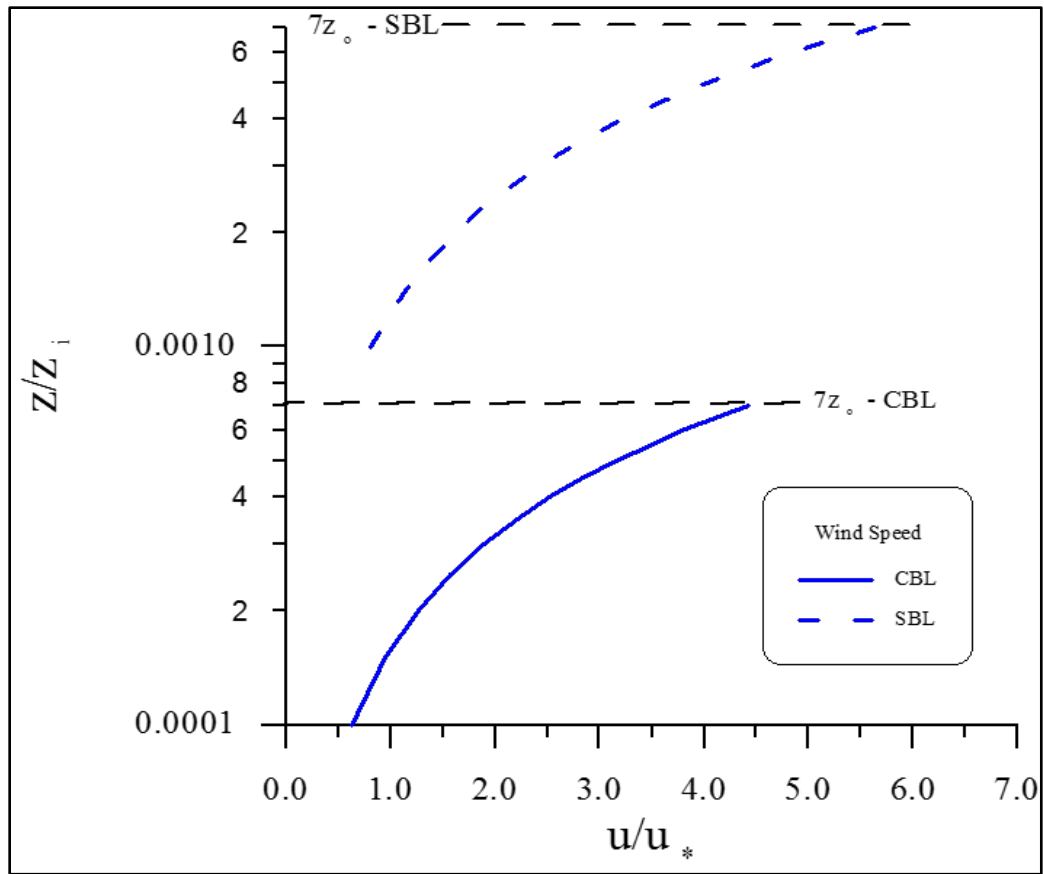


Figure 2. Wind speed profile, for both the CBL and SBL, in the region below  $7z_0$

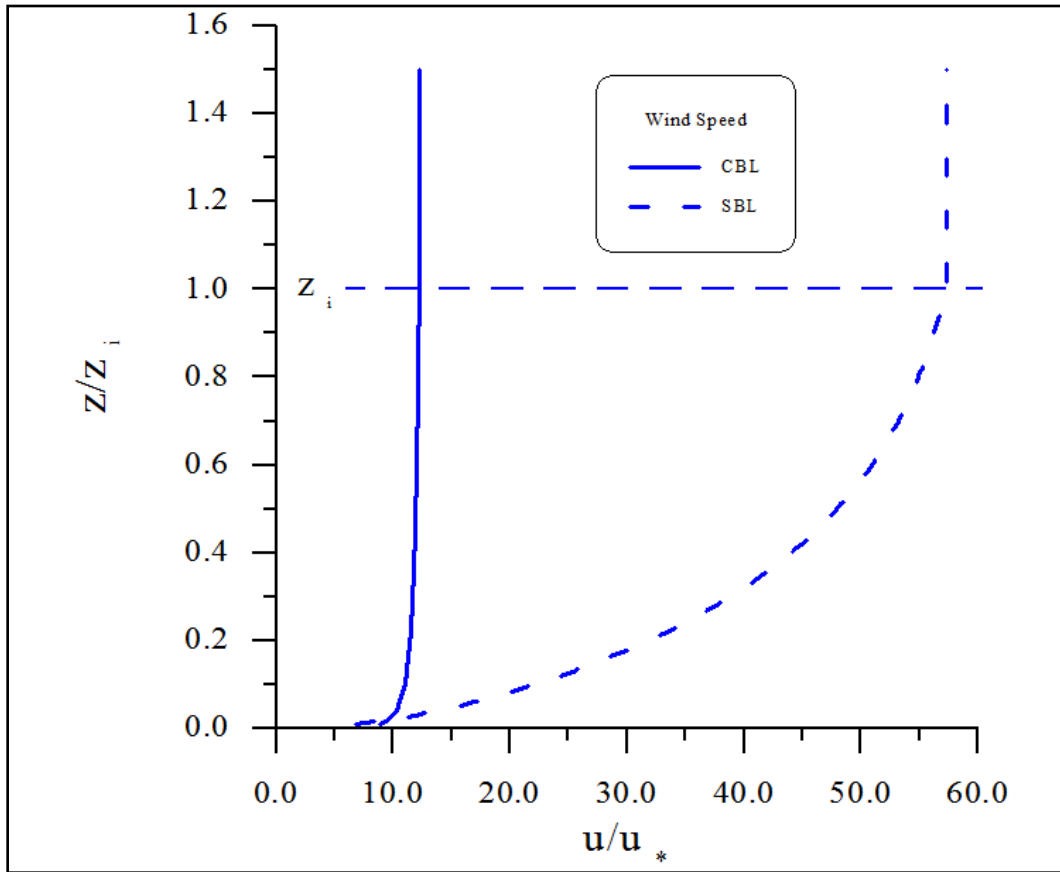


Figure 3. Wind speed profiling, for both the CBL and SBL, in the region above  $7z_0$

#### 4.1.2 Wind direction profiles

For both the CBL and SBL, wind direction is assumed to be constant with height both above the highest and below the lowest measurements. For intermediate heights, AERMOD linearly interpolates between measurements. At least one wind direction measurement is required for each AERMOD simulation.

#### 4.1.3 Profiles of the potential temperature gradient

Above the relatively shallow superadiabatic surface layer, the potential temperature gradient in the well mixed CBL is taken to be zero. The gradient in the stable interfacial layer

just above the mixed layer is taken from the morning temperature sounding. This gradient is an important factor in determining the potential for buoyant plume penetration into and above that layer. Above the interfacial layer, the gradient is typically constant and slightly stable. Although the interfacial layer depth varies with time, for the purposes of determining the strength of the stable stratification aloft, AERMET uses a fixed layer of 500 m to ensure that a sufficient layer of the morning sounding is sampled. A 500 m layer is also used by the CTDMPPLUS model (Perry 1992) for this same calculation. This avoids strong gradients (unrealistic kinks) often present in these data. For a typical mixed layer depth of 1000 m, an interfacial layer depth of 500 m is consistent with that indicated by Deardorff (1979). A constant value of  $0.005 \text{ K m}^{-1}$  above the interfacial layer is used, as suggested by Hanna and Chang (1991). Using the morning sounding to compute the interfacial temperature gradient assumes that as the mixed layer grows throughout the day, the temperature profile in the layer above  $z_i$  changes little from that of the morning sounding. Of course, this assumes that there is neither significant subsidence nor cold or warm air advection occurring in that layer. Field measurements (e.g. Clarke et al. (1971)) of observed profiles throughout the day lend support to this approach. These data point out the relative invariance of upper level temperature profiles even during periods of intense surface heating.

Below 100 m, in the SBL, AERMOD uses the definition of the potential temperature gradient suggested by Dyer (1974), as well as Panofsky and Dutton (1984). That is,

$$\begin{aligned} \frac{\partial \theta}{\partial z} &= \frac{\theta_*}{k(2)} \left[ 1 + 5 \frac{(2)}{L} \right] & \text{for } z \leq 2m \\ \frac{\partial \theta}{\partial z} &= \frac{\theta_*}{k z} \left[ 1 + 5 \frac{z}{L} \right] & \text{for } 2m < z \leq 100m. \end{aligned} \tag{30}$$

Eq. (30) is similar to that of Businger et al. (1971). Above 100 m the form of the potential temperature gradient, taken from Stull (1983) and van Ulden & Holtslag (1985) is

$$\frac{\partial \theta}{\partial z} = \frac{\partial \theta\{z_{mx}\}}{\partial z} \exp\left[-\frac{(z - z_{mx})}{0.44 z_{i\theta}}\right] \quad (31)$$

where  $z_{mx} = 100$  m,  $z_{i\theta} = \max[z_{im}; 100m]$ , and the constant 0.44 within the exponential term of eq. (31) is inferred from typical profiles taken during the Wangara experiment (Andre and Mahrt 1982). For all  $z$ ,  $\partial\theta/\partial z$  is limited to a minimum of  $0.002 \text{ K m}^{-1}$  (Paine and Kendall 1993).

In the SBL, if  $d\theta/dz$  measurements are available below 100 m and above  $z_o$ , then  $\theta_*$  is calculated from eq. (30) using the value of  $\partial\theta/\partial z$  at the lowest measurement level and  $z_{Tref}$  replaced by the height of the  $\partial\theta/\partial z$  measurements. The upper limit of 100 m for the vertical temperature gradient measurements is consistent with that imposed by AERMET for wind speed and temperature reference data used to determine similarity theory parameters such as the friction velocity and the Monin-Obukhov length. Similarly, the lower limit of  $z_o$  for the vertical temperature gradient measurements is consistent with that imposed for reference temperature data. If no measurements of  $\partial\theta/\partial z$  are available, in that height range, then  $\theta_*$  is calculated by combining eqs. (8) and (20).  $\theta_*$  is not used in the CBL.

Figure 4 shows the inverse height dependency of  $\partial\theta/\partial z$  in the SBL. To create this curve we assumed that:  $Z_{im}=100$  m; and therefore,  $Z_{i\theta} = 100$  m;  $L = 10$  m;  $u_* = .124$ , which is consistent with a mixing height of 100 m;  $T_{ref} = 293$  K; and therefore based on eq. (11)  $\theta_* = 0.115$  K. These parameter values were chosen to represent a strongly stable boundary layer. Below 2 m,  $\partial\theta/\partial z$  is persisted downward from its value of  $0.228 \text{ K m}^{-1}$  at 2m. Above 100 m,  $\partial\theta/\partial z$  is allowed to decay exponentially with height.

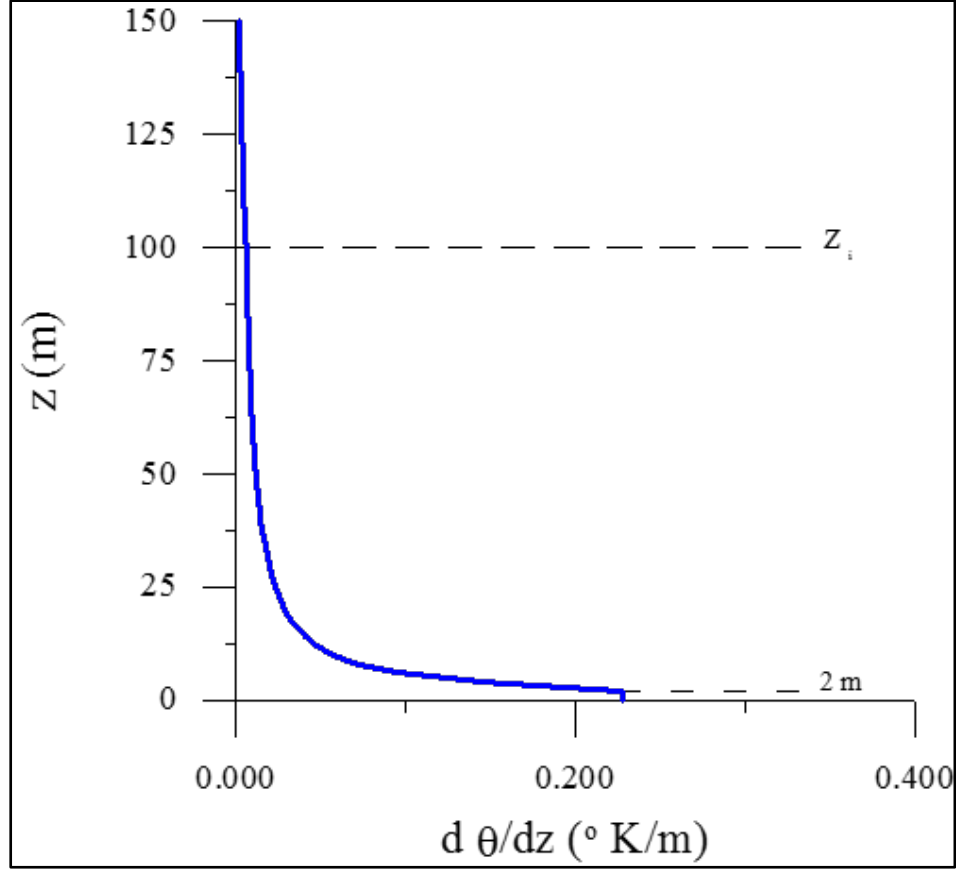


Figure 4. Profile of potential temperature gradient for the SBL

#### 4.1.4 Potential temperature profiling

For use in plume rise calculations, AERMOD develops the vertical profile of potential temperature from its estimate of the temperature gradient profile. First, the model computes the potential temperature at the reference height for temperature (i.e.,  $z_{Tref}$ ) as

$$\theta\{z_{Tref}\} = T_{ref} + \frac{g z_{msl}}{c_p}, \quad (32)$$

where  $z_{msl} = z_{ref} + z_{base}$  is the user specified elevation for the base of the temperature profile (i.e., meteorological tower). Then for both the CBL and SBL the potential temperature is calculated as follows:

$$\theta\{z + \Delta z\} = \theta\{z\} + \left. \frac{\partial \theta}{\partial z} \right|_z \Delta z \quad (33)$$

where  $\overline{\partial \theta} / \partial z$  is the average potential temperature gradient over the layer  $\Delta z$ . Note that for  $z < z_{Tref}$ ,  $\Delta z$  is negative.

#### 4.1.5 Vertical turbulence calculated

In the CBL, the vertical velocity variance or turbulence ( $\sigma_{wT}^2$ ) is profiled using an expression based on a mechanical or neutral stability limit ( $\sigma_{wm} \propto u_*$ ) and a strongly convective limit ( $\sigma_{wc} \propto w_*$ ). The total vertical turbulence is given as:

$$\sigma_{wT}^2 = \sigma_{wc}^2 + \sigma_{wm}^2 \quad (34)$$

This form is similar to one introduced by Panofsky et al. (1977) and included in other dispersion models (e.g., Berkowicz et al. (1986), Hanna and Paine (1989), and Weil (1988a)).

The convective portion ( $\sigma_{wc}^2$ ) of the total variance is calculated as:

$$\begin{aligned} \sigma_{wc}^2 &= 1.6 \left( \frac{z}{z_{ic}} \right)^{2/3} \cdot w_*^2 & \text{for } z \leq 0.1z_{ic} \\ \sigma_{wc}^2 &= 0.35w_*^2 & \text{for } 0.1z_{ic} < z \leq z_{ic} \\ \sigma_{wc}^2 &= 0.35w_*^2 \exp \left[ -\frac{6(z - z_{ic})}{z_{ic}} \right] & \text{for } z > z_{ic} \end{aligned} \quad (35)$$

where the expression for  $z \leq 0.1 z_{ic}$  is the free convection limit (Panofsky et al. 1977), for  $0.1z_{ic} < z \leq z_{ic}$  is the mixed-layer value (Hicks 1985), and for  $z > z_{ic}$  is a parameterization to connect the mixed layer  $\sigma_{wc}^2$  to the assumed near-zero value well above the CBL. An example profile of convective vertical turbulence described in eq. (35) is presented in Figure 5.

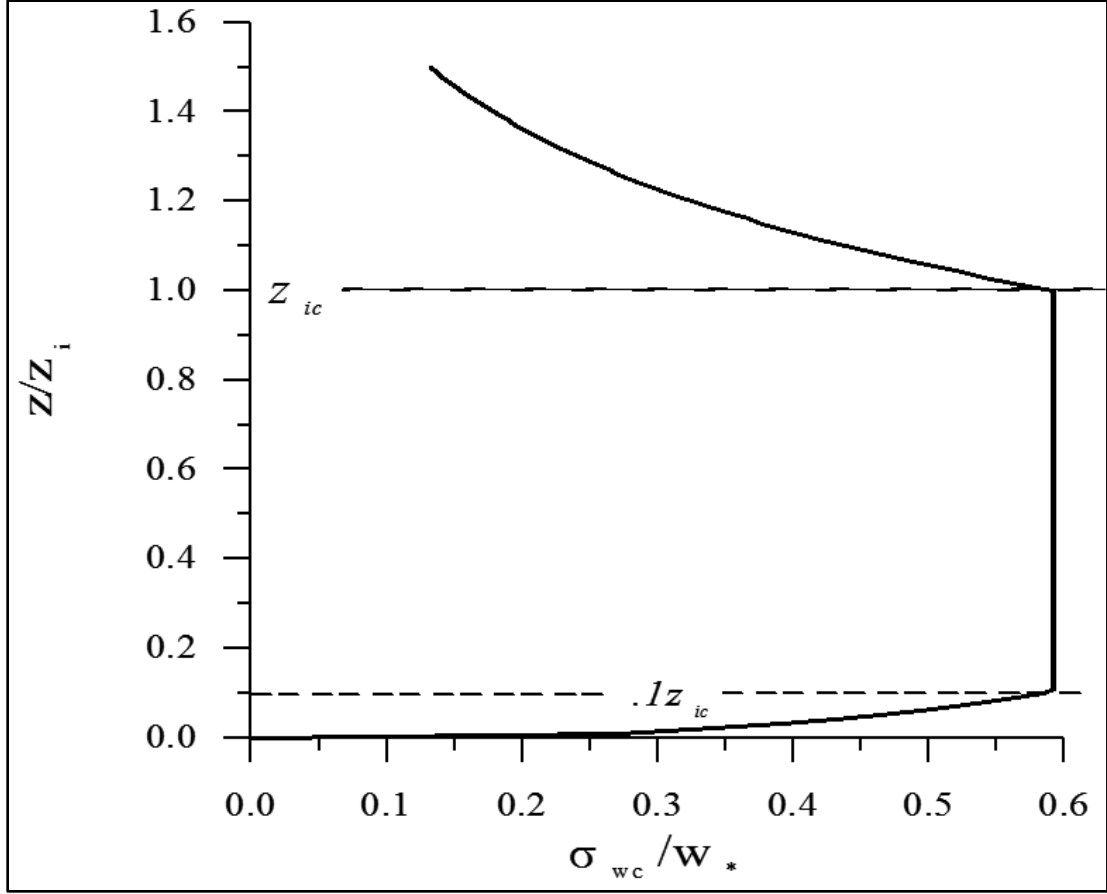


Figure 5. Convective portion of the vertical turbulence in the CBL

The mechanical turbulence ( $\sigma_{wm}$ ) is assumed to consist of a contribution from the boundary layer ( $\sigma_{wml}$ ) and from a “residual layer” ( $\sigma_{wmr}$ ) above the boundary layer ( $z > z_i$ ) such that,

$$\sigma_{wm}^2 = \sigma_{wml}^2 + \sigma_{wmr}^2. \quad (36)$$

This is done to satisfy the assumed decoupling between the turbulence aloft ( $z > z_i$ ) and that at the surface in the CBL shear layer, and to maintain a continuous variation of  $\sigma_{wm}^2$  with  $z$  near  $z = z_i$ . The expression for  $\sigma_{wml}$  following the form of Brost et al. (1982) is

$$\begin{aligned}
\sigma_{wml} &= 1.3u_* \left(1 - \frac{z}{z_i}\right)^{1/2} & \text{for } z < z_i \\
\sigma_{wml} &= 0.0 & \text{for } z \geq z_i
\end{aligned} \tag{37}$$

where the  $\sigma_{wml} = 1.3u_*$  at  $z = 0$  is consistent with Panofsky et al. (1977).

Above the mixing height,  $\sigma_{wmr}$  is set equal to the average of measured values in the residual layer above  $z_i$ . If measurements are not available, then  $\sigma_{wmr}$  is taken as the default value of  $0.02 u\{z_i\}$ . The constant 0.02 is an assumed turbulence intensity  $i_z (= \sigma_{wm} / u)$  for the very stable conditions presumed to exist above  $z_i$  (Briggs 1973). Within the mixed layer the residual turbulence ( $\sigma_{wmr}$ ) is reduced linearly from its value at  $z_i$  to zero at the surface. Figure 6 presents the profile of the mechanical portion of the vertical turbulence in the CBL. The effect of combining the residual and boundary layer mechanical turbulence (eq. (36)) can be seen in this figure.

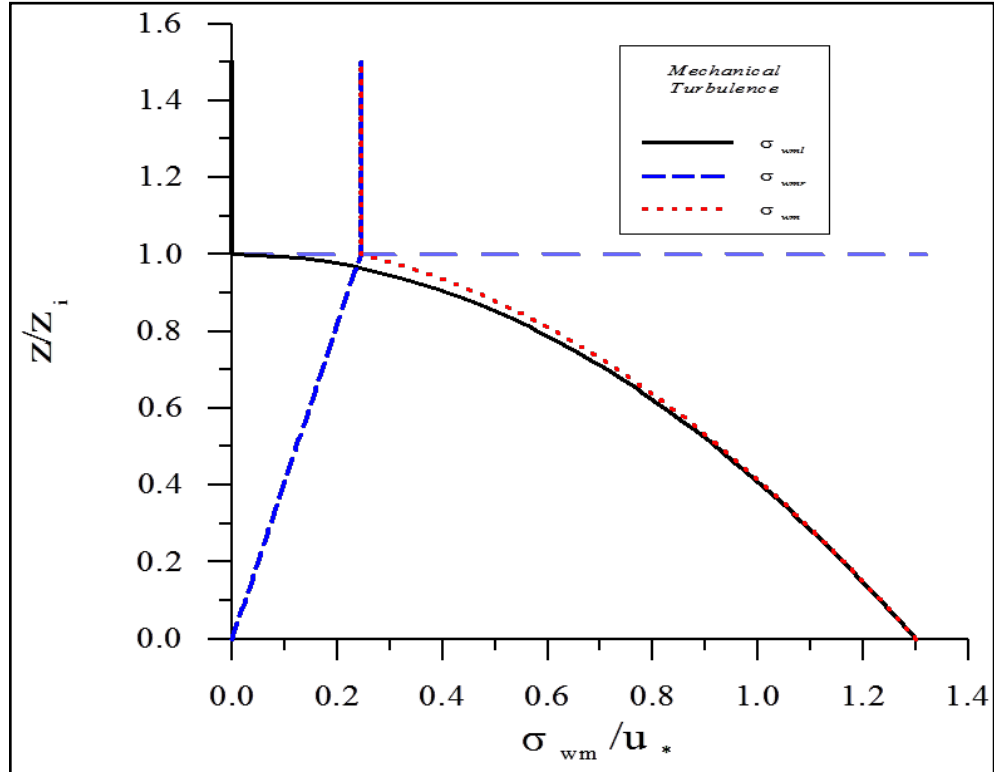


Figure 6. Mechanical portion of the vertical turbulence in the CBL

In the SBL the vertical turbulence contains only a mechanical portion which is given by eq. (36). The use of the same  $\sigma_{wm}^2$  expressions for the SBL and CBL is done to ensure continuity of turbulence in the limit of neutral stability. Figure 7 illustrates AERMOD's assumed vertical turbulence profile for the SBL. This is similar to the profile for the CBL except for a notable increase in the value of  $\sigma_{wmr}$ . Since values for  $\sigma_{wmr}$  are based on the magnitude of the wind speed at  $z_i$ , the differences in the two figures stem from setting  $z_o = 0.0001z_i$  in the CBL example case, while for the SBL case  $z_o = 0.001z_i$ .

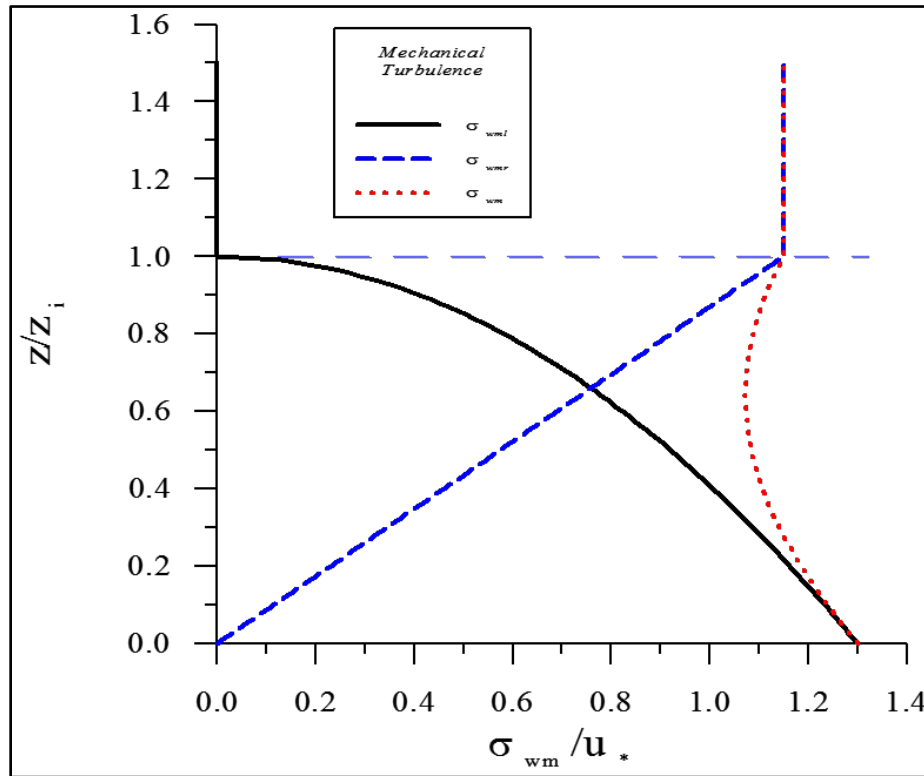


Figure 7. Profile of vertical turbulence in the SBL

#### 4.1.6 Lateral turbulence calculated by the interface

In the CBL the total lateral turbulence,  $\sigma_{vT}^2$ , is computed as a combination of a mechanical ( $\sigma_{vm}$ ) and convective ( $\sigma_{vc}$ ) portions such that

$$\sigma_{vT}^2 = \sigma_{vc}^2 + \sigma_{vm}^2. \quad (38)$$

In the SBL the total lateral turbulence contains only a mechanical portion. AERMOD, uses the same  $\sigma_{vm}$  expression in the CBL and SBL. This is done to maintain continuity of  $\sigma_{vm}$  in the limit of neutral stability. A description of mechanical and convective profiles of lateral turbulence follows.

#### 4.1.6.1 Mechanical portion of the lateral turbulence

The variation with height of the mechanical portion of the lateral turbulence is bounded by its value at the surface and an assumed residual value at the top of the mechanical mixed layer. The variation between these two limits is assumed to be linear. Based on observations from numerous field studies, Panofsky and Dutton (1984) report that, in purely mechanical turbulence, the lateral variance near the surface has the form

$$\sigma_{v0}^2 = C u_*^2 \quad (39)$$

where the constant,  $C$ , ranges between 3 and 5. Based on an analysis of the Kansas data, Izumi (1971) and Hicks (1985) support the form of eq. (39) with a value of 3.6 for  $C$ .

Between the surface and the top of the mechanically mixed layer,  $\sigma_{vm}^2$  is assumed to vary linearly as

$$\begin{aligned} \sigma_{vm}^2 &= \left[ \frac{\sigma_{vm}^2 \{z_{im}\} - \sigma_{vo}^2}{z_{im}} \right] z + \sigma_{vo}^2 \quad \text{for } z \leq z_{im} \\ \sigma_{vm}^2 &= \sigma_{vm}^2 \{z_{im}\} \quad \text{for } z > z_{im}, \end{aligned} \quad (40)$$

where  $\sigma_{vm}^2 \{z_m\} = \min[\sigma_{vo}^2; 0.25 \text{ m}^2 \text{s}^{-2}]$  and  $\sigma_{vo}^2$ , the surface value of the lateral turbulence, is equal to  $3.6 u_*^2$ . This linear variation of  $\sigma_{vm}^2$  with  $z$  is consistent with field observations (e.g., Brost et al. (1982)). In the SBL the total lateral turbulence contains only a mechanical portion and it is given by eq. (40).

Above the mixed layer, lateral turbulence is expected to maintain a modest residual level. Hanna (1983) analyzed ambient measurements of lateral turbulence in stable conditions. He found that even in the lightest wind conditions, the measurements of  $\sigma_{vc}$  were typically  $0.5 \text{ m s}^{-1}$  but were observed to be as low as  $0.2 \text{ m s}^{-1}$ . AERMOD adopts the lower limit of  $0.2 \text{ m s}^{-1}$  for  $\sigma_{vc}$  in near-surface conditions, as discussed below, but uses the more typical value of  $0.5 \text{ m s}^{-1}$  for the residual lateral turbulence above the mixed layer. Above the height of the CBL, the model linearly decreases  $\sigma_{vc}^2$  from  $\sigma_{vc}^2\{z_{ic}\}$  to  $0.25$  at  $1.2 z_{ic}$  and holds  $\sigma_{vc}^2$  constant above  $1.2 z_{ic}$ . However, if  $\sigma_{vc}^2\{z_{ic}\} < 0.25 \text{ m}^2 \text{ s}^{-2}$ , then  $\sigma_{vc}^2\{z_{ic}\}$  is persisted upward from  $z_{ic}$ . Furthermore, it was found that a value of the order  $\sigma_{vc}^2 = 0.25 \text{ m}^2 \text{ s}^{-2}$  provided consistently good model performance (for plumes commonly above  $z_{im}$ ) during the developmental evaluation (Perry et al. 2005) supporting the presence of residual lateral turbulence in this layer.

Figure 8 shows how the vertical profile of lateral mechanical turbulence changes over a range of mechanical mixing heights, and related friction velocities. The values of  $u^*$  used to produce these curves are consistent with the relationship between  $z_{im}$  and  $u^*$  which is found in eq. (24). For the SBL Figure 8 represents profiles of the total lateral turbulence. In the CBL these curves depict only the mechanical portion of the total lateral variance. Note that for  $z_{im} = 300 \text{ m}$  and  $100 \text{ m}$  the values  $\sigma_{vo}^2$  are less than  $0.25 \text{ m}^2 \text{ s}^{-2}$ . Therefore, the profiles are constant with height.

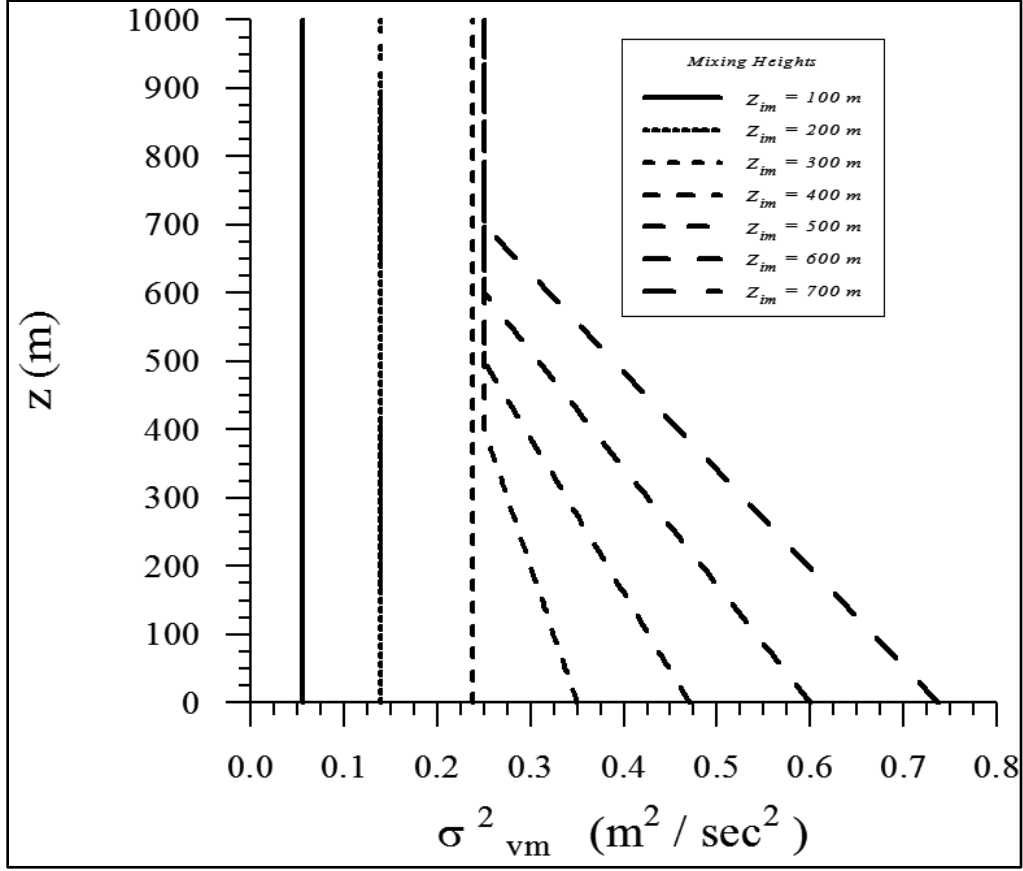


Figure 8. Family of lateral mechanical turbulence profiles over a range of mechanical mixing heights

#### 4.1.6.2 Convective portion of the lateral turbulence

The convective portion of the lateral turbulence within the mixed layer is constant and calculated as:

$$\sigma_{vc}^2 = 0.35w_*^2 \quad (41)$$

This constant value of  $\sigma_v^2/w_*^2 = 0.35$  is supported by the Minnesota data (Readings et al. 1974; Kaimal et al. 1976) and by data collected at Ashchurch, England (Caughey and Palmer 1979).

For  $z > z_{ic}$ , the model linearly decreases  $\sigma_{vc}^2$  from  $\sigma_{vc}^2\{z_{ic}\}$  to 0.25 at  $1.2 z_{ic}$  and holds  $\sigma_{vc}^2$  constant above  $1.2 z_{ic}$ . However, if  $\sigma_{vc}^2\{z_{ic}\} < .25 \text{ m}^2 \text{ s}^{-2}$ , then  $\sigma_{vc}^2\{z_{ic}\}$  is persisted upward from  $z_{ic}$ .

#### 4.2 Vertical inhomogeneity in the boundary layer as treated by the interface

AERMOD is designed to treat the effects on dispersion from vertical variations in wind and turbulence. Consideration of the vertical variation in meteorology is important for properly modeling releases in layers with strong gradients, for capturing the effects of meteorology in layers into which the plume may be vertically dispersing, and to provide a mechanism (in the CBL) by which sources that are released into, or penetrate into, an elevated stable layer can eventually re-enter the mixed layer. However, AERMOD is a steady-state plume model and therefore can use only a single value of each meteorological parameter to represent the layer through which these parameters are varying. Thus, the model "converts" the inhomogeneous values into equivalent effective or homogeneous values. This technique is applied to  $u$ ,  $\sigma_{vT}$ ,  $\sigma_{wT}$ ,  $\partial\theta/\partial z$ , and the Lagrangian time scale. The effective parameters are denoted by a tilde throughout the document (e.g., effective wind speed is denoted by  $\tilde{u}$ ).

Fundamental to this approach is the concept that the primary layer of importance, relative to receptor concentration, is the one through which plume material travels directly from source to receptor. Figure 9 presents a schematic illustration of the approach AERMOD uses to determine these effective parameters ( $\alpha$  is used to generically represent these parameters). The effective parameters are determined by averaging their values over that portion of the layer that contains plume material between the plume centroid height,  $H_p\{x\}$ , (a simplified surrogate for the height of the plume's center of mass) and the receptor height ( $z_r$ ). In other words, the averaging layer is determined by the vertical half-depth of the plume (defined as  $2.15 \sigma_z\{x_r\}$  where  $x_r$  is the distance from source to receptor) but is bounded by  $H_p\{x_r\}$  and  $z_r$ . The values

used in the averaging process are taken from AERMOD's vertical profiles. This technique is best illustrated with examples.

Consider the two receptors depicted in Figure 9. Both receptors are located at the same distance  $x_r$  from the source but at different heights above ground, i.e.,  $z_{r1}$  and  $z_{r2}$ . An example profile of some parameter  $\alpha$  is shown at the far left of the figure. The value of the effective parameter used by AERMOD to represent transport and diffusion from source to receptor depends on the location of the receptor. For receptor 1 the effective parameter value  $\tilde{\alpha}_1$  (shown

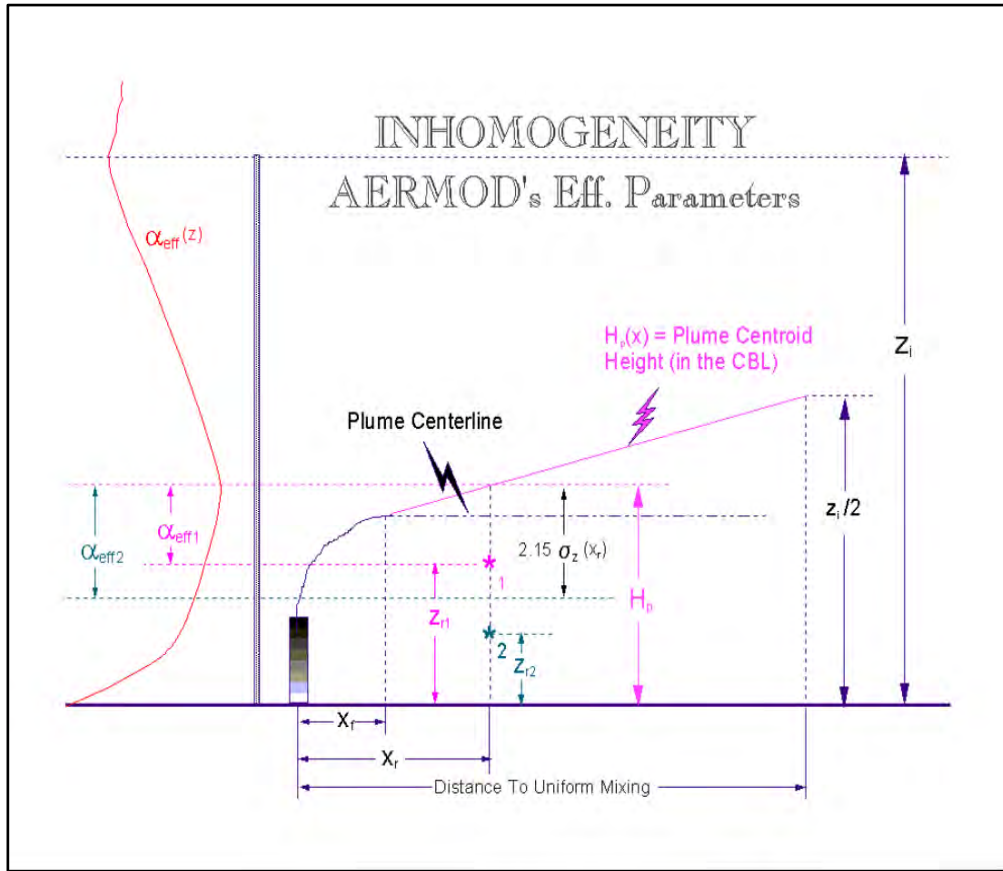


Figure 9. AERMOD's Treatment of the Inhomogeneous Boundary Layer

in the figure as  $\alpha_{eff1}$ ) is determined by averaging the values of  $\alpha\{z\}$  between  $H_p\{x_r\}$  and  $z_{r1}$ . Therefore, the layer over which this average is taken is smaller than the plume's half-depth. Whereas,  $\tilde{\alpha}_2$  (shown in the figure as  $\alpha_{eff2}$ ) is determined by averaging  $\alpha\{z\}$  over the full layer from  $H_p\{x_r\}$  down through a depth of  $2.15\sigma_z\{x_r\}$  since the receptor is located below the defined lower extent of the plume.

Since  $\sigma_z \{x_r\}$  depends on the effective values of  $\sigma_{wT}$  and  $u$ , the plume size is estimated by first using the plume height values of  $\sigma_{wT} \{H_p\}$  and  $u \{H_p\}$  to calculate  $\sigma_z \{x_r\}$ . As illustrated in Figure 9  $\sigma_z \{x_r\}$  is then used to determine the layer over which  $\tilde{\sigma}_{wT} \{x_r\}$  and  $\tilde{u} \{x_r\}$  are calculated. Once the averaging layer for a given plume and receptor is established the effective values,  $\tilde{\alpha}$ , are computed as simple averages:

$$\tilde{\alpha} = \frac{1}{(h_t - h_b)} \int_{h_b}^{h_t} \alpha \{z\} dz \quad (42)$$

where  $h_b$  and  $h_t$  are the bottom and top, respectively, of the layer of importance such that:

$$\begin{aligned} h_b &= \begin{cases} H_p \{x_r, y_r\}, & \text{if } H_p \{x_r, y_r\} \leq z_r \\ \text{MAX} \left\{ \left[ H_p \{x_r, y_r\} - 2.15 \sigma_z \{x_{sr}\} \right], z_r \right\}, & \text{if } H_p \{x_r, y_r\} > z_r \end{cases} \\ h_t &= \begin{cases} \text{MIN} \left\{ \left[ H_p \{x_r, y_r\} + 2.15 \sigma_z \{x_{sr}\} \right], z_r \right\}, & \text{if } H_p \{x_r, y_r\} \leq z_r \\ H_p \{x_r, y_r\}, & \text{if } H_p \{x_r, y_r\} > z_r \end{cases} \end{aligned} \quad (43)$$

For all plumes, both limits are bounded by either the  $z_r$  or  $H_p$ . For both the direct and indirect sources  $h_t$ , in eq. (43) is not allowed to exceed  $z_i$  and if  $h_b \geq z_i$  then  $\tilde{\alpha} = \alpha \{z_i\}$ .

For plumes in stable conditions and for the penetrated source in the CBL,  $H_p$  is always set equal to the plume centerline height ( $\Delta h_s + h_s$ ) where  $h_s$  is the stack height corrected for stack tip downwash and  $\Delta h_s$  is the stable source plume rise. The stable source plume rise  $\Delta h_s$  is calculated from expressions found in Section 5.6.2.

In the CBL, the specification of  $H_p$  is somewhat more complicated. Because of limited mixing in the CBL the center of mass of the plume will be the plume height close to the source and the mid-point of the PBL at the distance where it becomes well mixed. Beyond final plume rise,  $H_p$  is varied linearly between these limits.

Prior to plume stabilization, i.e.,  $x < x_f$  (distance to plume stabilization),

$$H_p = h_s + \Delta h_{d,p},$$

where  $\Delta h_d$  is the plume rise for the direct source (estimated from eq. (91)), and  $\Delta h_p (= h_{ep} - h_s)$  is the plume rise for the penetrated source, where  $h_{ep}$  (penetrated source plume height) is calculated from eq. (94).

The distance to plume stabilization,  $x_f$ , is determined following Briggs (Briggs 1975; Briggs 1971) as

$$\begin{aligned} x_f &= 49 F_b^{5/8} & \text{for } F_b < 55 \\ x_f &= 119 F_b^{2/5} & \text{for } F_b \geq 55 \end{aligned} \quad (44)$$

where the buoyancy flux ( $F_b$ ) is calculated from eq. (57).

For  $F_b = 0$  the distance to final rise is calculated from the ISCST3 ((U.S. Environmental Protection Agency, 1995)) expression

$$x_f = \frac{8r_s(w_s + 3u_p)^2}{w_s u_p} \quad (45)$$

where  $u_p$  is the wind speed at source height,  $r_s$  is the stack radius, and  $w_s$  is the stack exit gas velocity.

Beyond plume stabilization ( $x > x_f$ ),  $H_p$  varies linearly between the stabilized plume height ( $H\{x_f\}$ ) and the mid-point of the mixed layer ( $z_i/2$ ). This interpolation is performed over the distance range  $x_f$  to  $x_m$ , where  $x_m$  is the distance at which pollutants first become uniformly mixed throughout the boundary layer.

The distance  $x_m$  is taken to be the product of the average mixed layer wind speed and the mixing time scale,  $z_i/\overline{\sigma}_{wT}$ . That is,

$$x_m = \frac{\overline{u} z_i}{\overline{\sigma}_{wT}}, \quad (46)$$

where the averaging of  $u$  and  $\sigma_{wT}$  are taken over the depth of the boundary layer.

For distances beyond  $x_f$ ,  $H_p$  is assumed to vary linearly between the plume's stabilized height,  $H\{x_f\}$ , and  $z_i/2$  such that:

$$H_p = H\{x_f\} + \left( \frac{z_i}{2} - H\{x_f\} \right) \cdot \frac{(x - x_f)}{(x_m - x_f)} \quad (47)$$

Note that in the CBL, both the direct and indirect source will have the same  $\alpha$  (effective parameter) values. In eq. (43)  $\sigma_z$  is the average of the updraft  $\sigma_z$  and the downdraft  $\sigma_z$ , the maximum value of  $h_t$  is  $z_i$ , and when  $h_b \geq z_i$ ,  $\alpha = \alpha\{z_i\}$ .

As discussed previously, when multiple vertical measurements of wind direction are available a profile is constructed by linearly interpolating between measurements and persisting the highest and lowest measurements up and down, respectively. The approach taken for selecting a transport wind direction from the profile is different from the above. The transport wind direction is selected as the mid-point of the range between stack height and the stabilized plume height.

## 5. The AMS/EPA regulatory Model: AERMOD

AERMOD is a steady-state plume model in that it assumes that concentrations at all distances during a modeled hour are governed by the temporally averaged meteorology of the hour. The steady state assumption yields useful results since the statistics of the concentration distribution are of primary concern rather than specific concentrations at particular times and locations. AERMOD has been designed to handle the computation of pollutant impacts in both flat and complex terrain within the same modeling framework. In fact, with the AERMOD structure, there is no need for the specification of terrain type (flat, simple, or complex) relative to stack height since receptors at all elevations are handled with the same general methodology. To define the form of the AERMOD concentration equations, it is necessary to simultaneously discuss the handling of terrain.

In the stable boundary layer (SBL), the concentration distribution is assumed to be Gaussian in both the vertical and horizontal. In the convective boundary layer (CBL), the horizontal distribution is assumed to be Gaussian, but the vertical distribution is described with a bi-Gaussian probability density function (pdf). This behavior of the concentration distributions in the CBL was demonstrated by Willis and Deardorff (1981) and Briggs (1993). Additionally, in the CBL, AERMOD treats “plume lofting,” whereby a portion of plume mass, released from a buoyant source, rises to and remains near the top of the boundary layer before becoming vertically mixed throughout the CBL. The model also tracks any plume mass that penetrates into an elevated stable layer, and then allows it to re-enter the boundary layer when and if appropriate.

In urban areas, AERMOD accounts for the dispersive nature of the “convective-like” boundary layer that forms during nighttime conditions by enhancing the turbulence over that which is expected in the adjacent rural, stable boundary layer. The enhanced turbulence is the result of the urban heat flux and associated mixed layer which are estimated from the urban-rural temperature difference as suggested by Oke (1978; 1982).

In complex terrain, AERMOD incorporates the concept of the dividing streamline (Snyder et al., 1985) for stably-stratified conditions. Where appropriate, the plume is modeled

as a combination of two limiting cases: a horizontal plume (terrain impacting) and a terrain-following (terrain responding) plume. That is, AERMOD handles the computation of pollutant impacts in both flat and complex terrain within the same modeling framework. Generally, in stable flows, a two-layer structure develops in which the lower layer remains horizontal while the upper layer tends to rise over the terrain. The concept of a two-layer flow, distinguished at the dividing streamline height ( $H_c$ ), was first suggested by theoretical arguments of Sheppard (1956) and demonstrated through laboratory experiments, particularly those of Snyder et al. (1985). In neutral and unstable conditions  $H_c = 0$ .

A plume embedded in the flow below  $H_c$  tends to remain horizontal; it might go around the hill or impact on it. A plume above  $H_c$  will ride over the hill. Associated with this is a tendency for the plume to be depressed toward the terrain surface, for the flow to speed up, and for vertical turbulent intensities to increase. These effects in the vertical structure of the flow are accounted for in models such as the Complex Terrain Dispersion Model (CTDMPLUS) (Perry 1992). However, because of the model complexity, input data demands for CTDMPLUS are considerable. EPA policy (Code of Federal Regulations 1997) requires the collection of wind and turbulence data at plume height when applying CTDMPLUS in a regulatory application. As previously stated, the model development goals for AERMOD include having methods that capture the essential physics, provide plausible concentration estimates, and demand reasonable model inputs while remaining as simple as possible. Therefore, AERMIC arrived at a terrain formulation in AERMOD that considers vertical flow distortion effects in the plume, while avoiding much of the complexity of the CTDMPLUS modeling approach. Lateral flow channeling effects on the plume are not considered by AERMOD.

AERMOD captures the effect of flow above and below the dividing streamline by weighting the plume concentration associated with two possible extreme states of the boundary layer (horizontal plume and terrain-following). As is discussed below, the relative weighting of the two states depends on: 1) the degree of atmospheric stability; 2) the wind speed; and 3) the plume height relative to terrain. In stable conditions, the horizontal plume "dominates" and is given greater weight while in neutral and unstable conditions, the plume traveling over the terrain is more heavily weighted.

## 5.1 General structure of AERMOD including terrain

In general, AERMOD models a plume as a combination of two limiting cases: a horizontal plume (terrain impacting) and a terrain-following plume. Therefore, for all situations, the total concentration, at a receptor, is bounded by the concentration predictions from these states. In flat terrain the two states are equivalent. By incorporating the concept of the dividing streamline height, in elevated terrain, AERMOD's total concentration is calculated as a weighted sum of the concentrations associated with these two limiting cases or plume states (Venkatram et al. 2001).

The AERMOD terrain pre-processor (AERMAP) uses gridded terrain data to calculate a representative terrain-influence height ( $h_c$ ) for each receptor with which AERMOD computes receptor specific  $H_c$  values. Through this approach, AERMOD handles the computation of pollutant impacts in both flat and elevated terrain within the same modeling framework, thereby obviating the need to differentiate between the formulations for simple and complex terrain (as required with previous regulatory models).

The general concentration equation, which applies in stable or convective conditions is given by

$$C_T\{x_r, y_r, z_r\} = f \cdot C_{c,s}\{x_r, y_r, z_r\} + (1 - f) C_{c,s}\{x_r, y_r, z_p\} \quad (48)$$

where  $C_T\{x_r, y_r, z_r\}$  is the total concentration  $C_{c,s}\{z_r, y_r, z_r\}$  is the contribution from the horizontal plume state (subscripts  $c$  and  $s$  refer to convective and stable conditions, respectively),  $C_{c,s}\{z_r, y_r, z_r\}$  is the contribution from terrain-following state,  $f$  is the plume state weighting function,  $\{x_r, y_r, z_r\}$  is the coordinate representation of a receptor (with  $z_r$  defined relative to stack base elevation)  $z_p = z_r - z_t$  is the height of a receptor above local ground, and  $z_t$  is the terrain height at a receptor. Note that in flat terrain,  $z_t = 0$ ,  $z_p = z_r$  and the concentration (eq. (48)) reduces to the form for a single horizontal plume. It is important to note that for any concentration calculation all heights ( $z$ ) are referenced to stack base elevation. Figure 10 illustrates the relationship between the actual plume and AERMOD's characterization of it.

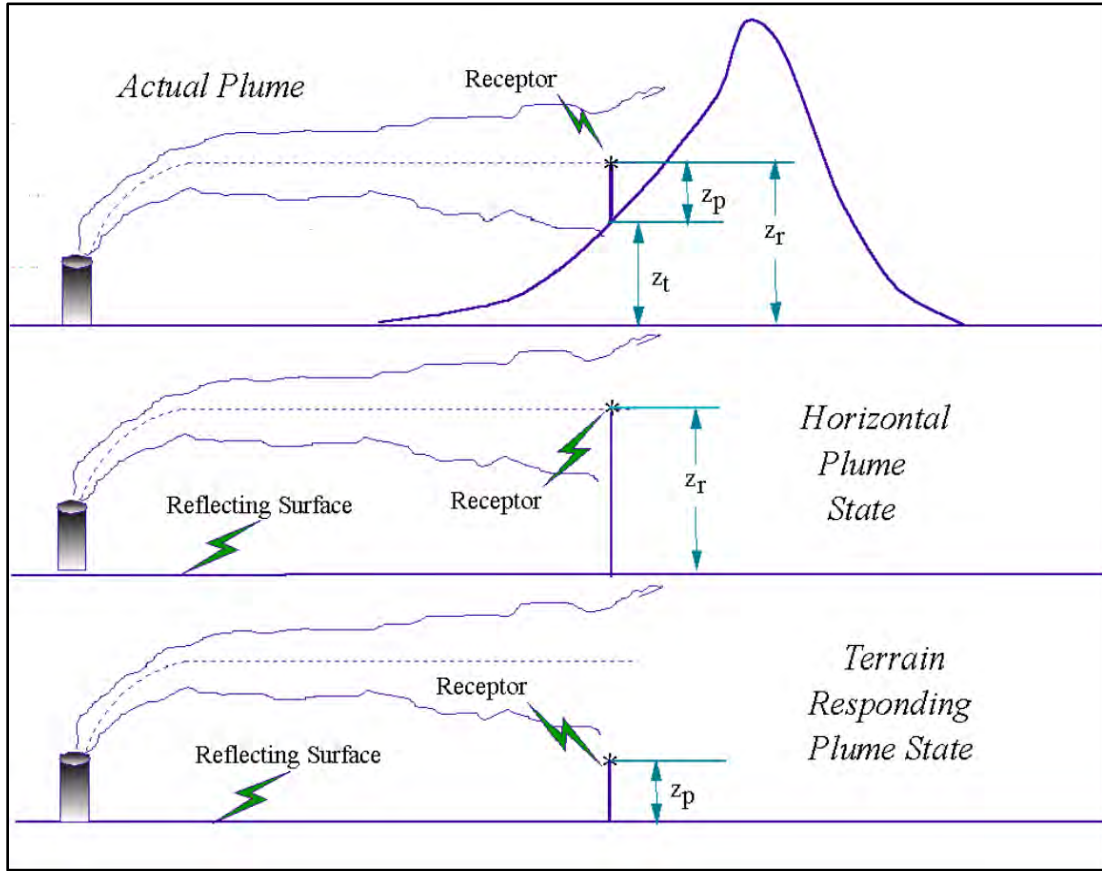


Figure 10. AERMOD two state approach. The total concentration predicted by AERMOD is the weighted sum of the two extreme possible plume states

The formulation of the weighting factor requires the computation of  $H_c$ . Using the receptor specific terrain height scale ( $h_c$ ) from AERMAP,  $H_c$  is calculated from the same algorithms found in CTDMPLUS as:

$$1/2 \cdot u^2 \{H_c\} = \int_{H_c}^{h_c} N^2 (h_c - z) dz. \quad (49)$$

where  $u \{H_c\}$  is the wind speed at height  $H_c$ , and  $N = \left[ \frac{g}{\theta} \frac{\partial \theta}{\partial z} \right]^{1/2}$  is the Brunt-Vaisala frequency. The height scale,  $h_c$ , characterizes the height of the surrounding terrain that most dominates the flow in the vicinity of the receptor.

The weighting between the two states of the plume depends on the relationship between  $H_c$  and the vertical concentration distribution at the receptor location. Assuming that the wind speed increases with height,  $H_c$  can be thought of as the level in the stable atmosphere where the flow has sufficient kinetic energy to overcome the stratification and rise to the height of the terrain. However, in determining the amount of plume material in the terrain-following state at a receptor, it is only important to know the lowest height in the flow where the kinetic energy is sufficient for a streamline to just maintain its height above the surface, i.e. terrain-following. Whether it will be deflected further and reach the top of some specified hill is not important for determining the amount of plume material in the terrain-following state for this receptor. Venkatram et al. (2001) first proposed the idea that for real terrain, often characterized by a number of irregularly shaped hills,  $H_c$  should be defined in relation to a terrain-following height at each receptor location. This is in contrast to the more classical definition where  $H_c$  is defined in relation to the top of a single representative hill upon which may reside many receptor locations.

In the AERMOD approach, plume height, receptor elevation, and  $H_c$  will determine how much plume material resides in each plume state. For a receptor at elevation  $z_r$  and an effective plume at height  $h_e$ , the height that the streamlines must reach to be in the terrain-following state is  $z_r + h_e$ . Therefore, the terrain height of importance,  $h_c$ , in determining  $H_c$  is simply equal to this local terrain-following height. Any actual terrain above  $h_c = z_r + h_e$  is of no consequence to the concentration at the receptor. This receptor and plume dependent approach to computing  $H_c$  assumes that there is sufficient terrain affecting the flow near the receptor to vertically force the streamlines to the terrain-following level. If the actual surrounding terrain does not reach the height of the terrain-following state,  $h_c$  is calculated from the highest actual terrain height in the vicinity of the receptor. Therefore, for any receptor,  $h_c$  is defined as the minimum of the highest actual terrain and the local terrain-following height. Given  $h_c$ , the dividing streamline height is computed with the same integral formula found in the CTDMPLUS model.

The fraction of the plume mass below  $H_c$  (i.e.,  $\phi_p$ ) is computed as:

$$\varphi_p = \frac{\int_0^{H_c} C_s\{x_r, y_r, z_r\} dz}{\int_0^{\infty} C_s\{x_r, y_r, z_r\} dz} \quad (50)$$

where  $C_s\{x_r, y_r, z_r\}$  is the concentration in the absence of the hill for stable conditions. In convective conditions  $H_c = 0$  and  $\varphi_p = 0$ . As described by Venkatram et al. (2001), the plume state weighting factor  $f$  is given by  $f = 0.5(1 + \varphi_p)$ . When the plume is entirely below  $H_c$  ( $\varphi_p = 1.0$  and  $f = 1.0$ ) the concentration is determined only by the horizontal plume. When the plume is entirely above the critical dividing streamline height or when the atmosphere is either neutral or convective, ( $\varphi_p = 0$  and  $f = 0.5$ ). Therefore, during convective conditions the concentration at an elevated receptor is simply the average of the contributions from the two states. As plumes above  $H_c$  encounter terrain and are deflected vertically, there is also a tendency for plume material to approach the terrain surface and to spread out around the sides of the terrain. To simulate this the estimated concentration is constrained to always contain a component from the horizontal state. Therefore, under no conditions is the plume allowed to completely approach the terrain-following state. For flat terrain, the contributions from the two states are equal, and are equally weighted.

Figure 11 illustrates how the weighting factor is constructed and its relationship to the estimate of concentration as a weighted sum of two limiting plume states.

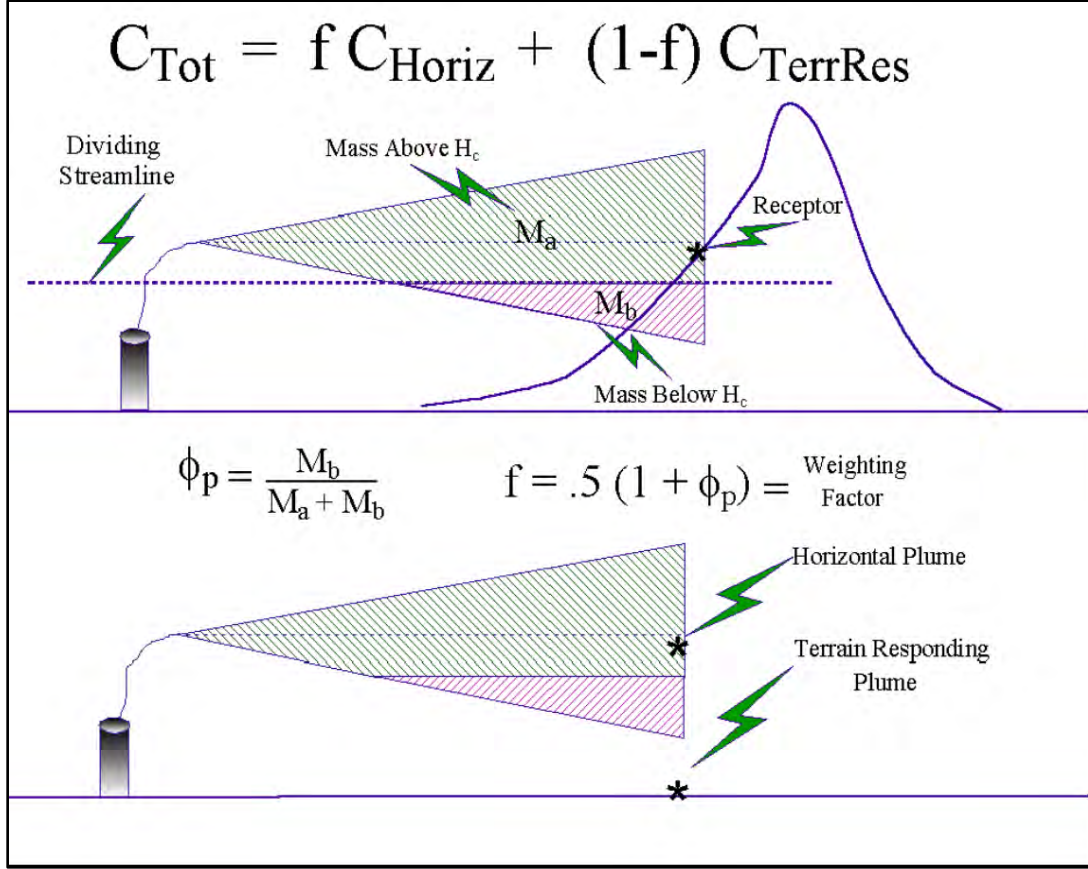


Figure 11. Treatment of Terrain in AERMOD. Construction of the weighting factor used in calculating total concentration

The general form of the expressions for concentration in each term of eq. (48) for both the CBL and the SBL can be written as follows:

$$C\{x, y, z\} = (Q/\tilde{u}) P_y\{y; x\} P_z\{z; x\}, \quad (51)$$

where  $Q$  is the source emission rate,  $\tilde{u}$  is the effective wind speed, and  $p_y$  and  $p_z$  are probability density functions (pdf) which describe the lateral and vertical concentration distributions, respectively. AERMOD assumes a traditional Gaussian pdf for both the lateral and vertical distributions in the SBL and for the lateral distribution in the CBL. The CBL's vertical distribution of plume material reflects the distinctly non-Gaussian nature of the vertical velocity distribution in convectively mixed layers. The specific form for the concentration distribution in the CBL is found in eq. (54) which uses the notation  $C_c\{x_r, y_r, z_r\}$ . Similarly, in the SBL, the

concentration takes the form of eq. (67) and used the notation  $C_s \{x_r, y_r, z_r\}$ .

AERMOD simulates five different plume types depending on the atmospheric stability and on the location in and above the boundary layer: 1) direct, 2) indirect, 3) penetrated, 4) injected and 5) stable. All of these plumes will be discussed, in detail, throughout the remainder of this document. During stable conditions, plumes are modeled with the familiar horizontal and vertical Gaussian formulations. During convective conditions ( $L < 0$ ), the horizontal distribution is still Gaussian; the vertical concentration distribution results from a combination of three plume types: 1) the direct plume material within the mixed layer that initially does not interact with the mixed layer lid; 2) the indirect plume material within the mixed layer that rises up and tends to initially loft near the mixed layer top; and 3) the penetrated plume material that is released in the mixed layer but, due to its buoyancy, penetrates into the elevated stable layer.

During convective conditions, AERMOD also handles a special case referred to as an injected source where the stack top (or release height) is greater than the mixing height. Injected sources are modeled as plumes in stable conditions, however the influence of the turbulence and the winds within the mixed layer are considered in the inhomogeneity calculations as the plume material passes through the mixed layer to reach receptors.

As described above, AERMOD accounts for the vertical variation of meteorology through the use of effective values of wind speed, turbulence, and the Lagrangian time scale. Being a steady state plume model, AERMOD uses a single value of each meteorological variable to represent the state of the dispersive layer for each modeling period (typically one hour). Specifically, the effective parameters are determined by averaging values from the meteorological profile within the layer between the plume's center of mass and the receptor. Effective variables or parameters are denoted by an overbar tilde (e.g.,  $\tilde{u}$ ).

## **5.2 Concentration predictions in the CBL**

In AERMOD, the dispersion formulation for the convective boundary layer (CBL) represents one of the more significant model advances by comparison with existing regulatory models. One assumes that plume sections are emitted into a traveling train of convective

elements - updrafts and downdrafts - that move with the mean wind. The vertical and lateral velocities in each element are assumed to be random variables and characterized by their probability density functions (pdf). The mean concentration is found from the pdf of the position of source-emitted “particles”; this position pdf in turn is derived from the pdf of the lateral and vertical velocities as described by Weil et al. (1997); also see Misra (1982), Venkatram (1983), and Weil (1988a).

In the CBL, the pdf of the vertical velocity ( $w$ ) is positively skewed and results in a non-Gaussian vertical concentration distribution,  $F_z$  (Lamb 1982). The positive skewness is consistent with the higher frequency of occurrence of downdrafts than updrafts; for an elevated non-buoyant source the skewness also leads to the decent of the plume centerline, as defined by the locus of maximum concentration (Lamb 1982; Weil 1988a). Figure 12 presents a schematic representation of an instantaneous plume in a convective boundary layer and its corresponding ensemble average. The base concentration prediction in AERMOD is representative of a one-hour average. Notice that since a larger percentage of the instantaneous plume is affected by downdrafts, the ensemble average has a general downward trend. Since downdrafts are more prevalent the average velocity of the downdrafts is correspondingly weaker than the average updraft velocity to ensure that mass is conserved. In AERMOD, a skewed vertical velocity pdf is modeled using a bi-Gaussian distribution, which has been shown to be a good approximation to laboratory convection tank data (Baerentsen and Berkowicz 1984). In contrast to the vertical component, the lateral velocity pdf is approximately Gaussian (Lamb 1982), and this pdf and the resulting concentration distribution,  $F_y$ , are assumed to be Gaussian.

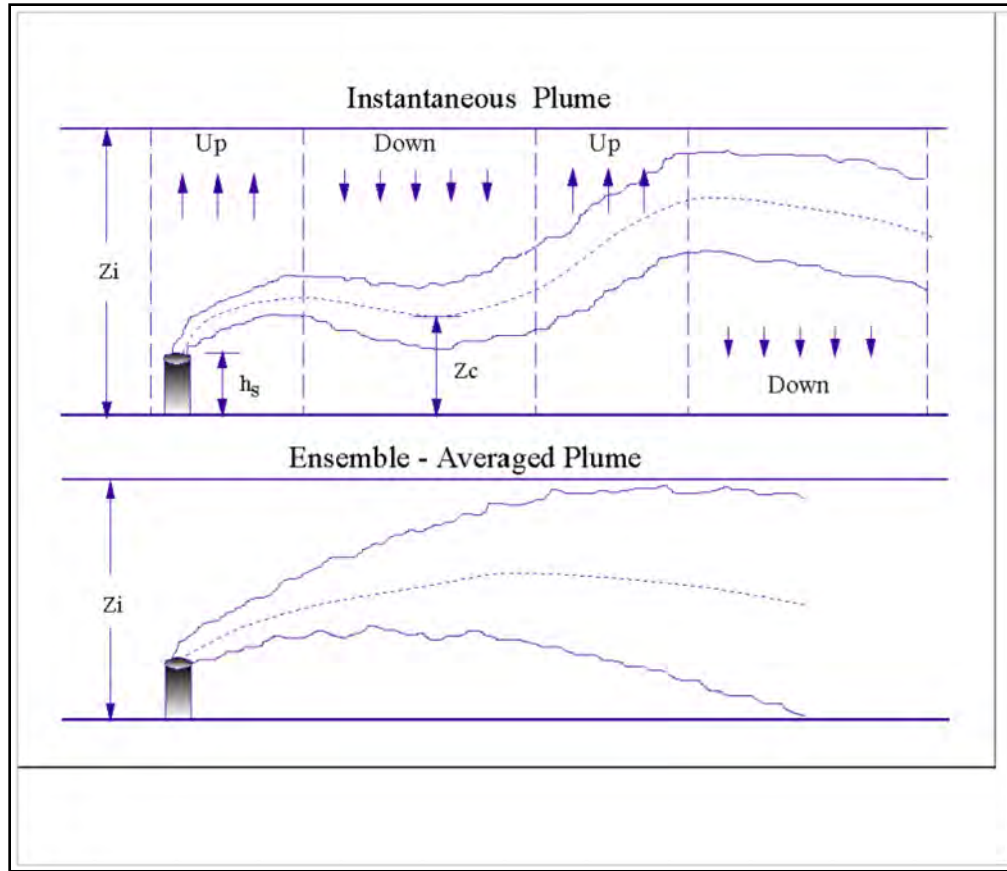


Figure 12. Instantaneous and corresponding ensemble-averaged plume in the CBL

In addition to the non-Gaussian  $F_z$ , AERMOD has the following features. For buoyant releases, there is no “final” plume rise assumed. Instead, the plume or particle trajectories are determined by the addition of a distance-dependent plume rise and the random vertical displacement caused by the vertical distribution of  $w$ . Ground level concentrations first appear when the negative or downdraft velocities are sufficiently large to overcome the plume rise velocity and carry plume sections to the surface. The direct transport of plume material to the ground is treated by the “direct” source located at the stack. That is, the direct source treats that portion of the plume’s mass to first reach the ground, and all subsequent reflections of the mass at  $z = z_i$  and 0 (where  $z_i$  is the mixed layer height in the CBL (Cimorelli et al., 2004)). For plume segments or particles initially rising in updrafts, an “indirect” or modified-image source is included (above the mixed layer) to address the initial quasi-reflection of plume material at  $z = z_i$ , i.e., for material that does not penetrate the elevated inversion. This source is labeled “indirect” because it is not a true image source (i.e., as is found in models such as ISC) - the plume is not

perfectly reflected about  $z_i$ . Thus, the indirect source treats that portion of the plume's mass that first reaches  $z_i$  and all subsequent reflections of that particular mass at  $z = 0$  and  $z_i$ . For the indirect source, a plume rise ( $\Delta h_i$ ) is added to delay the downward dispersion of material from the CBL top (see Figure 13); this mimics the plume's lofting behavior, i.e., the tendency of buoyant plumes to remain temporarily near  $z_i$  and resist downward mixing. For non-buoyant sources the indirect source reduces to the first image source (as found in ISCST3) resulting from the first reflection at  $z = z_i$ . Additionally, a "penetrated" source or plume (above the CBL top) is included to account for material that initially penetrates the elevated inversion but is subsequently reentrained by and disperses in the growing CBL.

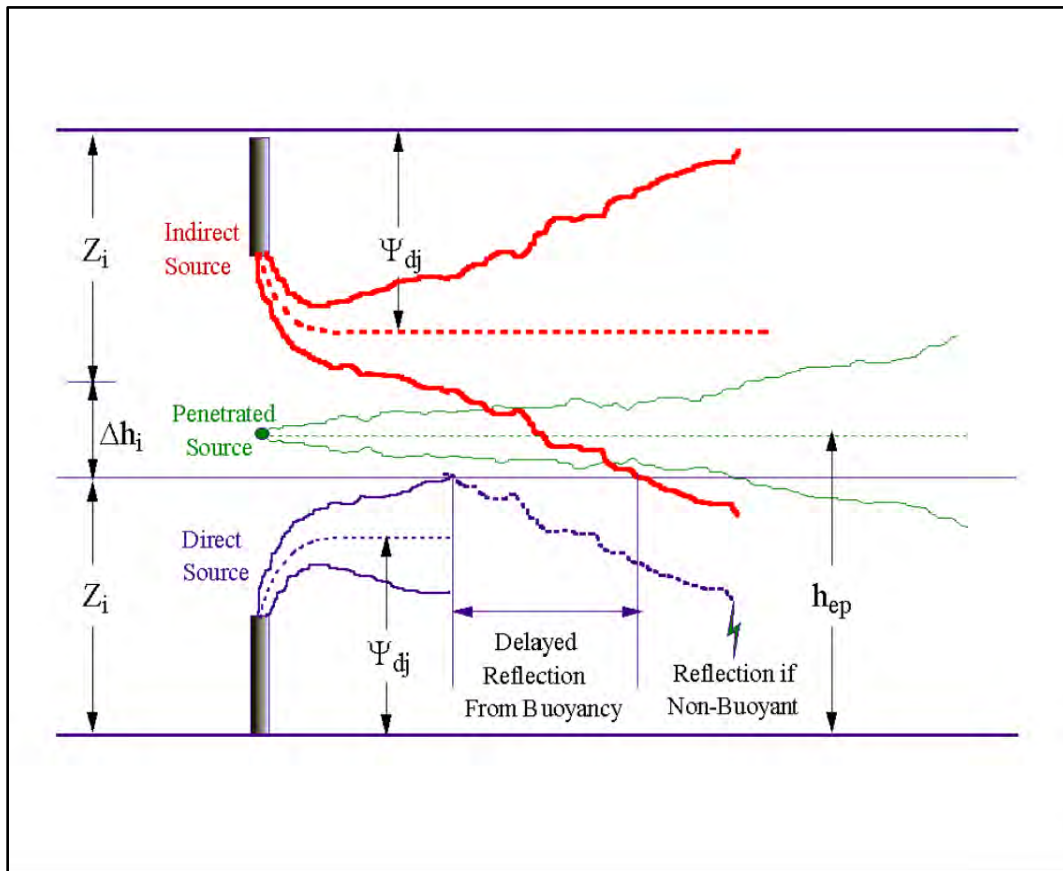


Figure 13. AERMOD's three plume treatment of the CBL

In line with the above concepts there are three main mathematical sources that contribute to the modeled concentration field: 1) the direct source (at the stack), 2) the indirect source, and 3) the penetrated source. The strength of the direct source is  $f_p Q$ , where  $Q$  is the source emission

rate and  $f_p$  is the calculated fraction of the plume mass trapped in the CBL ( $0 \leq f_p \leq 1$ ). Likewise, the indirect source strength is  $f_p Q$  since this (modified image) source is included to satisfy the no-flux boundary condition at  $z = z_i$  for the trapped material. The strength of the penetrated source is  $(1 - f_p)Q$ , which is the fraction of the source emission that initially penetrates into the elevated stable layer. In addition to the three main sources, other image sources are included to satisfy the no-flux conditions at  $z = 0$  and  $z_i$ .

For material dispersing within a convective layer, the conceptual picture (see Figure 12) is a plume embedded within a field of updrafts and downdrafts that are sufficiently large to displace the plume section within it. The relationship between the particle (or air parcel) height,  $z_c$  and  $w$  is found by superposing the plume rise ( $\Delta h$ ) and the vertical displacement due to  $w$  (i.e.,  $wx/u$ ), as

$$z_c = h_s + \Delta h + \frac{wx}{u}, \quad (52)$$

where  $h_s$  is the stack height (corrected for stack tip downwash),  $u$  is the mean wind speed (a vertical average over the convective boundary layer) and  $x$  is the downwind distance. The  $\Delta h$  above includes source momentum and buoyancy effects as given by eq. (91) below (see Briggs (1984)). The  $F_z$  or pdf of  $z_c$  is found from the vertical velocity pdf  $p_w$  as described in Weil et al. (1997). In the CBL a good approximation to  $p_w$  is the superposition of two Gaussian distributions (Baerentsen and Berkowicz 1984; Weil 1988a) such that

$$p_w = \frac{\lambda_1}{\sqrt{2\pi}\sigma_{w1}} \exp\left(-\frac{(w - \overline{w_1})^2}{2\sigma_{w1}^2}\right) + \frac{\lambda_2}{\sqrt{2\pi}\sigma_{w2}} \exp\left(-\frac{(w - \overline{w_2})^2}{2\sigma_{w2}^2}\right), \quad (53)$$

where  $\lambda_1$  and  $\lambda_2$  are weighting coefficients for the two distributions with  $\lambda_1 + \lambda_2 = 1$  (the subscripts 1 and 2 refer to the updraft and downdraft distributions, respectively). The parameters of the pdf ( $w_1, w_2, \sigma_{w1}, \sigma_{w2}, \lambda_1, \lambda_2$ ) are functions of  $\sigma_w$  (the “total” or overall root mean square vertical turbulent velocity), the vertical velocity skewness  $S = \overline{w^3}/\sigma_w^3$  (where  $\overline{w^3}$  is the third moment of

$w$ ), and a parameter  $R = \sigma_{w1}/\overline{w_1} = -\sigma_{w2}/\overline{w_2} = 2$ . An expanded discussion of the pdf parameters is given in Weil et al. (1997).

The instantaneous plume is assumed to have a Gaussian concentration distribution about its randomly varying centerline. The mean or average concentration is found by summing the concentrations due to all of the random centerline displacements. This averaging process results in a skewed distribution which AERMOD represents as a bi-Gaussian pdf (i.e., one for updrafts and the other for downdrafts). Figure 14 illustrates the bi-Gaussian approach to approximate the skewed vertical concentration distribution in the CBL. The figure shows two mean trajectories, each representing the average of many individual trajectories of parcels (or particles) released into downdrafts (the downdraft plume) or updrafts (the updraft plume). The velocities determining these mean trajectories are: 1) the mean horizontal wind speed ( $u$ ), 2) the vertical velocity due to plume buoyancy ( $v_{buoy}$ ), and 3) the mean updraft ( $\overline{w_1}$ ) or downdraft ( $\overline{w_2}$ ) velocity. The mean height of each trajectory,  $\overline{z_{c1}}$  or  $\overline{z_{c2}}$ , can be found by averaging eq. (53). These parcel (or particle) height distributions are thus related to concentration and are characterized by  $\sigma_{z1}$  ( $= \sigma_{w1}x/u$ ) and  $\sigma_{z2}$  ( $= \sigma_{w2}x/u$ ), the standard deviations of the two concentration distributions comprising the bi-Gaussian form as derived in Weil et al. (1997).

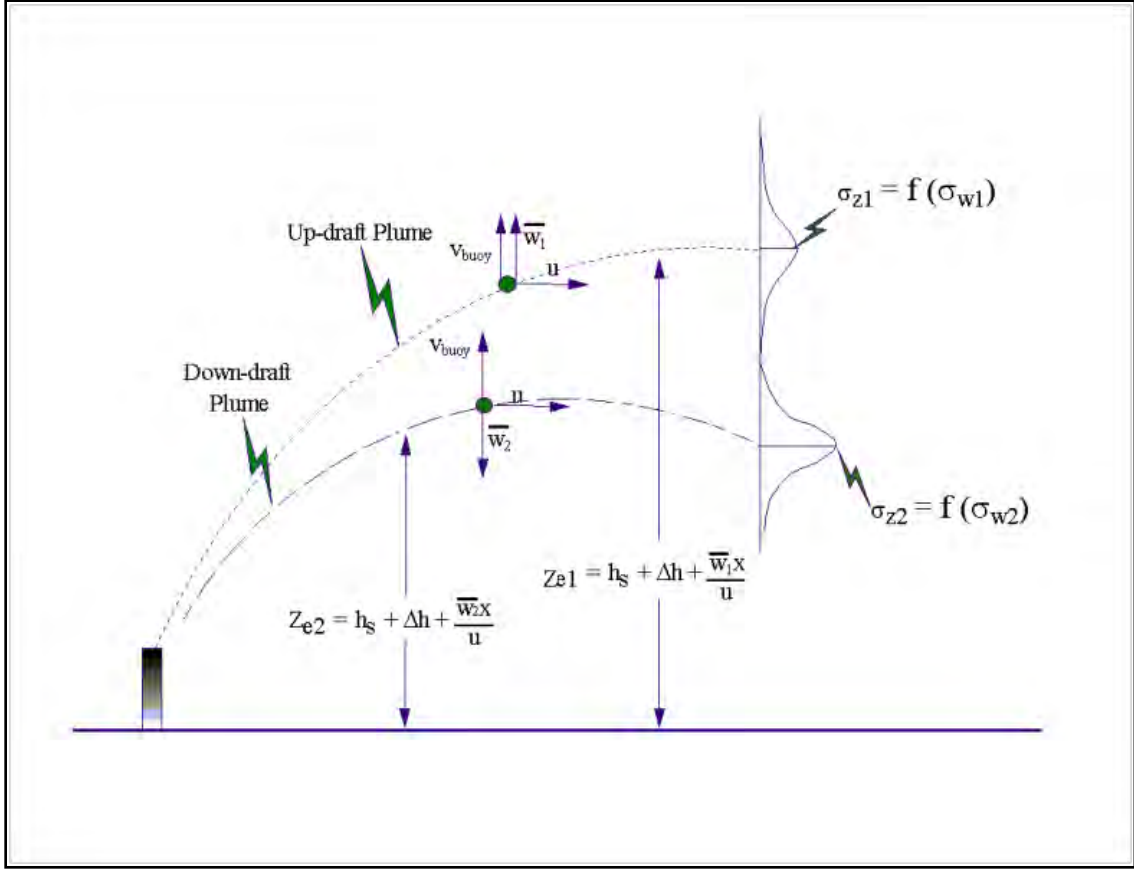


Figure 14. AERMOD's pdf approach for plume dispersion in the CBL. AERMOD approximates the skewed distribution by superimposing two Gaussian distributions, the updraft and downdraft distributions

Figure 15 compares the bi-Gaussian pdf with the Gaussian form, which is symmetric about  $w = 0$ . As can be seen, for the negative and positive tails of the distributions, the bi-Gaussian pdf is biased towards smaller and larger  $p_w$  values, respectively, than the Gaussian. In addition, for the bi-Gaussian forms, approximately 60% of the area under the  $p_w$  curve is on the negative side of the  $w$  axis and approximately 40% on the positive side. This is consistent with the results of numerical simulations and field observations (Lamb 1982; Weil 1988a).

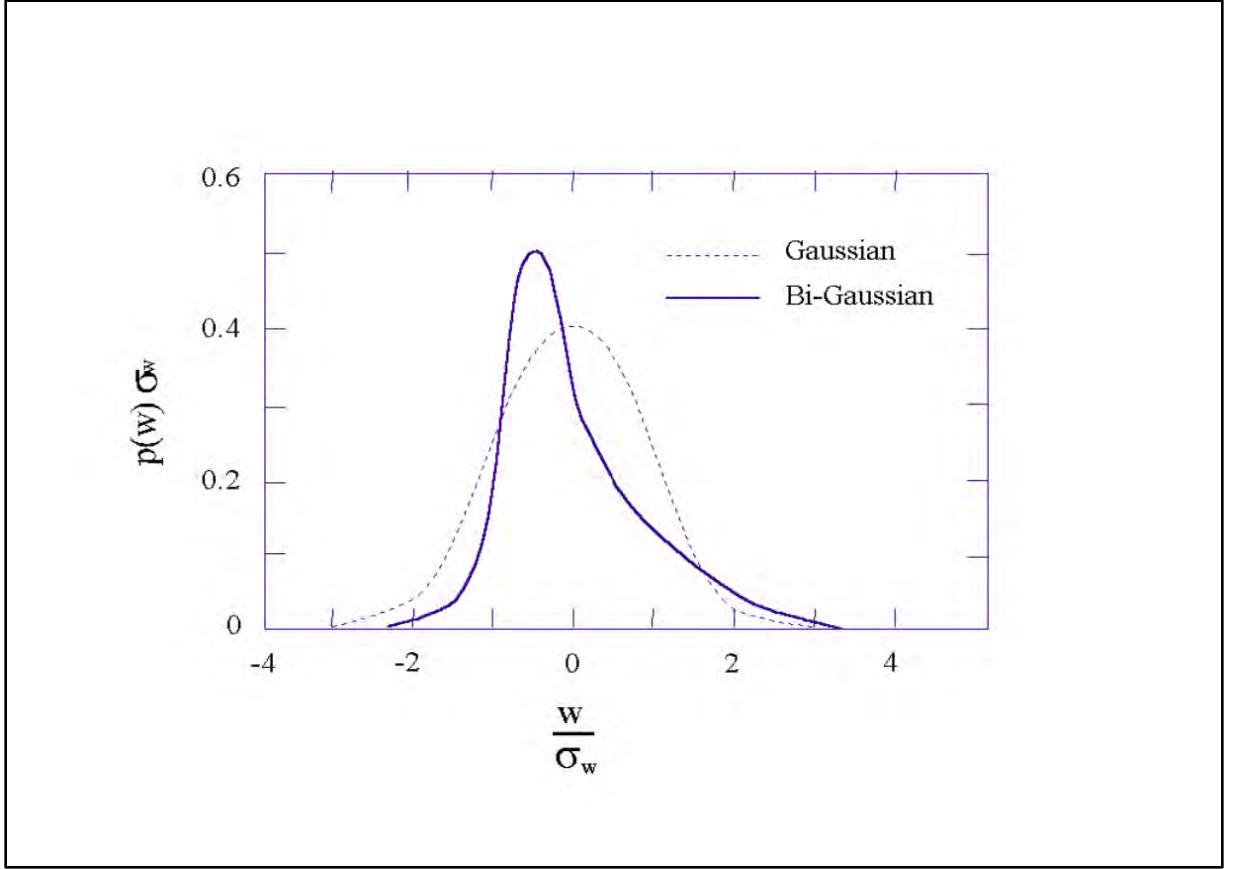


Figure 15. Probability density function of the vertical velocity. While the Gaussian curve is unskewed, the bi-Gaussian curve has a skewness of  $S=1$

In the pdf approach used here (Weil et al. 1997), there are, as mentioned in the previous section, three primary sources that contribute to the modeled concentration field: 1) the “direct” or real source at the stack, 2) an “indirect” source that the model locates above the CBL top to account for the slow downward dispersion of buoyant plumes that “loft” or remain near, but below,  $z_i$ , and 3) a “penetrated source” that contains the portion of plume material that has penetrated into the stable layer above  $z_i$ . The direct source describes the dispersion of plume material that reaches the ground directly from the source via downdrafts. The indirect source is included to treat the first interaction of the “updraft” plume with the elevated inversion - that is, for plume sections that initially rise to the CBL top in updrafts and return to the ground via downdrafts. Image sources are added to treat the subsequent plume interactions with the ground and inversion and to satisfy the zero-flux conditions at  $z = 0$  and at  $z = z_i$ . This source plays the same role as the first image source above  $z_i$  in the standard Gaussian model, but differs in the treatment of plume buoyancy. For the indirect source, a modified reflection approach is adopted

in which the vertical velocity is reflected at  $z = z_i$ , but an “indirect” source plume rise  $\Delta h_i$  is added to delay the downward dispersion of plume material from the CBL top. This is intended to mimic the lofting behavior. The penetrated source is included to account for material that initially penetrates the elevated inversion but subsequently can reenter the CBL via turbulent mixing of the plume and eventual reentrainment into the CBL. Figure 13 illustrates this three plume approach; a fundamental feature of AERMOD’s convective model. In AERMOD, the total concentration ( $C_c$ ) in the CBL is found by summing the contribution from the three sources. For the horizontal plume state, the  $C_c$  is given by

$$C_c\{x_r, y_r, z_r\} = C_d\{x_r, y_r, z_r\} + C_r\{x_r, y_r, z_r\} + C_p\{x_r, y_r, z_r\}, \quad (54)$$

where  $C_d$ ,  $C_r$ , and  $C_p$  are the contributions from the direct, indirect and penetrated sources, respectively. The total concentration for the terrain-following state has the form of eq. (54) but with  $z_r$  replaced by  $z_p$ .

The fraction  $f_p$  of the source material that remains trapped in the CBL is found from

$$\begin{aligned} f_p &= 0 & \text{if } \Delta h_h < 0.5\Delta h_{eq} \\ f_p &= 1 & \text{if } \Delta h_h > 1.5\Delta h_{eq} \\ f_p &= \frac{\Delta h_h}{\Delta h_{eq}} - 0.5 & \text{if } 0.5\Delta h_{eq} < \Delta h_h < 1.5\Delta h_{eq}. \end{aligned} \quad (55)$$

where  $\Delta h_h = z_i - h_s$ , and  $\Delta h_{eq}$  is the equilibrium plume rise in a stable environment. The  $\Delta h_{eq}$  has the form Berkowicz et al. (1986)

$$\Delta h_{eq} = \left( 2.6^3 P_s + (2/3)^3 \right)^{1/3} \Delta h_h \quad (56)$$

where  $P_s = F_b / u N_h^2 \Delta h_h^3$  is the penetration parameter, and the stack buoyancy flux ( $F_b$ ), and Brunt-Vaisala frequency ( $N_h$ ) are given respectively by

$$F_b = g w_s r_s^2 \frac{\Delta T}{T_s} \quad (57)$$

and

$$N_h = \left[ \frac{g}{\theta\{z_i\}} \frac{\partial \theta}{\partial z} \Big|_{z > z_i} \right]^{1/2}. \quad (58)$$

Here,  $u$  is the wind speed at stack height;  $g$  is the gravitational acceleration;  $w_s$ ,  $r_s$ , and  $T_s$  are the stack exit velocity, radius, and temperature, respectively; and  $\theta$  is the ambient potential temperature. The  $N_h$  in eq. (58) is based on the potential temperature gradient in the elevated stable layer, provided by AERMET, capping the CBL. In general, this layer is within  $z_i$  and  $z_i + 500$  m.

### 5.2.1 Direct Source contribution to concentration calculations in the CBL

Following Weil et al. (1997), the concentration due to the direct plume is given by:

$$C_d\{x_r, y_r, z\} = \frac{Q f_p}{\sqrt{2\pi} \tilde{u}} F_y \cdot \sum_{j=1}^2 \sum_{m=0}^{\infty} \frac{\lambda_j}{\sigma_{zj}} \left[ \exp\left(-\frac{(z - \Psi_{dj} - 2mz_i)^2}{2\sigma_{zj}^2}\right) + \exp\left(-\frac{(z + \Psi_{dj} + 2mz_i)^2}{2\sigma_{zj}^2}\right) \right], \quad (59)$$

where

$$\Psi_{dj} = h_s + \Delta h_d + \frac{\overline{w}_j x}{u}, \quad (60)$$

$u$  is the wind speed at stack top,  $F_y \left( = \frac{1}{\sqrt{2\pi}\sigma_y} \exp\left(\frac{-y^2}{2\sigma_y^2}\right) \right)$  the lateral distribution function with meander (discussed in Section 5.4),  $\overline{w}_j = a_j w_*$  ( $a_j$  is defined below in eq. (62)),  $\Delta h_d$  is the direct source plume rise calculated from eq. (91), and  $z = z_r$  and  $z_p$  in the horizontal and terrain-following states, respectively. Here,  $\Psi_{dj}$  and  $\sigma_{zj}$  are the effective source height and vertical

dispersion parameter corresponding to each of the two distributions in eq. (53). The subscript  $j$  is equal to 1 for updrafts and 2 for downdrafts. The lateral and vertical dispersion parameters ( $\sigma_y$  and  $\sigma_{zj}$ ), resulting from the combined effects of ambient, buoyancy-induced, and building-induced turbulence are calculated as discussed in Sections 5.5.1.1 and 5.5.1.2 respectively. Here,  $\sigma_{zj}$  (with  $j = 1$  or  $2$ ) is the vertical dispersion parameter corresponding to each of the Gaussian distributions used in the bi-Gaussian pdf, (see Section 5.5.1.2) and  $\lambda_j$ , the weighting coefficient for each distribution in eq.(53), is calculated from Weil et al. (1997) as

$$\begin{aligned}\lambda_1 &= +\frac{\bar{w}_2}{\bar{w}_2 - \bar{w}_1} = +\frac{a_2}{a_2 - a_1} \\ \lambda_2 &= -\frac{\bar{w}_1}{\bar{w}_2 - \bar{w}_1} = -\frac{a_1}{a_2 - a_1}\end{aligned}\tag{61}$$

where

$$\begin{aligned}a_1 &= \frac{\tilde{\sigma}_{wT}}{w_*} \left( \frac{\alpha S}{2} + \frac{1}{2} \left( \alpha^2 S^2 + \frac{4}{\beta} \right)^{1/2} \right) \\ a_2 &= \frac{\tilde{\sigma}_{wT}}{w_*} \left( \frac{\alpha S}{2} - \frac{1}{2} \left( \alpha^2 S^2 + \frac{4}{\beta} \right)^{1/2} \right)\end{aligned}\tag{62}$$

Recall that  $\tilde{\sigma}_{wT}$  is the total effective vertical turbulence and is calculated from eq. (34).

The parameters appearing in eq. (62) are given by

$$\begin{aligned}\frac{\bar{w}^3}{w_*^3} &= 0.125 & \text{for } H_p\{x\} \geq 0.1 z_i \\ \frac{\bar{w}^3}{w_*^3} &= 1.25 \frac{H_p\{x\}}{z_i} & \text{for } H_p\{x\} < 0.1 z_i\end{aligned}\tag{63}$$

where,

$$\begin{aligned}
\alpha &= \frac{1 + R^2}{1 + 3R^2} \\
\beta &= 1 + R^2 \\
S &= \frac{\bar{w}^3 / w_*^3}{(\tilde{\sigma}_{wT} / w_*)^3} \equiv \text{Skewness factor},
\end{aligned} \tag{64}$$

and  $R$  is assumed to be 2.0 (Weil et al., 1997). Likewise, the term  $\bar{w}_j x/u$  in eq. (60) follows from the  $F_z$  derivation and the  $w_j$  appearing in the bi-Gaussian form (see discussion of eq. (53)). The lateral dispersion parameter ( $\sigma_{y,}$ ) is calculated from eq. (75) (Weil et al., 1997).

In eq. (59), an image plume is used to satisfy the no-flux condition at the ground, i.e., an image plume from a source at  $z = -h_s$ , which results in the exponential terms containing  $z + \Psi_{dj}$  on the right-hand side of eq. (59). This image source results in a positive flux of material at  $z = z_i$ , and additional image sources are introduced at  $z = 2z_i + h_s, -2z_i - h_s, 4z_i + h_s, -4z_i - h_s$ , etc. to satisfy all the subsequent no-flux conditions occurring at  $z = 0$  and  $z_i$ .

### 5.2.2 Indirect Source contribution to concentration calculations in the CBL

The concentration due to the indirect source is calculated from:

$$C_r\{x_r, y_r, z\} = \frac{Qf_p}{\sqrt{2\pi}\tilde{u}} \cdot F_y \cdot \sum_{j=1}^2 \sum_{m=1}^{\infty} \frac{\lambda_j}{\sigma_{zj}} \left[ \exp\left(-\frac{(z + \Psi_{rj} - 2mz_i)^2}{2\sigma_{zj}^2}\right) + \exp\left(-\frac{(z - \Psi_{rj} + 2mz_i)^2}{2\sigma_{zj}^2}\right) \right], \tag{65}$$

where  $\Psi_{rj} = \Psi_{dj} - \Delta h_i$ , and  $z$  is either  $z_r$  (for the horizontal plume state) or  $z_p$  (for the terrain-following state). As shown in Figure 13, the indirect plume is modeled as a reflected version of the direct plume with an adjustment ( $\Delta h_i$  - calculated from eq. (92)) to the reflected plume height to account for the delay in vertical mixing due to plume lofting at the top of the boundary layer.

### 5.2.3 Penetrated source contribution to concentration calculations in the CBL

For the penetrated source the concentration expression has a Gaussian form in both the vertical and lateral directions. The concentration due to this source is given by:

$$C_p\{x_r, y_r, z\} = \frac{Q(1-f_p)}{\sqrt{2\pi}\tilde{u}\sigma_{zp}} F_y \cdot \sum_{m=-\infty}^{\infty} \left[ \exp\left(-\frac{(z-h_{ep}+2mz_{ieff})^2}{2\sigma_{zp}^2}\right) + \exp\left(-\frac{(z+h_{ep}+2mz_{ieff})^2}{2\sigma_{zp}^2}\right) \right] \quad (6)$$

where  $z_{ieff}$  is the height of the upper reflecting surface in a stable layer (see Section 5.3) and  $z$  is either  $z_r$  for the horizontal plume state or  $z_p$  for the terrain-following state. The vertical dispersion parameters ( $\sigma_{zp}$ ) are calculated as described in Section 5.5.1.2.

The penetrated plume height,  $h_{ep}$ , is taken as the height of the plume centroid above the mixed layer and is calculated from eq. (94).

### 5.3 Concentrations in the SBL

For stable conditions, the AERMOD concentration expression ( $C_s$  in eq. (48)) has the Gaussian form, and is similar to that used in many other steady-state plume models (e.g., HPDM (Hanna and Paine 1989)). The  $C_s$  is given by

$$C_s\{x_r, y_r, z\} = \frac{Q}{\sqrt{2\pi}\tilde{u}\sigma_{zs}} \cdot F_y \cdot \sum_{m=-\infty}^{\infty} \left[ \exp\left(-\frac{(z-h_{es}-2mz_{ieff})^2}{2\sigma_{zs}^2}\right) + \exp\left(-\frac{(z+h_{es}+2mz_{ieff})^2}{2\sigma_{zs}^2}\right) \right], \quad (67)$$

where  $z_{ieff}$  is the effective mechanical mixed layer height,  $\sigma_{zs}$  is the total vertical dispersion in the SBL (see discussion in Section 5.5), and  $h_{es}$  is the plume height (i.e., stack height plus the plume rise - see Section 5.6.2).

Above the mechanical mixed layer height,  $z_{im}$  (eq. (26)), the turbulence level is generally expected to be small and thus supports little vertical mixing of the plume. AERMOD is

designed (in the SBL) with an effective mixing lid,  $z_{ieff}$ , that retards but does not prevent plume material from spreading into the region above the estimated mechanical mixed layer. When the final plume height is well below  $z_{im}$ , the plume does not interact with  $z_{im}$ . When the plume is below  $z_{im}$  yet the “upper edge” (plume height plus  $2.15 \sigma_{zs}$ ) of the stabilized plume reaches  $z_{im}$ , the effective mixing lid is allowed to increase and remain at a level near the upper edge of the plume. In this way, AERMOD allows the plume to disperse downwards, but where the turbulence aloft is low, vertical plume growth is limited by an effective reflecting surface that is folding back only the extreme tail of the vertical plume distribution. There is no strong concentration doubling effect as occurs with reflections from an assumed hard lid. Downward dispersion is primarily a factor of  $\sigma_w$  averaged from the receptor to the plume height. If the plume height is above the mixed layer height, the calculation of the effective  $\sigma_w$  will include regions in which  $\sigma_w$  is likely to be small. This, in effect, retards plume growth by an amount dependent upon how much of the plume is above  $z_{im}$ . Therefore, whether the plume is above or below  $z_{im}$ , the region of low turbulence above  $z_{im}$  will have an appropriate effect on the concentration distribution within the mixing layer.

When the plume buoyancy carries the rising plume into the relatively non-turbulent layer above  $z_{im}$ , the reflecting surface is still placed at  $2.15 \sigma_{zs}$  above the effective plume height because there will be plume spread due to plume buoyancy and downward mixing is still important. Therefore, in the SBL, plume material is assumed to reflect off an elevated surface which is defined as:

$$z_{ieff} = MAX[(h_{es} + 2.15\sigma_{zs}\{h_{es}\}; z_{im})]. \quad (68)$$

where  $\sigma_{zs}$  in eq. (68) is determined from equations found in Section 5.5.1.2 with  $\sigma_{wT}$  and  $u$  evaluated at  $h_{es}$ ; not as an effective parameter. It is important to note that  $z_{ieff}$  depends on downwind distance since  $\sigma_{zs}$  is distance dependent. In fact, as eq. (68) suggests, this effective reflecting surface is only folding back the extreme tail of the upward distribution. Also, if the height of the receptor  $z_r \geq z_{ieff}$  then the effective reflecting surface is not considered. This approach is also implemented for the penetrated source. For the penetrated and injected sources  $z_{ieff}$  is calculated using eq. (68) with  $\sigma_{zs}$  and  $h_{es}$  replaced by  $\sigma_{zp}$  and  $h_{ep}$  respectively.

## 5.4 Treatment of lateral plume meander

In AERMOD we include the effect that lower-frequency, non-diffusing eddies (i.e., meander) have on plume concentration. Meander (or the slow lateral back and forth shifting of the plume) decreases the likelihood of seeing a coherent plume after long travel times. This effect on plume concentration could best be modeled with a particle trajectory model, since these models estimate the concentration at a receptor by counting the number of times a particle is seen in the receptor volume. However, as a simple steady state model, AERMOD is not capable of producing such information. AERMOD accounts for meander by interpolating between two concentration limits: the coherent plume limit (which assumes that the wind direction is distributed about a well-defined mean direction with variations due solely to lateral turbulence) and the random plume limit, (which assumes an equal probability of any wind direction).

For the coherent plume, the horizontal distribution function ( $F_{yC}$ ) has the familiar Gaussian form:

$$F_{yC} = \frac{1}{\sqrt{2\pi}\sigma_y} \exp\left(\frac{-y^2}{2\sigma_y^2}\right) \quad (69)$$

where  $\sigma_y$  is the lateral dispersion parameter (see Section 5.5). For the random plume limit, the wind direction (and plume material) is uniformly distributed through an angle of  $2\pi$ . Therefore, the horizontal distribution function  $F_{yR}$  takes the simple form:

$$F_{yR} = \frac{1}{2\pi x_r} \quad (70)$$

where  $x_r$  is radial distance to the receptor. Although the form of the vertical distribution function remains unchanged for the two plumes, its magnitude is based on downwind distance for the coherent plume and radial distance for the random plume.

Once the two concentration limits ( $C_{Ch}$  - coherent plume;  $C_R$  - random plume) have been calculated, the total concentration for stable or convective conditions ( $C_{c,s}$ ) is determined by interpolation. Interpolation between the coherent and random plume concentrations is accomplished by assuming that the total horizontal “energy” is distributed between the wind’s mean and turbulent components. That is,

$$C_{c,s} = C_{Ch} \left(1 - \sigma_r^2 / \sigma_h^2\right) + C_R \left(\sigma_r^2 / \sigma_h^2\right) \quad (71)$$

where  $\sigma_h^2$  is a measure of the total horizontal wind energy and  $\sigma_r^2$  is a measure of the random component of the wind energy. Therefore, the ratio  $\sigma_r^2 / \sigma_h^2$  is an indicator of the importance of the random component and can therefore be used to weight the two concentrations as done in eq. (71).

The horizontal wind is composed of a mean component  $\bar{u}$ , and random components  $\sigma_u$  and  $\sigma_v$ . Thus, a measure of the total horizontal wind “energy” (given that the alongwind and crosswind fluctuations are assumed equal i.e.,  $\sigma_u = \sigma_v$ ), can be represented as

$$\sigma_h^2 = 2\tilde{\sigma}_v^2 + \bar{u}^2 \quad (72)$$

where  $\bar{u} = (\tilde{u}^2 - 2\tilde{\sigma}_v^2)^{1/2}$ . The random energy component is initially  $2\tilde{\sigma}_v^2$  and becomes equal to  $\sigma_h^2$  at large travel times from the source when information on the mean wind at the source becomes irrelevant to the predictions of the plume’s position. The evolution of the random component of the horizontal wind energy can be expressed as

$$\sigma_r^2 = 2\tilde{\sigma}_v^2 + \bar{u}^2 \left(1 - \exp\left(-x_r / \tilde{u}T_r\right)\right) \quad (73)$$

where  $T_r$  is a time scale (= 24 hrs) at which mean wind information at the source is no longer correlated with the location of plume material at a downwind receptor. Analyses involving autocorrelation of wind statistics (Brett and Tuller 1991) suggest that after a period of approximately one complete diurnal cycle, plume transport is “randomized.” Equation (73)

shows that at small travel times,  $\sigma_r^2 = 2\tilde{\sigma}_v^2$ , while at large times (or distances)  $\sigma_r^2 = 2\tilde{\sigma}_v^2 + \bar{u}^2$ , which is the total horizontal kinetic energy ( $\sigma_h^2$ ) of the fluid. Therefore, the relative contributions of the coherent and random horizontal distribution functions (eq. (71)) are based on the fraction of random energy contained in the system (i.e.,  $\sigma_r^2/\sigma_h^2$ ).

The application of eq. (71) is relatively straight forward in the SBL. Since concentrations in the SBL are represented as a single plume,  $C_s$  can be calculated directly from eq. (71). By contrast, for convective conditions the situation is complicated by the inclusion of plume penetration. Since  $\sigma_r^2$  depends on the effective parameters (eq. (73)), the concentration weighting factors found in eq. (71) will be different for the non-penetrated and penetrated plumes of the CBL. This is handled by combining the penetrated and non-penetrated weighting factors ( $\sigma_r^2/\sigma_h^2|_P$  and  $\sigma_r^2/\sigma_h^2|_{NP}$ ) into a single effective factor ( $\sigma_r^2/\sigma_h^2|_{CBL}$ ). That is,

$$\left. \frac{\sigma_r^2}{\sigma_h^2} \right|_{CBL} = f_p \cdot \left. \frac{\sigma_r^2}{\sigma_h^2} \right|_P + (1 - f_p) \cdot \left. \frac{\sigma_r^2}{\sigma_h^2} \right|_{NP} \quad (74)$$

where  $f_p$  (see eq. (55)) is the fraction of the source material that remains trapped in the CBL. Using eq. (74), concentrations in the CBL ( $C_c$ ) are calculated from eq. (71) with  $(\sigma_r^2/\sigma_h^2)$  replaced by  $(\sigma_r^2/\sigma_h^2|_{CBL})$ .

## 5.5 Estimation of dispersion coefficients

The overall standard deviations ( $\sigma_{y,z}$ ) of the lateral and vertical concentration distributions are a combination of the dispersion (represented by  $\sigma_{ya}$ ,  $\sigma_{za}$ ) resulting from ambient turbulence, and dispersion ( $\sigma_b$ ) from turbulence induced by plume buoyancy. Building induced dispersion is not included here since a separate approach (see Section 5.5.3) is taken for situations in which building wake effects contribute to the total dispersion. Dispersion induced by ambient turbulence is known to vary significantly with height, having its strongest variation near the earth's surface. Unlike present regulatory models, AERMOD has been designed to account for the effect of variations of turbulence with height on dispersion through its use of “effective parameters” (see Section 4.2), which are denoted by an overscript tilde, e.g.,  $\tilde{\sigma}_{wT}$ .

AERMOD treats vertical dispersion from ambient turbulence ( $\sigma_{za}$ ) as a combination of a specific treatment for surface dispersion and the more traditional approach based on Taylor (1921) for elevated dispersion. Using this approach, good agreement with observations was achieved in the SBL. However, the results in the CBL indicated that the treatment of lateral dispersion near the surface was problematic. This problem was corrected through the development of an empirical relationship for  $\sigma_{ya}$  near the surface using the full (CBL and SBL) Prairie Grass data set. A description of the resulting formulations for  $\sigma_{ya}$  and  $\sigma_{za}$  is presented in the next section.

The approach used to combine the above contributions to dispersion assumes that the effects are independent of one another. Thus, the total dispersion coefficients, for situations that do not include building downwash effects, are calculated from the following general expression (Pasquill and Smith 1983):

$$\sigma_{y,z}^2 = \sigma_{ya,za}^2 + \sigma_b^2, \quad (75)$$

where the subscripts  $y$  and  $z$  are deleted from  $\sigma_b$  because  $\sigma_{yb}$  is assumed equal to  $\sigma_{zb}$ . With the exception of the CBL's penetrated source the form of eq. (75) applies to all source dispersion in both the CBL and SBL such that  $\sigma_{y,z}$  becomes  $\sigma_{ys,zs}$  and  $\sigma_{yjs,zj}$  and  $\sigma_{ya,za}$  becomes  $\sigma_{yas,zas}$  and  $\sigma_{yajs,zaj}$  for the SBL and CBL, respectively. For the penetrated source, the total dispersion is assumed to include ambient and buoyancy induced turbulence only; building wakes are assumed to have little influence. For the injected source, the total dispersion is calculated as if the source were in the SBL.

A comment on notation: eq. (75) applies for both lateral and vertical dispersion in the SBL and CBL. In references to the SBL,  $\sigma_z$  appears as  $\sigma_{zs}$  in the dispersion equation;  $\sigma_{za}$  appears as  $\sigma_{zas}$ . In reference to the CBL,  $\sigma_z$  appears as  $\sigma_{zj}$  for the dispersion expression applicable to the direct and indirect sources and  $\sigma_{za}$  appears as  $\sigma_{aj}$ ; for the penetrated source  $\sigma_z$  appears as  $\sigma_{zp}$  in the dispersion expression.

### 5.5.1 Dispersion from ambient turbulence

#### 5.5.1.1 Lateral dispersion from ambient turbulence

In general terms, the ambient component of the lateral dispersion is based upon Taylor (1921) such that:

$$\sigma_{ya} = \frac{\tilde{\sigma}_v x}{\tilde{u} \left( 1 + \frac{x/\tilde{u}}{2T_{Ly}} \right)^p} \quad (76)$$

where  $p = 0.5$ ,  $u$  is the wind speed,  $\sigma_v$  is the root-mean-square lateral turbulence velocity, and  $T_{Ly}$  is the Lagrangian integral time for the lateral turbulence. Application of eq. (76) in a preliminary version of AERMOD yielded poor concentration estimates in comparison to those found in the Prairie Grass field experiments (Barad 1958). Specifically, the lateral spread was not well matched. Therefore, the lateral dispersion expression was reformulated to allow for an empirical fit to the Prairie Grass data.

Using an approach similar to that of Venkatram et al. (1984),  $T_{Ly}$  is found to be  $l/\sigma_v$  where  $l$  is an appropriate length scale for lateral turbulence. Equation (76) can be written in terms of the non-dimensional downwind distance  $X$  and a non-dimensional height scale  $\alpha$  as:

$$\sigma_{ya} = \frac{\tilde{\sigma}_v x}{\tilde{u} (1 + \alpha X)^p} \quad (77)$$

where  $X (= \tilde{\sigma}_v x / \tilde{u} z)$  is the non-dimensional distance with  $u$  and  $\sigma_v$  given by effective parameters, where  $\alpha = z_i / l$ , and  $z_i$  is the mixed layer height.

Based on a preliminary comparison of  $\sigma_{ya}$  (eq. (77)) with selected stable and convective cases from the Prairie Grass experiment (Barad 1958),  $\alpha$  was found equal to 78 and  $p$  equal to

0.3. As such,  $\alpha$  is treated as a fitting parameter. In later comparisons against the full Prairie Grass data set (Figure 16), eq. (77) tended towards the lower envelope of this widely scattered data (i.e., lateral dispersion estimates are on the lower end of the distribution of measurements). However, the preliminary values of  $\alpha$  ( $= 78$ ) and  $p$  ( $= 0.3$ ) produced good agreement between AERMOD concentration predictions and observations (Brode 2002). Therefore, these preliminary values were retained in AERMOD, and eq. (77) applies for the calculation of  $\sigma_{ya}$  for all plumes in both the SBL and CBL.

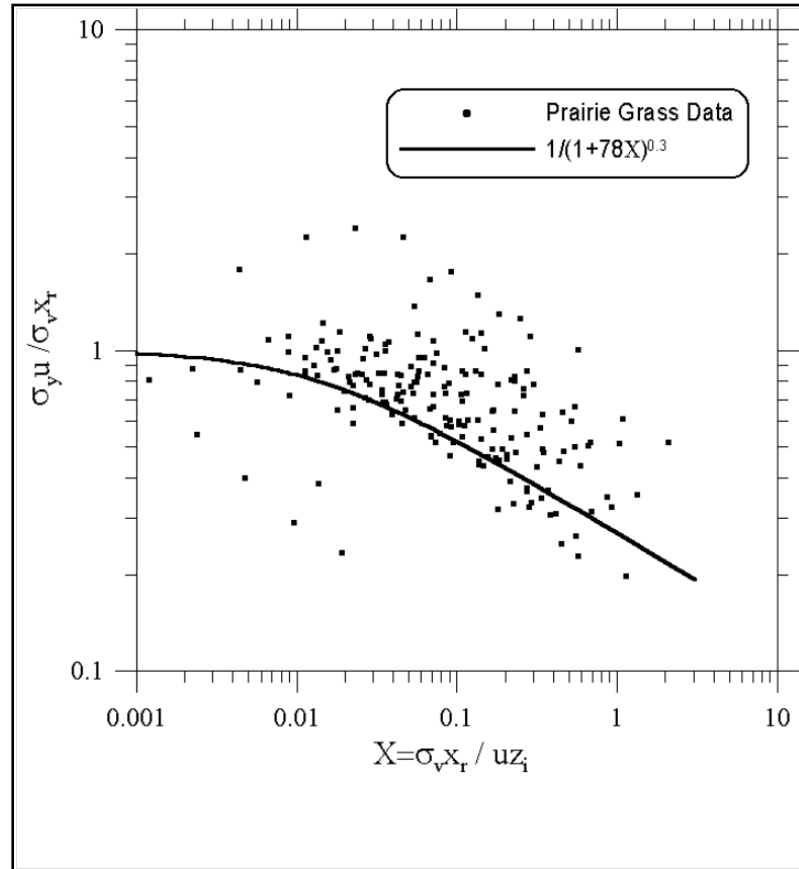


Figure 16. Lateral spread ( $F_y$ ) as a function of non-dimensional distance ( $X$ ). The data is taken from the Prairie Grass experiment (Barad, 1958)

The ambient component of the lateral dispersion for the penetrated source, i.e. a source which has been released below  $z_i$ , but penetrates above, is calculated using eq. (77) with  $h_{es}$  set equal to  $h_{ep}$  (the height of the penetrated source). However, for the injected source, i.e. source released above  $z_i$ , no substitution is needed since these sources are modeled as a stable source.

To account for the increase in the turbulence length scale and hence the Lagrangian time scale with release heights greater than that at Prairie Grass,  $\alpha$  is scaled as follows:

$$\alpha = 78 \left( \frac{z_{PG}}{z_{max}} \right) \quad (78)$$

where  $z_{PG} = 0.46$  m (Prairie Grass release height), and  $z_{max} = \max(z; z_{PG})$ . To insure that  $\alpha$  does not become unrealistically large for surface releases,  $z$  is not allowed below  $z_{PG}$  (i.e., 0.46 m). In the SBL,  $z = h_{es}$ ; in the CBL  $z = h_s$ ; for penetrated sources,  $z = h_{ep}$ . . As  $\alpha$  becomes small for large release heights,  $\sigma_{ya}$  would tend to grow linearly with downwind distance.

#### 5.5.1.2 Vertical dispersion from ambient turbulence

For sources in the SBL (and for sources in the CBL that are emitted directly into the stable layer above the mixed layer), the ambient portion of the vertical dispersion ( $\sigma_{zas}$ ) is composed of an elevated ( $\sigma_{zes}$ ) and near-surface ( $\sigma_{zgs}$ ) component. For  $h_{es} < z_i$  simple interpolation provides a smooth transition between the two components.

$$\sigma_{zas} = \left( 1 - \frac{h_{es}}{z_i} \right) \sigma_{zgs} + \left( \frac{h_{es}}{z_i} \right) \sigma_{zes}. \quad (79)$$

For  $h_{es} \geq z_i$   $\sigma_{zas}$  is set equal to  $\sigma_{zes}$ . The expressions for calculating  $h_{es}$  are found in Section 5.6.2. It should be noted, for sources in the SBL, that  $\sigma_{zas}$  is the specific form of the ambient portion of the vertical dispersion (i.e.,  $\sigma_{za}$  in eq. (75)).

In the SBL, the elevated portion of the vertical dispersion follows the form of eq. (76):

$$\sigma_{zes} = \tilde{\sigma}_{wT}(x/\tilde{u}) / \left( 1 + \frac{x/\tilde{u}}{2T_{Lzs}} \right)^{1/2}, \quad (80)$$

where  $\sigma_{wT}$  is the vertical turbulence due to the mechanical mixing (Cimorelli et al., 2004).

As with the lateral component, the Lagrangian time scale ( $T_{Lzs}$ ) for the vertical turbulence can be written in the form (Venkatram et al. 1984)

$$T_{Lzs} = \frac{l}{\tilde{\sigma}_{wT}} \quad (81)$$

The length scale  $l$  is an interpolation between the limiting length scales for neutral conditions and stable conditions

$$\frac{1}{l} = \frac{1}{l_n} + \frac{1}{l_s}. \quad (82)$$

where  $l_n = 0.36 h_{es}$  and  $l_s = 0.27 \tilde{\sigma}_{wT}/N$ . Under very stable conditions or at large heights,  $l$  approaches  $l_s$ . When conditions are near neutral,  $N$  is very small and  $l$  approaches  $l_n$ .

By combining eqs. (80), (81), and (82) we find the following expression that is used by AERMOD to compute  $\sigma_{zes}$ , the elevated portion of the vertical dispersion for the stable source:

$$\sigma_{zes} = \frac{\tilde{\sigma}_{wT} t}{\left[ 1 + \frac{\tilde{\sigma}_{wT} t}{2} \left( \frac{1}{0.36 h_{es}} + \frac{N}{0.27 \tilde{\sigma}_{wT}} \right) \right]^{1/2}}. \quad (83)$$

Finally, to complete the description of eq. (79), the surface portion of vertical dispersion ( $\sigma_{zgs}$ ) in the SBL, is calculated from Venkatram (1992) as

$$\sigma_{zgs} = \sqrt{\frac{2}{\pi}} \left( \frac{u_* x}{\tilde{u}} \right) \left( 1 + 0.7 \frac{x}{L} \right)^{-1/3} \quad (84)$$

For the direct and indirect sources in the CBL, the ambient portion of the vertical dispersion ( $\sigma_{za}$  of eq. (75)) is denoted as  $\sigma_{zaj}$  ( $j = 1, 2$ ) to distinguish between updrafts and downdrafts.  $\sigma_{zaj}$  is composed of an elevated ( $\sigma_{zej}$ ) and surface ( $\sigma_{zg}$ ) portion and is given by

$$\sigma_{zaj}^2 = \sigma_{zej}^2 + \sigma_{zg}^2, \quad (85)$$

where the elevated portion ( $\sigma_{zej}$ ) is obtained from Weil et al. (1997) as

$$\sigma_{zej} = \alpha_b \frac{\sigma_{wj} x}{\tilde{u}}, \quad (86)$$

where  $\sigma_{wj}$  is a parameter in the bi-Gaussian pdf (eq. (53)).

The expression  $\alpha_b = \min(0.6 + 4H_p/z_i, 10.0)$  designed to be 1.0 above the surface layer ( $H_p > 0.1 z_i$ ) and to otherwise match Venkatram's (1992) result for vertical dispersion from a surface source in a neutral boundary layer.

For the CBL, the vertical dispersion from a source within the surface layer ( $H_p\{x\} < 0.1 z_i$ ) is parameterized by

$$\sigma_{zg} = b_c \left( 1 - 10 \left( \frac{H_p}{z_i} \right) \right) \cdot (u_*/\tilde{u})^2 \cdot (x^2/|L|) \quad (87)$$

where  $b_c = 0.5$ ,  $u_*$  is the friction velocity, and  $L$  is the Monin-Obukhov length; above the surface layer ( $H_p > 0.1 z_i$ ),  $\sigma_{zg}$  is assumed to equal zero. In the limit of a surface release ( $H_p = 0$ ), the parameterization of eq. (87) follows the form suggested by Venkatram (1992) for vertical dispersion in the unstable surface layer; i.e.,  $\sigma_z \propto (u_*/\tilde{u})^2 x^2/|L|$ . The parameterization is designed to: 1) agree with Venkatram's result in the limit of a surface release, 2) provide good agreement between the modeled and observed concentrations from the Prairie Grass experiment (Perry et al., 2005), and 3) decrease with source height in the surface layer and ultimately vanish

for above the surface layer. The constant  $b_c$  was chosen to satisfy the second design requirement. In the limit of a neutral boundary layer  $\sigma_{zg}$  is equal to zero.

The total vertical dispersion for the penetrated source  $\sigma_{zp}$  ( $= \sigma_z$  in eq. (75)) is a combination of both ambient and buoyancy effects. The ambient portion of the vertical dispersion for the penetrated source contains only an elevated component  $\sigma_{zes}$  ( $= \sigma_{zss}$ ) since it is assumed to be decoupled from the ground surface by its location above  $z_i$  and therefore unaffected by the underlying surface. The ambient vertical dispersion for the penetrated source is computed as the elevated portion of a stable source ( $\sigma_{zes}$  of eq. (83)) with  $N = 0$  and with no contribution from the surface component. The Brunt-Vaisala frequency,  $N$ , is set to zero because the penetrated plume passes through the well mixed layer (where  $N \approx 0$ ) prior to dispersing to receptors within the mixed layer.

#### 5.5.2 Buoyancy induced dispersion (BID) component of $\sigma_y$ and $\sigma_z$

For all plumes, the buoyancy induced dispersion (BID) is calculated following Pasquill (Pasquill 1976) and Weil (1988b) as

$$\sigma_b = \frac{0.4\Delta h}{\sqrt{2}}, \quad (88)$$

where  $\Delta h$  is the plume rise appropriate for each of the plume types (direct, indirect, penetrated, and stable plumes). The direct source plume rise is calculated from eq. (91), stable plume rise ( $\Delta h_s$ ) is calculated from eq. (95) and the plume rise for the penetrated source  $\Delta h_p = h_{ep} - h_s$  where  $h_{ep}$  is calculated from eq. (94)).

#### 5.5.3 Treatment of building downwash

AERMOD incorporates the Plume Rise Model Enhancements (PRIME) (Schulman et al. 2000) algorithms for estimating enhanced plume growth and restricted plume rise for plumes affected by building wakes (U.S. Environmental Protection Agency, 1995). PRIME partitions plume mass between a cavity recirculation region and a dispersion enhanced wake region based

upon the fraction of plume mass that is calculated to intercept the cavity boundaries. These boundaries are established from estimates of the locations of the lateral and vertical separation streamlines. Dispersion of the recirculated cavity mass is based on building geometry and is assumed to be uniformly mixed in the vertical. At the boundary of the cavity region, cavity mass is emitted into the wake region. Here, it is combined with plume mass that was not captured by the cavity and dispersed at an enhanced rate based on source location, release height and building geometry. The enhancement of turbulence within the wake decays gradually with distance, allowing for a smooth transition to ambient levels of turbulence in the far-field. A probability density function model and an eddy diffusivity model (Weil 1996) are used for dispersion estimates in the near-wake and far-wake regions, respectively. Plume rise, for sources influenced by a building, is estimated using a numerical model that includes effects from streamline deflection near the building, vertical wind speed shear, enhanced dilution from the turbulent wake and velocity deficit. In general, these building induced effects act to restrict the rise that the plume would have in the absence of the building.

PRIME was originally designed (Schulman et al., 2000) to enhance plume growth using Pasquill Gifford (PG) dispersion (Pasquill 1961; Gifford 1961). AERMOD's estimate of plume growth is based on dispersion parameters derived from profiles of turbulence (see Section 4), not from radiation base turbulence surrogates as is done in the PG approach. A basic design tenet for incorporating PRIME into AERMOD was to be as faithful as possible to the PRIME formulation while ensuring that 1) AERMOD's ambient dispersion was used in place of PG dispersion and 2) far beyond the wake region, where building influences should be insignificant, concentrations approach the AERMOD estimate. Therefore, within the wake, PRIME algorithms are used exclusively to calculate concentration with AERMOD-derived ambient turbulent intensities as input. To ensure a smooth transition between concentrations estimated by PRIME, within the wake, and AERMOD estimates in the far field, concentrations beyond the wake are estimated as the weighted sum of the two calculations. That is, beyond the wake the total concentration ( $C_{total}$ ) is calculated as follows:

$$C_{Total} = \gamma C_{Prime} + (1 - \gamma) C_{AERMOD} \quad (89)$$

where  $C_{prime}$  is the concentration estimated using the PRIME algorithms with AERMOD-derived meteorological inputs,  $C_{AERMOD}$  is the concentration estimated using AERMOD without considering building wake effects, and  $\gamma$  the weighting parameter. The weighting parameter,  $\gamma$ , is designed such that the contribution from the PRIME calculation decreases exponentially with vertical, lateral and downwind distance from the wake. It is calculated as follows:

$$\gamma = \exp\left(\frac{-(x - \sigma_{xg})^2}{2\sigma_{xg}^2}\right) \exp\left(\frac{-(y - \sigma_{yg})^2}{2\sigma_{yg}^2}\right) \exp\left(\frac{-(z - \sigma_{zg})^2}{2\sigma_{zg}^2}\right) \quad (90)$$

where  $x$  is the downwind distance from the upwind edge of the building to the receptor,  $y$  is the lateral (crosswind) distance from the building centerline to the receptor,  $z$  is the receptor height above ground,  $\sigma_{xg}$  is longitudinal dimension of the wake,  $\sigma_{yg}$  is the distance from the building centerline to lateral edge of the wake, and  $\sigma_{zg}$  is the height of the wake at the receptor location.

## 5.6 Plume rise calculations in AERMOD

### 5.6.1 Plume rise in the CBL

The plume rise for the direct source is given by the superposition of source momentum and buoyancy effects following Briggs (1984).

$$\Delta h_d = \left( \frac{3F_m x}{\beta_1^2 u_p^2} + \frac{3}{2\beta_1^2} \cdot \frac{F_b x^2}{u_p^3} \right)^{1/3} \quad (91)$$

where  $F_m = (T/T_s)w_s^2 r_s^2$  the stack momentum flux,  $F_b = g w_s r_s^2 (\Delta T/T_s)$  is the stack buoyant flux,  $r_s$  is the stack radius corrected for stack tip downwash, and  $\beta_1 (= 0.6)$  is an entrainment parameter. It should be noted that  $u_p$  is the wind speed used for calculating plume rise. In the CBL  $u_p$  is set equal to  $u\{h_s\}$ .

As shown in Figure 13, the indirect plume, which is included to treat the no flux condition at  $z = z_i$ , is modeled as a reflected version of the direct plume with an adjustment ( $\Delta h_i$ ) to the reflected plume height to account for the delay in vertical mixing due to plume lofting at the top of the boundary layer. That height adjustment is given by

$$\Delta h_i = \left( \frac{2F_b z_i}{\alpha_r u_p r_y r_z} \right)^{1/2} \frac{x}{u_p}, \quad (92)$$

where  $r_y$  and  $r_z$  are the lofting plume half-widths in the lateral and vertical directions,  $u_p$  is the wind speed used for plume rise, and  $\alpha_r = 1.4$ . The produce of cross-wind dimensions of the assumed elliptical plume is calculated from Weil et al. (1997) as

$$r_y r_z = r_h^2 + \frac{a_e \lambda_y^{3/2}}{4} \cdot \frac{w_*^2 x^2}{u_p^2} \quad (93)$$

where  $r_h = \beta_2(z_i - h_s)$ ,  $\beta_2 = 0.4$ ,  $\lambda_y = 2.3$ , and  $a_e = 0.1$  (dimensionless entrainment parameter). For a derivation and discussion of  $\Delta h_i$  see Weil et al. (1997).

The height that the penetrated source achieves above  $z_i$  is calculated as the equilibrium plume rise in a stratified environment and is determined by the source buoyancy flux, the stable stratification above  $z_i$ , and the mean wind speed. In line with Weil et al. (1997), the penetrated source plume height,  $h_{ep}$ , is taken as the centroid of plume material above the inversion. For complete penetration ( $f_p = 0$ )  $h_{ep} = h_s + \Delta h_{eq}$ . However, for partial penetration ( $f_p > 0$ ),  $h_{ep}$  is chosen as the average of the heights of the upper plume edge  $h_s + 1.5 \Delta h_{eq}$  and  $z_i$ , or

$$h_{ep} = \frac{h_s + z_i}{2} + 0.75 \Delta h_{eq}. \quad (94)$$

where  $\Delta h_{eq}$  is defined in eq.(56).

### 5.6.2 Plume rise in the SBL

Plume rise in the SBL is taken from Weil (1988b), which is modified by using an iterative approach which is similar to that found in Perry et al. (1989). When a plume rises in an atmosphere with a positive potential temperature gradient, plume buoyancy decreases because the ambient potential temperature increases as the plume rises; thus, plume buoyancy with respect to the surroundings decreases. To account for this, the plume rise equations have to be modified. With this modification, AERMOD computes stable plume rise,  $\Delta h_s$ , from Weil et al. (1988b) as

$$\Delta h_s = 2.66 \left( \frac{F_b}{N^2 u_p} \right)^{1/3} \cdot \left[ \frac{N' F_m}{F_b} \sin \left( \frac{N' x}{u_p} \right) + 1 - \cos \left( \frac{N' x}{u_p} \right) \right]^{1/3}, \quad (95)$$

where  $N' = 0.7N$  with  $N$  given by eq. (58).  $N$  and  $u$  are evaluated initially at stack height. Once plume rise has been computed, subsequent plume rise estimates are made (iteratively until convergence) by averaging the  $u$  and  $N$  values at stack top with those at  $h_s + \Delta h_s/2$ . Equation (95) is used for downwind distances that are less than the distance to final rise ( $x_f$ ). Beyond  $x_f$ ,  $\Delta h_s$  remains constant. The distance at which the stable plume reaches its maximum rise is given by

$$x_f = \frac{u_p}{N'} \arctan \left( \frac{-F_m N'}{F_b} \right). \quad (96)$$

Upon substituting eq. (95) for  $x$  in eq. (97) the maximum final rise of the stable plume  $\Delta h_s\{x_f\}$  reduces to:

$$\Delta h_s\{x_f\} = 2.66 \left( \frac{F_b}{u_p N^2} \right)^{1/3}. \quad (97)$$

As with eq. (95), the velocity,  $u_p$ , and  $N$  in eq. (97) are evaluated initially at stack height and then iteratively.

When the atmosphere is close to neutral, the Brunt Vaisala frequency,  $N$ , is close to zero, and eq. (95) can predict an unrealistically large plume rise. Under, these circumstances, plume rise is limited by atmospheric turbulence. This happens when the rate of plume rise under neutral conditions is comparable to  $\sigma_w$ . Under these conditions, stable plume rise (eq. (97)) is limited by the neutral rise calculated from Weil (1985) as

$$\Delta h_s = 1.2 L_n^{3/5} (h_s + 1.2 L_n)^{2/5} \quad (98)$$

where the neutral length scale  $L_n = F_b / (u_p u_*^2)$ .

As the wind speed approaches zero, eq. (95) again predicts unrealistic values. In these near-calm conditions the stable plume rise (eq. (97)) is limited by the calm rise expression that is based on the work of Morton et al. (1956) and Briggs (1969) such that,

$$\Delta h_s = \frac{4 F_b^{1/4}}{N^{3/4}}. \quad (99)$$

Finally, the stable plume rise is limited by a calculation of the unstable rise (see Section 5.6.1).

## 5.7 Source characterization

AERMOD gives the user the ability to characterize a source as either a point, a volume, an area, a roadway, or a buoyant line. AERMOD additionally has the capability of characterizing irregularly shaped area sources.

Point sources are characterized exactly as in the ISC3 model (U.S. Environmental Protection Agency, 1995). The input to the model includes the location, elevation, emission rate,

stack height, stack gas temperature, stack gas exit velocity, and stack inside diameter. The temperature, exit velocity, and diameter are required for plume rise calculations.

Similarly, volume sources require the same input as the ISC3 model. This includes the location, elevation height (optional), height of release, emission rate, the initial lateral plume size ( $\sigma_y$ ) and initial vertical plume size ( $\sigma_z$ ). AERMOD differs from ISC3 in the treatment of volume sources only in how the initial plume size is implemented. Where ISC3 uses the virtual source technique to account for initial plume size, AERMOD adds the square of the initial plume size to the square of the ambient plume size:

$$\sigma_y^2 = \sigma_{yl}^2 + \sigma_{yo}^2 \quad (100)$$

where  $\sigma_{yo}$  is the initial horizontal plume size,  $\sigma_{yl}$  is the plume size before accounting for the initial size, and  $\sigma_y$  is the resultant plume size after accounting for the initial size.

The area source treatment is enhanced from that available in ISC3. In addition to being input as squares or rectangles, area sources may be input as circles or polygons. A polygon may be defined by up to 20 vertices. A circle is defined by inputting its center location and radius. The AERMOD code uses this information to create an equivalent, nearly circular polygon of 20 sides, with the same area as the circle.

As with ISC3, AERMOD allows for the calculation of a simple half-life decay.

The buoyant line source algorithm from the Buoyant Line and Point Source (BLP) model (Schulman and Scire, 1980) was incorporated into AERMOD beginning with version 15181. The input to the model includes emission rate and average release height for individual lines, and average building length, average building height, average building width, average line source width, average building separation, and average buoyancy for the single source.

## 5.8 Plume volume molar ration method (PVMRM)

PVMRM was first introduced in AERMOD in version 04300 as an option for modeling the conversion of NO<sub>x</sub> to NO<sub>2</sub> in the presence of ozone. The implementation is based on the work of Hanrahan (1999) and adapted for AERMOD. Details regarding the formulation of the PVMRM option in AERMOD, and preliminary model evaluation results are available in U.S. Environmental Protection Agency (2015).

### 5.8.1 Definition of plume volume

#### 5.8.1.1 Total vs. relative dispersion

The PVMRM determines the conversion rate for NO<sub>x</sub> to NO<sub>2</sub> based on a calculation of the NO<sub>x</sub> moles emitted into the plume, and the amount of O<sub>3</sub> moles contained within the volume of the plume between the source and receptor. The dispersion algorithms in AERMOD and other steady-state plume models are based on the use of total dispersion coefficients, which are formulated to represent the time-averaged spread of the plume. A more appropriate definition of the volume of the plume for purposes of determining the ozone moles available for conversion of NO<sub>x</sub> is based on the instantaneous volume of the plume, which is represented by the use of relative dispersion coefficients, (Cole and Summerhays, 1979; Bange, 1991). The implementation of PVMRM in AERMOD is based on the use of relative dispersion coefficients to calculate the plume volume. Weil (1996 and 1998) has defined formulas for relative dispersion that are consistent with the AERMOD treatment of dispersion, and which can be calculated using meteorological parameters available within AERMOD.

#### 5.8.1.2 Calculation of relative dispersion coefficients

The formula for relative dispersion combines the effects of buoyancy-induced turbulence, which should dominate close to the source, and ambient turbulence, which begins to dominate further downwind. Since the travel time from the source to the receptor is important for defining relative dispersion, the relative dispersion coefficients are calculated based on the radial distance from source to receptor. Weil (1996 and 1998) assumes relative dispersion ( $\sigma_r$ )

to be isotropic, so that  $\sigma_{rx} = \sigma_{ry} = \sigma_{rz} = \sigma_r$ . The relative dispersion ( $\sigma_r$ ) due to the combined effects of buoyancy- induced turbulence ( $\sigma_{rb}$ ) and ambient turbulence ( $\sigma_{ra}$ ) is parameterized as follows:

$$\sigma_r = (\sigma_{rb}^3 + \sigma_{ra}^3)^{1/3} \quad (101)$$

The buoyancy-induced dispersion term,  $\sigma_{rb}$ , is calculated in AERMOD as

$$\sigma_{rb} = \frac{0.4 \Delta h}{\sqrt{2}} \quad (102)$$

where  $\Delta h$  is the plume rise. Relative dispersion due to ambient turbulence,  $\sigma_{ra}$ , is parameterized by

$$\sigma_{ra} = \frac{a_1 \varepsilon^{1/2} t^{3/2}}{1 + a_2 t / T_{Lr}} \quad (103)$$

where  $a_1$  is a constant ( $= 0.57$ ),  $a_2 = 0.62 a_1$ ,  $t$  is the plume travel time ( $= x/U$ ), and  $T_{Lr}$  is a Lagrangian time scale for relative dispersion defined as

$$T_{Lr} = a_{r1} \frac{z_i}{\sigma_w} \quad (104)$$

where  $a_{r1} = 0.46$ ,  $z_i$  is the mixing height, and  $\sigma_w$  is the vertical turbulence parameter. The turbulence dissipation rate,  $\gamma$ , is calculated as follows, based on Weil (1996):

$$\varepsilon = \frac{b \sigma_w^2}{T_{Lr}} \quad (105)$$

where  $b$  is a constant ( $= 0.78$ ). The values of wind speed ( $U$ ) and  $\sigma_w$  used in eqs. (103) through (105) are the effective values, calculated as averages across the layer from the plume centroid height to the receptor height (up to  $2.15\Phi_z$ ), following the procedure used in AERMOD to calculate effective values. Using the effective values of  $\sigma_w$ , AERMOD calculates effective values of the turbulence dissipation rate,  $\gamma$ .

Since the relative dispersion coefficients are source- and meteorology-dependent in AERMOD, the model generates a table of relative dispersion coefficients as a function of distance for the dominant source for each receptor and each hour in order to complete the plume volume calculation.

The original PVMRM utilized the relative dispersion coefficients described above to define the plume volume. These relative dispersion coefficients are applicable to unstable/convective conditions but are likely to overpredict the plume volume for stable conditions, resulting in overpredictions of NO<sub>2</sub> concentrations. The PVMRM algorithm was modified for version 15181 to use the “standard” total dispersion coefficients incorporated in AERMOD to define the plume volume during stable conditions.

#### 5.8.1.3 Treatment of volume and area sources

If the dominant source is a volume source, then the initial lateral and vertical dimensions of the volume source are included in the calculation of the relative dispersion coefficients for purposes of calculating the plume volume, as follows:

$$\sigma_r = (\sigma_{rb}^3 + \sigma_{ra}^3 + \sigma_0^3)^{1/3} \quad (106)$$

where  $\sigma_0$  is the initial dispersion coefficient of the volume source calculated as  $\sqrt{\sigma_{y0}\sigma_{z0}}$  based on the initial lateral ( $\Phi_{y0}$ ) and vertical ( $\Phi_{z0}$ ) dimensions input by the user. If a volume source is included among the major contributing sources, it is treated the same as a point source in defining the combined plume volume.

For application of PVMRM to area sources, the plume volume is extended laterally, if necessary, to include the projected width of the area source or sources that are included among the major contributing sources. The emissions from an area source are included in the calculation of the NO<sub>x</sub> moles emitted into the plume if the centroid of the area source is within the box defined by the along-wind and crosswind extent of major contributing sources. In

addition, if an area source is the dominant source, then the relative dispersion coefficients are calculated based on the radial distance from the centroid of the area source to the receptor.

#### 5.8.1.4 Defining extent of plume

The original implementation of PVMRM in AERMOD used four (4) times the relative dispersion coefficients to define the plume volume, which accounts for more than 99.99% of the plume. The original implementation also used a minimum value 5.0m for the plume radius to account for near-source effects (e.g., downwash), which is consistent with the initial plume volume assumed by Hanrahan (1999). Given the fact that the PVMRM option in AERMOD assumes full and instantaneous mixing of the NO and O<sub>3</sub> within the plume, using such a large percentage of the plume volume may introduce a bias to overpredict ambient concentrations of NO<sub>2</sub>. Beginning with version 16216, the PVMRM option uses 2.58 times the relative dispersion coefficients to define the plume volume for unstable conditions, which accounts for about 99% of the plume, and a minimum plume radius of 15.0m. For stable conditions, the PVMRM option uses 1.282 times the total dispersion coefficients to define the plume volume, consistent with the original approach proposed by Hanrahan (1999), which accounts for about 80 percent of the plume volume, and minimum plume radius of 9.0m. Since AERMOD incorporates a horizontal meander algorithm that increases lateral plume spread beyond that accounted for based on dispersion coefficients, the number of sigmas used to define the plume volume for stable conditions is adjusted to account for meander, i.e.,

$$NSUBZ = \min \left( 2.15, 1.282 * \left( \frac{SYEFF}{SY} \right) \right)$$

where NSUBZ is the number of sigmas used to define the plume volume and SYEFF is the effective  $\sigma_y$  value that replicates the plume centerline associated with meander but based on a standard Gaussian plume calculation. An upper bound of 2.15 is applied, which corresponds with the point at which the concentration is 10 percent of the centerline value, and is used to define the extent of the plume in other contexts (e.g., initial dispersion coefficients for volume sources). The minimum value of the dispersion coefficient is also adjusted based on the ratio 1.282/NSUBZ, where NSUBZ is the adjusted value.

The original implementation of PVMRM used the radial distance from source to receptor to calculate the plume volume and the moles of NO<sub>x</sub> contained in the plume. Beginning with version 16216, the downwind distance is used to calculate these values. Use of the downwind distance provides a more realistic estimate of NO<sub>x</sub> conversion consistent with a straight-line, steady-state plume model, such as AERMOD.

#### 5.8.1.5 Adaption for AERMOD terrain algorithm

The vertical dimension of the plume volume is based on the relative dispersion coefficient for the dominant source and the range in plume heights for the major contributing sources. Since the effective plume heights differ for the terrain following and terrain responding components, the vertical dimension was modified to calculate the range of plume heights separately for both the terrain following and terrain responding components, and then use a weighted value for the vertical dimension based on the terrain (plume state) weighting factor,  $f$ , defined in Section 5.1.

#### 5.8.1.6 Treatment of penetrated plumes

For unstable conditions with partial or full plume penetration above the mixing height,  $z_i$ , separate relative dispersion coefficients are calculated for the penetrated portion of the dominant plume. For cases with partial penetration for the dominant plume, AERMOD calculates two plume volumes, one based on relative dispersion coefficients for the direct source and another based on the relative dispersion coefficients for the penetrated source. Since AERMOD uses the same dispersion coefficients for the direct and indirect sources, separate values of relative dispersion coefficients for the indirect source are not needed. The effective plume volume used in the application of PVMRM is based on a weighted average of the direct and penetrated plume volumes using the plume penetration factor (PPF) for the dominant source. The model stores the plume centroid heights for both the direct and penetrated plumes for all sources at each receptor, and these are used to incorporate the effect of the major contributing sources on the volumes for the direct and penetrated plumes.

### 5.8.2 Minimum ozone concentration for stable conditions

Conditions for implementation with ISCST3, due to the fact that surface measurements may be artificially low during nighttime stable conditions due to the formation of a stable vertical temperature gradient. Since the AERMOD model does not use Pasquill-Gifford (P-G) stability categories, this minimum ozone concentration was modified to use Monin-Obukhov length as the stability parameter. The AERMOD model first keeps track of the maximum ozone concentration over the previous 24 hours. If the Monin-Obukhov length is positive (i.e. stable), with a value of less than 50 meters (very stable), then the maximum ozone concentration over the previous 24 hours is used as the minimum value. If the Monin-Obukhov length is positive and the value is over 500 meters (nearly neutral), then no minimum ozone concentration is applied for that hour. If the Monin-Obukhov length is between 50 meters and 500 meters, then the minimum ozone concentration is determined by linear interpolation, i.e., the minimum value is calculated as  $O3MAX * (500 - L)/450$ , where O3MAX is the maximum ozone concentration over the previous 24 hours, and L is the Monin-Obukhov length in meters.

## **5.9 Adjustments for the urban boundary layer**

Although urban surface characteristics (roughness, albedo, etc.) influence the boundary layer parameters at all times, the effects of the urban sublayer on the structure of the boundary layer is largest at night and relatively absent during the day (Oke 1998). An urban “convective-like” boundary layer forms during nighttime hours when stable rural air flows onto a warmer urban surface. Following sunset, the urban surface cools at a slower rate than the rural surface because buildings in the urban area trap the outgoing thermal radiation and the urban subsurface has a larger thermal capacity. AERMOD accounts for this by enhancing the turbulence above that found in the rural stable boundary layer (i.e., a convective-like urban contribution to the total turbulence in the urban SBL). The convective contribution is a function of the convective velocity scale, which in turn, depends on the surface heat flux and the urban mixed layer height. The upward heat flux is a function of the urban-rural temperature difference.

The urban-rural temperature difference depends on a large number of factors that cannot easily be included in applied models such as AERMOD. For simplicity, the data presented in

Oke (1973; 1982) is used to construct an empirical model. Oke presents observed urban-rural temperature differences for a number of Canadian cities with populations varying from about 1000 up to 2,000,000. These data represent the maximum urban effect for each city since they were collected during ideal conditions of clear skies, low winds, and low humidities. An empirical fit to the data yields the following relationship

$$\Delta T_{u-r} = \Delta T_{\max} \left[ 0.1 \ln \left( \frac{P}{P_o} \right) + 1.0 \right], \quad (107)$$

where  $\Delta T_{\max} = 12^\circ\text{C}$ ,  $P_o = 2,000,000$  (the city population associated with the maximum temperature difference in Oke's data), and  $P$  is the population of the urban area being modeled.

Since the ambient nighttime temperature of an urban area is higher than its surrounding rural area, an upward surface heat flux must exist in the urban area. It is assumed that this upward surface heat flux is related to the urban-rural temperature difference through the following relationship

$$H_u = \alpha \rho c_p \Delta T_{u-r} u_*, \quad (108)$$

where  $\alpha$  is an empirical constant,  $\rho$  is the density of air, and  $c_p$  is the specific heat at constant pressure. This expression is analogous to the bulk transfer parameterization of heat flux over a homogeneous surface (e.g., Businger (1973)), with  $\alpha$  defined as the “bulk” transfer coefficient. We chose  $\alpha$  to ensure that the upward heat flux is consistent with maximum measured values of the order of  $0.1 \text{ m s}^{-1} ^\circ\text{C}$ . Because  $\Delta T_{u-r}$  has a maximum value on the order of  $10^\circ\text{C}$ , and  $u_*$  is on the order of  $0.1 \text{ m s}^{-1}$ ,  $\alpha$  should have a maximum value on the order of 0.1. Although we assume that  $\alpha$  has a maximum (city center) value of about 0.1, AERMOD uses an effective value of  $\alpha$  that is averaged over the entire urban area. Assuming a linear variation of  $\alpha$  from 0 at the edge of the urban area to about 0.1 at the center of the urban area results in an area average equal to one-third of that at the center (since the volume of cone is one-third of that of a right circular cylinder of the same height). Therefore, AERMIC tested an area-averaged value of  $\alpha$  equal to 0.03 against the Indianapolis data. This choice for  $\alpha$  is consistent with measured values of the

upward heat flux in Canadian cities reported by Oke (1973; 1982). The results of the developmental testing indicated that this choice for  $\alpha$  resulted in an adequate fit between observations and AERMOD-predicted concentrations.

The mixing height in the nighttime urban boundary layer,  $z_{iu}$ , is based on empirical evidence presented in Oke (1973; 1982) that, in turn, suggests the following relationships:

$$z_{iu} \approx R^{1/2} \text{ and } R \approx P^{1/2}, \quad (109)$$

where  $R$  is a measure of the city size and  $P$  is the population of the city. The first relationship is based on the observed growth of the internal convective boundary layer next to shorelines (Venkatram 1978). The second relationship implicitly assumes that population densities do not vary substantially from city to city.

Equation (103) leads to the following equation for the nocturnal urban boundary layer height due to convective effects alone:

$$z_{iuc} = z_{iuo} \left( P/P_o \right)^{1/4} \quad (110)$$

where  $z_{iuo}$  is the boundary layer height corresponding to  $P_o$ . Based on lidar measurements taken in Indianapolis (1991) and estimates of  $z_{iu}$  found by Bornstein (1968) in a study conducted in New York city,  $z_{iuo}$  is set to 400 m in AERMOD.

In addition, since effects from urban heating should not cause  $z_{iu}$  to be less than the mechanical mixing height,  $z_{iu}$  is restricted from being less than  $z_{im}$ . Therefore, the mixed layer height for the nighttime urban boundary layer is computed as:

$$z_{iu} = \text{Max}[z_{iuc}; z_{im}]. \quad (111)$$

Once the urban mixing height has been estimated, a surrogate convective velocity scale (appropriate for the magnitude of convective turbulence present) is computed by substituting  $z_{iuc}$  and  $H_u$  into the definitional equation for  $w^*$  (Deardorff 1970). That is,

$$w_{*u} = \left( \frac{g H_u z_{iuc}}{\rho c_p T} \right)^{1/3} \quad (112)$$

where  $w_{*u}$  is the urban nighttime convective velocity scale and  $T$  is the near-surface air temperature.

Having estimated  $w_{*u}$  the turbulence in the nighttime urban can be enhanced using the expressions found in Section 4.1.5. However, since for low level sources  $\sigma_{wT}$  depends primarily on  $u_*$  (see eqs. (34) and (35)) it is not possible to directly enhance  $\sigma_{wT}$  for these sources using  $w_{*u}$ . Therefore, an effective friction velocity ( $u_{*eff}$ ) is developed as a surrogate for  $w_{*u}$  in the lower portion of urban PBL. We define  $u_{*eff}$  as the friction velocity that is consistent with  $\sigma_{wm} = \sigma_{wc}$  at  $z = 7z_o$ . Assuming that  $z = 7z_o$  is always less  $0.1z_{iuc}$ ,  $u_{*eff}$  is estimated by equating  $\sigma_{wc}$  (eq. (35)) with  $\sigma_{wm}$  (eq. (37)) and solving for  $u_*$ . Once  $u_{*eff}$  is found, the urban friction velocity for nighttime conditions ( $u_{*u}$ ) is calculated as the maximum of  $u_{*eff}$  and  $u_*$  (the rural and daytime urban friction velocity).

Then using the enhanced velocity scales  $u_{*u}$  and  $w_{*u}$ , the nighttime convective portion of the turbulence in the urban boundary layer is computed using the expressions turbulence found in Section 4.1.5. That is,  $\sigma_{wc}$  and  $\sigma_{wm}$  are calculated from eqs. (35) and (37), respectively, with  $w_{*u}$  used in place of the daytime convective velocity scale ( $w^*$ ) and  $u_{*u}$  substituted for the rural  $u_*$ . Furthermore, for consistency purposes, an urban nighttime Monin-Obukhov length is calculated using eq. (8) with substitutions  $u_{*u}$  for  $u_*$  and  $H_u$  (eq. (108)) for  $H$ .

Finally, the total nighttime turbulence in the urban boundary layer is calculated as the sum (in quadrature) of the convective and mechanical portions. With these enhanced levels, vertical dispersion due to ambient turbulence ( $\sigma_{za}$ ) in the urban boundary layer is calculated from eq. (83) (the SBL formulation for  $\sigma_{za}$ ) with the urban PBL assumed to be neutral (i.e.,  $N =$

0). For the lateral dispersion in the urban boundary layer,  $\sigma_{ya}$  is calculated using the SBL formulation given by eq. (76).

The potential temperature gradient in the night-time urban boundary layer is set equal to the upwind rural profile (Section 4.1.3) for all heights above  $z_{iu}$ , and is assumed to be equal to a small positive value below  $z_{iu}$ ; i.e.,

$$\begin{aligned} \partial\theta/\partial z &= 10^{-5} & \text{for } z \leq z_{iu} \\ \partial\theta/\partial z &= \text{rural value} & \text{for } z > z_{iu}. \end{aligned} \quad (113)$$

For plumes below  $z_{iu}$ , the effective reflection surface is set equal to the height of the urban boundary layer (i.e.,  $z_{ieff} = z_{iu}$ ). Plumes that rise above  $z_{iu}$  ( $h_{es} > z_{iu}$ ) are modeled with a  $z_{ieff}$  that is calculated from eq. (68) with  $z_{im}$  replaced by  $z_{iu}$ . Plume rise in the urban stable boundary layer is calculated from eqs. (95)-(99) with  $\partial\theta/\partial z$  taken from eq. (113).

Use of this value for  $\partial\theta/\partial z$  provides an appropriate near-neutral plume rise formulation that is expected within the nocturnal urban boundary layer. However, plume height in these conditions is not allowed to exceed  $1.25 z_{iu}$ .

For daytime conditions ( $L < 0$ ) in urban areas, AERMOD uses the same formulations as in rural areas (i.e., no urban-related adjustments to boundary layer characteristics).

Urban boundary layer adjustments have been implemented as an ALPHA option in version 19191 for the RLINE and RLINEXT source types. Based on algorithms for the AERMOD area source, modification was introduced so when a RLINE or RLINEXT source is specified as an urban source, the  $u^*$  urban nighttime Monin-Obukhov length,  $z_{iu}$ , and  $z_o$  parameters are recalculated for morning transition and stable hours. As initial integration of the RLINE and RLINEXT source types in version 19191 is based on algorithms of version 1.2 of the Research LINE source (R-LINE) model (Snyder et al, 2013), the R-LINE methodology for calculation of  $w^*$ , is included. The methodology incorporates a check to set any negative  $w^*$  values to 0.0, associated with stable meteorological conditions, unlike other AERMOD source

types that accept negative  $w^*$  values. The resultant  $w^*$  values are then used in the calculation of  $\sigma_v$  for RLINE and RLINEXT sources only.

## 6. List of symbols

$B_o$	Bowen ratio - ratio of the sensible to latent heat fluxes (dimensionless)
$C_{\text{AERMOD}}$	concentration estimated using AERMOD without considering building wake effects ( $\text{g m}^{-3}$ )
$C_{c,s}\{x_r, y_r, z_r\}$	concentration contribution from the horizontal plume state - convective and stable ( $\text{g m}^{-3}$ )
$C_{c,s}\{x_r, y_r, z_p\}$	concentration contribution from the terrain-following plume state - convective and stable ( $\text{g m}^{-3}$ )
$C_c\{x_r, y_r, z_r\}$	total concentration (CBL) ( $\text{g m}^{-3}$ )
$C_d\{x_r, y_r, z_r\}$	concentration contribution from the direct source (CBL) ( $\text{g m}^{-3}$ )
$C_p\{x_r, y_r, z_r\}$	concentration contribution from the penetrated source (CBL) ( $\text{g m}^{-3}$ )
$C_r\{x_r, y_r, z_r\}$	concentration contribution from the indirect source (CBL) ( $\text{g m}^{-3}$ )
$C_s\{x_r, y_r, z_r\}$	total concentration (SBL) ( $\text{g m}^{-3}$ )
$C_T\{x_r, y_r, z_r\}$	total concentration (CBL) ( $\text{g m}^{-3}$ )
$C_{ch}$	concentration from the coherent plume used in meander calculations ( $\text{gm}^{-3}$ )
$C_R$	concentration from the random plume used in meander calculations ( $\text{g m}^{-3}$ )
$C_D$	neutral drag coefficient ( $\text{cal g}^{-1} \text{ } ^\circ\text{C}^{-1}$ )
$C_{\text{prime}}$	concentration estimated using the PRIME algorithms with AERMOD-derived meteorological inputs ( $\text{g m}^{-3}$ )
$c_p$	specific heat at constant pressure ( $= 1004 \text{ J g}^{-1} \text{ K}^{-1}$ )
$F_b$	plume buoyancy flux ( $\text{m}^4 \text{ s}^3$ )
$F_y$	total horizontal distribution function - with meander ( $\text{m}^{-1}$ )
$F_{yC}$	horizontal distribution function for a coherent plume ( $\text{m}^{-1}$ )
$F_{yR}$	horizontal distribution function for a random plume ( $\text{m}^{-1}$ )
$F_G$	flux of heat into the ground ( $\text{W m}^{-2}$ )
$F_m$	plume momentum flux ( $\text{m}^4 \text{ s}^2$ )
$F_z$	total vertical distribution function ( $\text{m}^{-1}$ )
$f$	plume state weighting function (dimensionless)
$f_p$	fraction of plume mass contained in CBL = (1 - penetration factor) dimensionless)
$g$	acceleration due to gravity ( $9.8 \text{ m s}^{-2}$ )
$H$	sensible heat flux ( $\text{W m}^{-2}$ )
$H_c$	critical dividing streamline (m)
$H_p$	plume centroid height (m)
$H_u$	heat flux in the nighttime boundary layer ( $\text{W m}^{-2}$ )
$h_c$	receptor specific terrain height scale (m)
$h_{ep}$	penetrated source plume height above stack base (m)
$h_s$	stack height corrected for stack tip downwash (m)
$\Delta h$	general symbol for distance dependent plume rise (m)

$\Delta h_d$	plume rise for the direct source (m)
$\Delta h_{eq}$	equilibrium plume rise in a stable environment (m)
$\Delta h_h$	depth of the layer between $z_i$ and the stack top (m)
$\Delta h_p$	plume rise for the penetrated source (m)
$\Delta h_i$	plume rise for the indirect source (m)
$\Delta h_s$	plume rise for the stable source (m)
$i_z$	vertical turbulence intensity
$k$	von Karman constant $k = 0.4$ (dimensionless)
$l$	length scale used in determining the Lagrangian time scale (m)
$l_n$	neutral length scale - a component of $l$ (m)
$l_s$	stable length scale - a component of $l$ (m)
$L$	Monin-Obukhov length (m)
$N$	Brunt-Vaisala frequency ( $s^{-1}$ )
$N_h$	Brunt-Vaisala frequency above $z_i$ ( $s^{-1}$ )
$n$	cloud cover (fractional)
$P$	population of urban area
$p_y$	lateral probability density function
$p_z$	vertical probability density function
$p_w$	probability density function of the instantaneous vertical velocities
$Q$	source emission rate (g/s)
$R$	solar insolation ( $W m^{-2}$ )
$R_n$	net radiation ( $W m^{-2}$ )
$R_o$	<i>clear sky solar insolation</i> ( $W m^{-2}$ )
$r(\phi)$	Albedo {solar elevation} (dimensionless)
$r'$	noontime albedo (dimensionless)
$r_s$	stack radius - corrected for stack tip downwash (m)
$r_y$	lateral dimension of an elliptical plume
$r_z$	vertical dimension of an elliptical plume
$S$	skewness factor (dimensionless)
$T$	ambient temperature (K)
$T_{Ly}$	lateral lagrangian time scale (sec)
$T_{Lzc}$	vertical lagrangian time scale for the CBL (sec)
$T_{Lzs}$	vertical lagrangian time scale for the SBL (sec)
$T_r$	time scale used in the meander algorithm (sec)
$T_{ref}$	ambient temperature - at reference temperature height (K)
$T_s$	stack gas temperature (K)
$T_u$	urban surface temperature (K)
$t$	time (sec)
$\Delta T$	difference between stack gas and ambient temperature (K)
$\Delta T_{u-r}$	urban-rural temperature difference (K)

$u$	wind speed ( $\text{m s}^{-1}$ )
$u_{cr}$	minimum speed for which the expression for $u^*$ , in the SBL, has a real valued solution ( $\text{m s}^{-1}$ )
$u_o$	defined in eq. (14) and used in eq. (15)
$u_p$	wind speed that is used for plume rise ( $\text{m s}^{-1}$ )
$u_{ref}$	wind speed at reference height ( $\text{m s}^{-1}$ )
$u_{th}$	wind speed instrument threshold - separate value for each data set (offsite & onsite) ( $\text{m s}^{-1}$ )
$u^*$	surface friction velocity ( $\text{m s}^{-1}$ )
$u^{*eff}$	effective surface friction velocity - surrogate for $w_{*u}$ ( $\text{m s}^{-1}$ )
$u_{*u}$	surface friction velocity for nighttime urban conditions ( $\text{m s}^{-1}$ )
$w$	random vertical velocity in the CBL ( $\text{m s}^{-1}$ )
$\overline{w}_j$	mean vertical velocity for the updraft ( $j = 1$ ) and the downdraft ( $j = 2$ ) distributions ( $\text{m-s}^{-1}$ )
$w_s$	stack exit gas velocity ( $\text{m-s}^{-1}$ )
$w^*$	convective velocity scale ( $\text{m-s}^{-1}$ )
$w_{*u}$	urban nighttime convective velocity scale ( $\text{m-s}^{-1}$ )
$X$	non-dimensional downwind distance (dimensionless)
$x_r$	downwind distance to a receptor (m)
$x_f$	distance to final plume rise (m) - eq. (44) for the CBL; eq. (96) for the SBL
$x_m$	downwind distance at which plume material uniformly mixed throughout the boundary layer (m)
$(x_r, y_r, z_r)$	receptor location
$(x_t, y_t, z_t)$	terrain point location
$z_{base}$	user specified elevation for the base of the temperature profile (i.e., meteorological tower)
$z_c$	total height of the plume in the CBL considering both plume rise and effects from convective turbulence (m)
$z_i$	mixing height (m): $z_i = \text{MAX} [z_{ic}; z_{im}]$ in the CBL and $z_i = z_{im}$ in the SBL
$z_{ic}$	convective mixing height (m)
$z_{ie}$	equilibrium height of stable boundary layer
$z_{ieff}$	height of the reflecting surface in the SBL or in the stable layer above the above the CBL (m)
$z_{im}$	mechanical mixing height (m)
$z_{iu}$	urban nighttime boundary layer mixing height (m)
$z_{iuc}$	urban nighttime boundary layer mixing height due to convective effects alone (m)
$z_{msl}$	height of stack base above mean sea level (m)
$z_o$	surface roughness length (m)

$z_{PG}$	release height used in the Prairie Grass experiment (m)
$z_p$	receptor “flagpole” height - height of a receptor above local terrain (m)
$z_r$	height of the receptor above local source base (m)
$z_{ref}$	reference height for wind (m)
$z_{Tref}$	reference height for temperature (m)
$z_t$	height of the terrain above mean sea level (m)
$\tilde{\alpha}$	general symbol used to represent the effective parameters in the treatment of the inhomogeneous boundary layer. In the text the effective values of the parameters $u$ , $\sigma_w$ , $\sigma_v$ and $TL$ are denoted by underscoring the character
$\gamma$	parameter used to weight $C_{AERMOD}$ and $C_{Prime}$ in estimating concentrations that are influenced by building downwash (dimensionless)
$\theta$	potential temperature (K)
$\theta_*$	temperature scale (K)
$\lambda_j$	weighting coefficient for the updraft ( $j = 1$ ) and downdraft ( $j = 2$ ) distributions of eqs. (53),(59) and (65)
$\rho$	density of air ( $\text{kg m}^{-3}$ )
$\sigma_b$	buoyancy induced dispersion for the direct & indirect sources (m)
$\sigma_h^2$	total horizontal wind “energy” used in the meander algorithm ( $\text{m}^2$ )
$\sigma_r^2$	random “energy” component of the total horizontal wind “energy” used in the meander algorithm ( $\text{m}^2$ )
$\sigma_{SB}$	Stephen Boltzman constant ( $5.67 \times 10^{-8} \text{ Wm}^{-2}\text{K}^{-4}$ )
$\sigma_u$	along-wind turbulence ( $\text{m s}^{-1}$ )
$\sigma_v$	lateral turbulence ( $\text{m s}^{-1}$ )
$\sigma_{vc}$	convective portion of the lateral turbulence ( $\text{m s}^{-1}$ )
$\sigma_{vo}$	surface value of the lateral turbulence ( $\text{m s}^{-1}$ )
$\sigma_{vm}$	mechanical portion of the lateral turbulence ( $\text{m s}^{-1}$ )
$\sigma_{vT}$	total lateral turbulence ( $\text{m s}^{-1}$ )
$\sigma_w$	vertical turbulence ( $\text{m s}^{-1}$ )
$\sigma_{wc}$	convective portion of the vertical turbulence ( $\text{m s}^{-1}$ )
$\sigma_{wm}$	mechanical portion of the vertical turbulence ( $\text{m s}^{-1}$ )
$\sigma_{wml}$	mechanical portion of the vertical turbulence generated in the PBL ( $\text{m s}^{-1}$ )
$\sigma_{wmr}$	mechanical portion of the vertical turbulence above the PBL (residual) ( $\text{m s}^{-1}$ )
$\sigma_{wT}$	total vertical turbulence ( $\text{m s}^{-1}$ )
$\sigma_{xg}$	longitudinal dimension of the building wake (m)
$\sigma_y$	total lateral dispersion for the direct & indirect sources (m)
$\sigma_{ya,zaj}$	ambient turbulence induced dispersion for the direct & indirect sources (m)
$\sigma_{zas}$	ambient dispersion for the stable source (m)
$\sigma_{yg}$	distance from the building centerline to lateral edge of the building wake (m)
$\sigma_{yl}$	lateral spread from combined effects of ambient turbulence and building downwash (m)

$\sigma_{zp}$	total dispersion for the penetrated source (m)
$\sigma_{zs}$	total dispersion for the stable source (m)
$\sigma_{zaj}$	ambient vertical dispersion for the updraft & downdrafts plumes ( $j = 1,2$ ), respectively, for both the direct & indirect sources (m)
$\sigma_{zej}$	elevated portion of $\sigma_{zaj}$ (m)
$\sigma_{zes}$	elevated portion of $\sigma_{zas}$ (m)
$\sigma_{zg}$	height of the building wake at the receptor location (m)
$\sigma_{zj}$	total vertical dispersion for the updrafts and downdrafts ( $j = 1,2$ respectively), for both the direct and indirect sources
$\sigma_{zg}$	surface portion of $\sigma_{zaj}$ (m)
$\sigma_{zgs}$	surface portion of $\sigma_{zas}$ (m)
$\tau$	time constant controlling the temporal interpolation of $z_{im}$ (sec)
$\varphi$	solar elevation angle
$\varphi_p$	fraction of plume mass below $H_c$ (dimensionless)
$\Psi_{dj}$	total height of the direct source plume (i.e. release height + buoyancy + convection) (m)
$\Psi_{rj}$	total height of the indirect source plume (m)
$\psi_m$	similarity function for momentum (stability correction) - eq. (7) for the CBL and eq. (29) for the SBL (dimensionless)

## Appendix A. Input / output needs and data usage

### A.1 AERMET input data needs

Besides defining surface characteristics, the user provides several files of hourly meteorological data for processing by AERMET. At the present time AERMET is designed to accept data from any for the following sources: 1) standard hourly National Weather Service (NWS) data from the most representative site; 2) morning soundings of winds, temperature, and dew point from the nearest NWS upper air station; and 3) site-specific wind, temperature, turbulence, pressure, and radiation measurements (if available).

The minimum measured and/or derived data needed to run the AERMOD modeling system are as follows:

#### A.1.1 Meteorology

- wind speed ( $u$ );
- wind direction;
- cloud cover - opaque first then total ( $n$ );
- ambient temperature ( $t$ );
- morning sounding.

Cloud cover is also used in dry deposition calculations in the AERMOD model. Therefore, if cloud cover is missing and the Bulk Richardson Number Scheme is being used (see 3.3.1) then an equivalent cloud cover is calculated as follows, based on van Ulden and Holtslag (van Ulden and Holtslag 1985):

$$n_{eq} = \left( \frac{1 - \theta_*/0.09}{0.5} \right)^{0.5} \quad (114)$$

where  $\theta_*$  is the temperature scale as calculated from eq. (18).

### A.1.2 Directionally and/or Monthly Varying Surface Characteristics

- noon time albedo ( $r$ );
- Bowen ratio ( $B_o$ );
- roughness length ( $z_o$ ) -

For AERMET, the user can specify monthly variations of three surface characteristics. These include: the albedo ( $r$ ), which is the fraction of radiation reflected by the surface; the Bowen ratio ( $B_o$ ), which is the ratio of the sensible heat flux to the evaporation heat flux; and the surface roughness length ( $z_o$ ), which is the height above the ground at which the horizontal wind velocity is typically zero. Values for albedo and Bowen ratio should be based on a 10 km x 10 km area centered on the meteorological tower. Values for surface roughness should be based on a 1 km radius around the meteorological tower and can be differentiated for up to 12 wind sectors. Surface characteristics should be determined with the aid of the AERSURFACE program (U.S. Environmental Protection Agency, 2020). Refer to the AERSURFACE and AERMET User's Guides (U.S. Environmental Protection Agency, 2021a) for additional information on determining appropriate surface characteristic values.

### A.1.3 Other

- Latitude;
- longitude;
- time zone;
- wind speed instrument threshold for each data set ( $u_{th}$ ).

### A.1.4 Optional

- solar radiation;
- net radiation ( $R_n$ );
- profile of vertical turbulence ( $\sigma_w$ );
- profile of lateral turbulence ( $\sigma_v$ )

## **A.2 Selection and use of measured winds, temperature, and turbulence in AERMET**

### **A.2.1 Threshold Wind Speed**

The user is required to define a threshold wind speed ( $u_{th}$ ) for site-specific data sets. Although the current version of AERMOD cannot accept a separate  $u_{th}$  for NWS data, a separate  $u_{th}$  should be selected for each on-site data set being used.

### **A.2.2 Reference Temperature and Height**

The reference height for temperature ( $z_{Tref}$ ), and thus the reference temperature, is selected as the lowest level of data which is available between  $z_o$  & 100 m.

### **A.2.3 Reference Wind Speed and Height**

The reference height for winds ( $z_{ref}$ ), and thus the reference wind speed ( $u_{ref}$ ), is selected as the lowest level of data which is available between  $7 z_o$  & 100m. Although the current version of AERMOD cannot accept a separate  $z_{ref}$  for offsite data, we believe that a separate  $z_{ref}$  should be selected for each data set being used.

If no valid observation of the reference wind speed or direction exists between these limits the hour is considered missing and a message is written to the AERMET message file. For the wind speed to be valid its value must be greater than or equal to the threshold wind speed. AERMOD processes hours of invalid wind speed, e.g. calms, in the same manner as ISC (EPA calms policy).

All observed wind speeds in a measured profile that are less than  $u_{th}$  are set to missing and, are therefore, not used in the construction of the wind speed profile (profiling of winds is accomplished in AERMOD).

### **A.2.4 Calculating the Potential Temperature Gradient above the Mixing Height from Sounding Data**

AERMET calculates  $d\theta/dz$  for the layer above  $z_i$  as follows:

- If the sounding extends at least 500 m above  $z_i$  the first 500 m above  $z_i$  is used to determine  $d\theta/dz$  above  $z_i$ .
- If the sounding extends at least 250 m above  $z_i$  (but not 500 m) then the available sounding above  $z_i$  is used to determine  $d\theta/dz$  above  $z_i$ .
- AERMET limits  $d\theta/dz$  above  $z_i$  to a minimum of  $0.005 \text{ K m}^{-1}$ .
- If the sounding extends less than 250 m above  $z_i$  then set  $d\theta/dz = 0.005 \text{ K m}^{-1}$  (a default value).

#### A.2.5 Measured Turbulence

All measured turbulence values are passed to AERMOD if the hour is non-missing. This is true even for those levels where the wind speed is below  $u_{th}$ . Based on measurements with research grade instruments, reasonable minimum turbulence levels in non-calm conditions for vertical turbulence ( $\sigma_w$ ) and lateral turbulence ( $\sigma_v$ ) values are set by AERMOD to  $0.02 \text{ m s}^{-1}$  and  $0.2 \text{ m s}^{-1}$ , respectively. Although these lower limits are applied to the measured values of the turbulence the calculated profile values of  $\sigma_w$  and  $\sigma_v$  are not subjected to any lower limits. We do not restrict these estimated profiles because it would bias the calculation of the effective values of turbulence, which are averages through the layer between the receptor and the plume height, in determining the dispersion of the plume. However, as discussed in Section A.9, these limits are applied to the effective values of turbulence and wind speed.

#### A.2.6 Data Substitution for Missing On-Site Data

If on-site data are missing for an hour, the hour is considered missing unless the user specifies a substitute data set. AERMET does not default to NWS (or any other offsite) data.

### **A.3 Information passed by AERMET to AERMOD**

The following information is passed from AERMET to AERMOD for each hour of the meteorological data record.

- All observations of wind speed ( $u$ ); wind direction; ambient temperature ( $T$ ); lateral turbulence ( $\sigma_v$ ); & vertical turbulence ( $\sigma_w$ ) with their associated measurement heights.

- Sensible heat flux ( $H$ ), friction velocity ( $u^*$ ), Monin Obukhov length  $L$ ,  $z_{im}$  (for all hours),  $z_{ic}$  &  $w^*$  (for convective hours only),  $z_o$ ,  $r\{\phi\}$ , &  $B_o$ ,  $d\theta/dz$  (above  $z_i$ ),  $u_{ref}$ , wind direction at the reference height,  $z_{ref}$ , ambient temperature at the reference height ( $T_{ref}$ ) (not used in AERMOD), & the reference height for temperature ( $z_{Tref}$ )

#### A.4 Restrictions on the growth of the PBL height

AERMET restricts the growth of  $z_i$  to a reasonable maximum of 4000 m. This restriction applies to both calculated and measured mixing heights. Although mixing heights in excess of 4000 m may occur on rare occasions, in desert climates, the additional effect on surface concentration is most likely insignificant.

#### A.5 Initializing the mechanical mixing height smoothing procedure

If  $\{t + \Delta t\}$ , in eq. (26), is the first hour of the data set then no smoothing takes place. Furthermore, if a missing value occurs at time step  $t$  then smoothing is not performed at time step  $\{t + \Delta t\}$  but is restarted for subsequent hours.

#### A.6 Determining the mixing height when the sounding is too shallow

The left-hand side of eq. (22) is determined from the morning temperature sounding and the right-hand side from the daytime history of surface heat flux. When the temperature sounding, obtained from the NWS, does not reach a height which is greater than the convective mixing height, we must assume a profile for the potential temperature gradient in order to estimate  $z_{ic}$ . This is accomplished as follows:

- Determine  $d\theta/dz$  in the top 500 m layer of the sounding. However, if part of the 500 m layer is within the first 100 m of the PBL, the layer should be reduced (to a minimum thickness of 250 m) to avoid using the portion of the sounding that is below 100 m. If the above conditions cannot be satisfied, then  $z_{ic}$  is defined as missing.
- Extend the sounding by persisting  $d\theta/dz$  up and recomputing  $z_{ic}$ .
- Provide warning messages which tell users
  - the height of the actual sounding top,
  - that  $d\theta/dz$  has been extrapolated above the sounding  $z_{ic}$ , and

- that  $z_{ic}$  has been recomputed.
- Allow the user to reject the “fixed-up” value for  $z_{ic}$  by defining it as missing.

### A.7 Input data needs for AERMAP

The following data is required input for AERMAP

- DEM formatted terrain data (  $x_t, y_t, z_t$  ),
- Design of receptor grid; AERMAP accepts either polar, Cartesian or discrete receptors.

### A.8 Information passed by AERMAP to AERMOD

AERMAP passes the following parameters to AERMOD:  $x_r, y_r, z_r, z_t$ , & the height scale ( $h_c$ ) for each receptor.

### A.9 Wind speed and turbulence limits used in model calculations

When calculating the effective parameters, limits are placed on the such that:

$$\begin{aligned}\sigma_w\{z\} &= \text{Max}\left[\sigma_w\{z\}; 0.02 \text{ m s}^{-1}\right] \\ \sigma_v\{z\} &= \text{Max}\left[\sigma_v\{z\}; 0.05 u\{h_s\}; 0.2 \text{ m s}^{-1}\right].\end{aligned}\tag{115}$$

These limits are also applied when selecting the turbulence for plume rise calculations.

Dilution of the plume is determined by the wind that corresponds to the average over the magnitudes of the wind vectors during a given time interval. But measurements only give the vector averaged wind, which can be zero, even though the dilution wind is not zero. We can estimate the dilution wind by assuming that the vector wind,  $u_v$ , can be expressed as

$$u_v = (\bar{u} + u', v')\tag{116}$$

where  $\bar{u}$  is the mean measured wind, and the primed quantities refer to the turbulent fluctuations.

The assumption being made is  $\overline{u_v} = \overline{u}$ . If we assume that the measured velocity fluctuations correspond only to the angular variations of a constant vector,  $u_v$ , we can write from eq. (116) that

$$u_v^2 = \overline{u}^2 + \sigma_v^2 + \sigma_u^2. \quad (117)$$

In this simple model,  $u_v$ , is the dilution wind. If we take  $\sigma_u = \sigma_v$ , the dilution wind can be written as

$$u\{h_s\} = \sqrt{u\{h_s\}^2 + 2\sigma_v^2}. \quad (118)$$

This formulation assures that the dilution wind is not zero as long as either  $\overline{u}$  or  $\sigma_v$  is not zero. Similarly, at the time of plume rise calculations, the effective turbulence and effective wind speed will be recalculated using eqs. (115) and (118), where the turbulence and winds will be evaluated at stack top.

#### **A.10 Using profiles for interpolating between observations**

When observations are available AERMOD uses the similarity profile functions to interpolate adjacent measurements. Figure 17 illustrates how AERMOD's INTERFACE uses the expected shape of a meteorological profile to interpolate between observations.

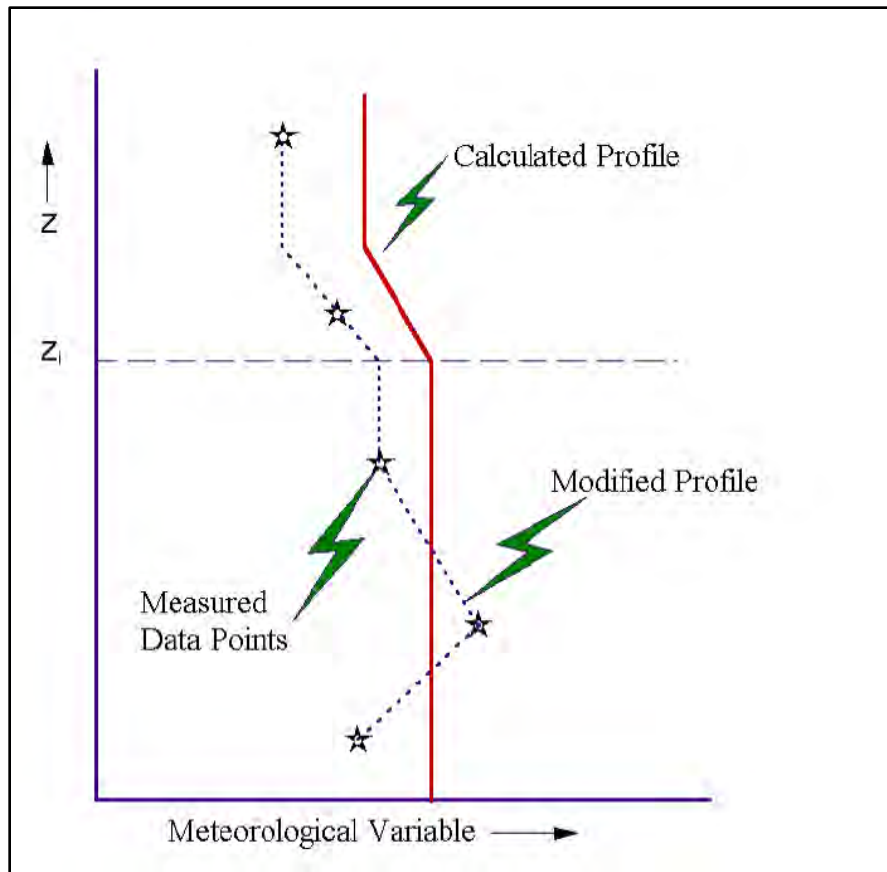


Figure 17. AERMOD's construction of a continuous meteorological profile by interpolating between observations.

For a gridded profile height between two observed profile heights, the observations are interpolated to the gridded height while maintaining the shape of the similarity profile. This is accomplished as follows:

1. the observations are linearly interpolated to the gridded profile height;
2. the similarity function is evaluated at the gridded profile height;
3. the similarity function is evaluated at the observed profile heights immediately above and below the grid height and linearly interpolated to the grid height;
4. the ratio of the value obtained in 2 to the value obtained in 3 is applied to the value obtained in 1.

For a gridded profile height above the highest observation, the procedure is modified slightly:

1. the observation at the highest observed profile height is extrapolated by persisting the value upward;
2. the similarity function is evaluated at the grid height;
3. the similarity function is evaluated at the highest height in the observed profile;
4. the ratio of the value obtained in 2 to the value obtained in 3 is applied to the value obtained in 1.

A similar procedure for extrapolating to heights above the observed profile is applied to heights below the lowest observed profile height.

### **A.11 Using measured mixing heights**

If measured mixing heights are available, then they are treated in the following manner: If  $L > 0$  (SBL) the measured mixing height is defined as  $z_{ie}$  and it is treated the same as a calculated mechanical mixing height. If  $L < 0$  (CBL) the measured mixing height is defined as  $z_{ic}$ , and  $z_{ie}$  is calculated from eq. (24), smoothed, then proceed as if both  $z_{ic}$  and the smoothed  $z_{im}$  had been calculated values.

If a user has “measured” mixing heights available (and chooses to use them), AERMET defaults to substituting calculated mixing heights for missing measurements and a message is written that a substitution has occurred. If the user elects to substitute calculations for missing measurements, AERMET will print out a message to the message file for each hour that a substitution has occurred.

## **Appendix B. Model evaluation results**

### **B.1 Introduction**

This evaluation presents a benchmark of model performance based on the original field studies presented in Cimorelli, et al, 2005 and Perry, et al, 2005. The evaluation focused on the performance of the final (16216) versions of the AERMOD modeling system associated with the 2016 update to the *Guideline on Air Quality Models* and previous update (18081). The statistical analysis determines the best performing version of the model for 14 of the original 17 databases, including the adjust u\* option formally adopted as a regulatory option in the final version of AERMOD (16216r).

### **B.2 Database descriptions**

The 14 databases used in this evaluation are briefly described in this section and summarized in Table 1. The stack heights, terrain complexity, urban/rural status, importance of downwash, inclusion of turbulence parameters and meteorological data included for the database are listed for each area. A more complete description of these databases can be found in U.S. EPA, 2003. The databases are arranged by the following hierarchy: Two categories of turbulence inclusion (inclusion of turbulence or no turbulence). Within each of those categories, databases were ordered by complexity of terrain (complex or flat), and within those two categories, databases were ordered by increasing height.

Table 1. AERMOD evaluation databases used for comparisons of AERMOD 15181 and AERMOD 16216. Databases in gray are also subject to the EPA's protocol for determining best performing model.

Location	Stack heights	Urban /rural	Terrain	Downwash	Turbulence parameters	Site specific AERMET inputs
Martins Creek	59, 76, 183 m	Rural	Complex	Yes	10 m $\sigma_v$ , $\sigma_w$	10m wind, temperature; 90-420 m wind (every 30 m).
Tracy	91 m	Rural	Complex	No	$\sigma_v$ , $\sigma_w$	10 and 50-400 m (every 25 m) wind, temperature
Lovett	145 m	Rural	Complex	No	$\sigma_v$ , $\sigma_w$	10, 50, and 100 m wind, temperature
Westvaco	190 m	Rural	Complex	No	$\sigma_v$ , $\sigma_w$	30, 210, 326, 366, and 416 m wind, temperature <sup>1</sup>
DAEC	1 m, 24 m, 46 m	Rural	Flat	Yes	$\sigma_v$	Insolation, 10, 23.5 and 50 m wind, temperature
EOCR	1, 25, 30 m	Rural	Flat	Yes	$\sigma_v$	4, 10, and 30 m wind, temperature
Alaska	39.2 m	Rural	Flat	Yes	$\sigma_v$ , $\sigma_w$	33 m wind, temperature
Indianapolis	84 m	Urban	Flat	No	$\sigma_v$ , $\sigma_w$	Station pressure, net radiation, 10 m wind, temperature
Kincaid	187 m	Rural	Flat	No	$\sigma_v$ , $\sigma_w$	Net radiation, insolation, 10 , 30, and 50 m wind, temperature
AGA	9.8, 14.5, 24.4 m	Rural	Flat	Yes	None	10 m wind and temperature
Millston	3 stacks 29 m (freon) 48 m (SF6)	Rural	Flat	Yes	None	10 m wind speed ; 43.3 m wind and temperature
Bowline	2 stacks 86.87 m	Rural	Flat	Yes	None	100 m winds and temperature
Baldwin	3 stacks 184.4 m	Rural	Flat	Yes	None <sup>2</sup>	10 and 100 m wind, temperature
Clifty Creek	3 stacks 207.9 m	Rural	Flat/Elev	No	None	10 m temperature; 60 m wind

- 1. 30 m observations removed from AERMOD profile before running AERMOD.

### B.2.1 Martin's Creek

The Martins Creek Steam Electric Station is located in a rural area along the Delaware River on the Pennsylvania/New Jersey border, approximately 30 km northeast of Allentown, PA and 95 km north of Philadelphia, PA (Figure B-1). The area is characterized by complex terrain rising above the stacks. Sources included multiple tall stacks ranging from 59 to 183 m in height, including Martins Creek and three background sources located between 5 and 10 km from Martins Creek. The seven SO<sub>2</sub> monitors were located on Scotts Mountain, which is about 2.5 - 8 km southeast of the Martins Creek facility. On-site meteorological data covered the period from 1 May 1992 through 19 May 1993. Hourly temperature, wind speed, wind direction, and sigma-theta (standard deviation of the horizontal wind direction) at 10 m were recorded from an instrumented tower located in a flat area approximately 2.5 km west of the plant. In addition, hourly multi-level wind measurements were taken by a sodar located approximately three km southwest of the Martins Creek station.

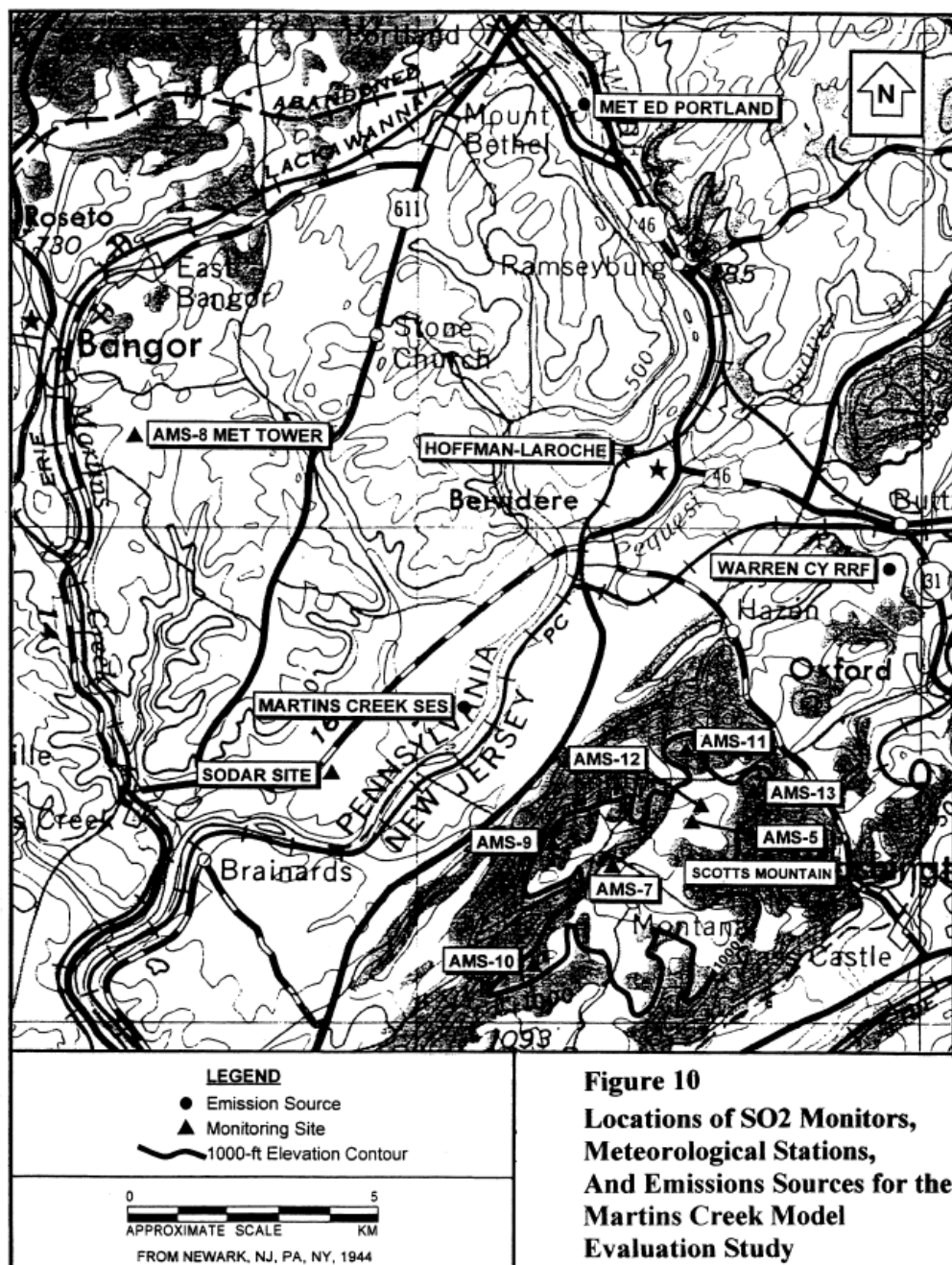


Figure B-1. Martin's Creek study area.

### B.2.2 Tracy

The Tracy Power Plant is located 27 km east of Reno, Nevada in the rural Truckee River valley completely surrounded by mountainous terrain (Figure B-2). A field tracer study was conducted at the power plant in August 1984 with SF<sub>6</sub> being released with the moderately buoyant plume from a 91-m stack. A total of 128 hours of data were collected over 14 experimental periods. Stable atmospheric conditions were dominant for this study. Site-specific meteorological data (wind, temperature, and turbulence) for Tracy were collected from an instrumented 150-m tower located 1.2 km east of the power plant. The wind measurements from the tower were extended above 150 meters using a Doppler acoustic sounder and temperature measurements were extended with a tether sonde.

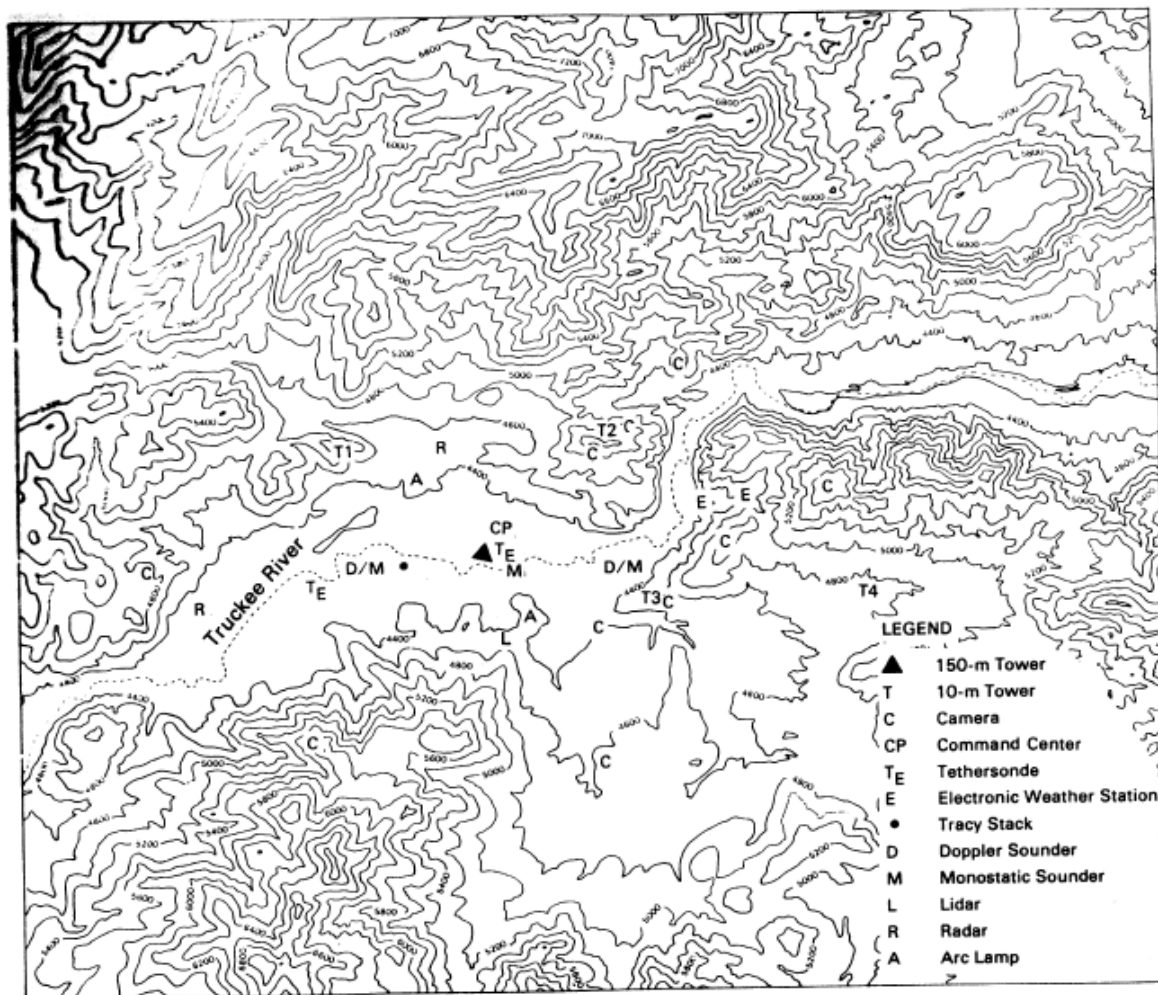


Figure B-2. Tracy power plant study area.

### B.2.3 Lovett

The Lovett Power Plant study consisted of a buoyant, continuous release of SO<sub>2</sub> from a 145-m tall stack located in a complex terrain, rural area in New York State (Figure B-3). The data spanned one year from December 1987 through December 1988. Data were collected from 12 monitoring sites (ten on elevated terrain and two near stack-base elevation) that were located about 2 to 3 km from the plant. The monitors provided hourly-averaged concentrations. The important terrain features rise approximately 250 m to 330 m above stack base at about 2 to 3 km downwind from the stack. Meteorological data include winds, turbulence, and  $\Delta T$  from a tower instrumented at 10 m, 50 m, and 100 m. National Weather Service surface data were available from a station 45 km away.

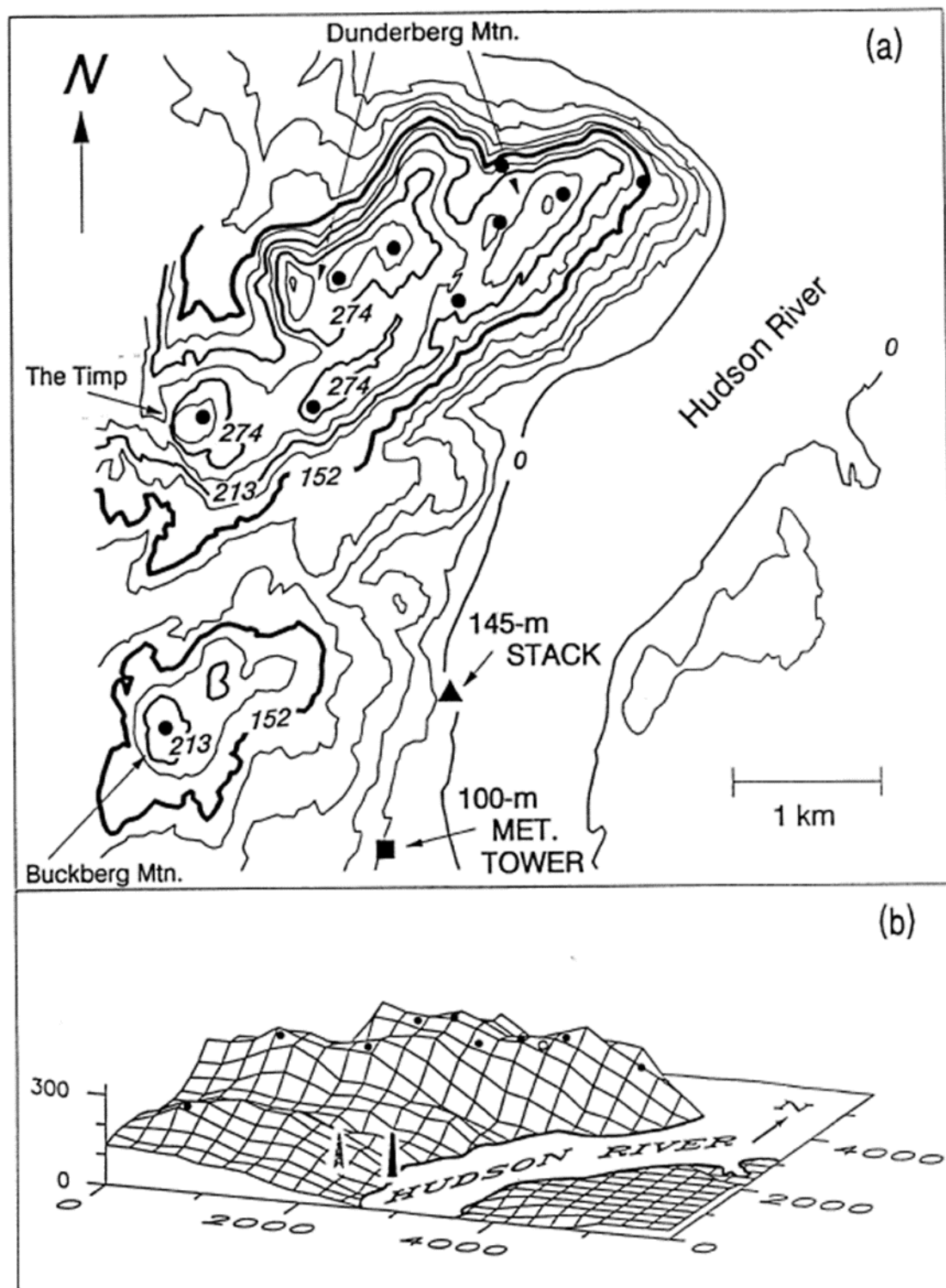


Figure B-3. Lovett study area.

#### B.2.4 Westvaco

The Westvaco Corporation's pulp and paper mill in rural Luke, Maryland is located in a complex terrain setting in the Potomac River valley (Figure B-4). A single 183-m buoyant source was modeled for this evaluation. There were 11 SO<sub>2</sub> monitors surrounding the facility, with eight monitors well above stack top on the high terrain east and south of the mill at a distance of 800 - 1500 m. Hourly meteorological data (wind, temperature, and turbulence) were collected between December 1980 and November 1991 at three instrumented towers: the 100-m Beryl tower in the river valley about 400 m southwest of the facility; the 30-m Luke Hill tower on a ridge 900 meters north-northwest of the facility; and the 100-m Met tower located 900 m eastsoutheast of the facility on a ridge across the river.

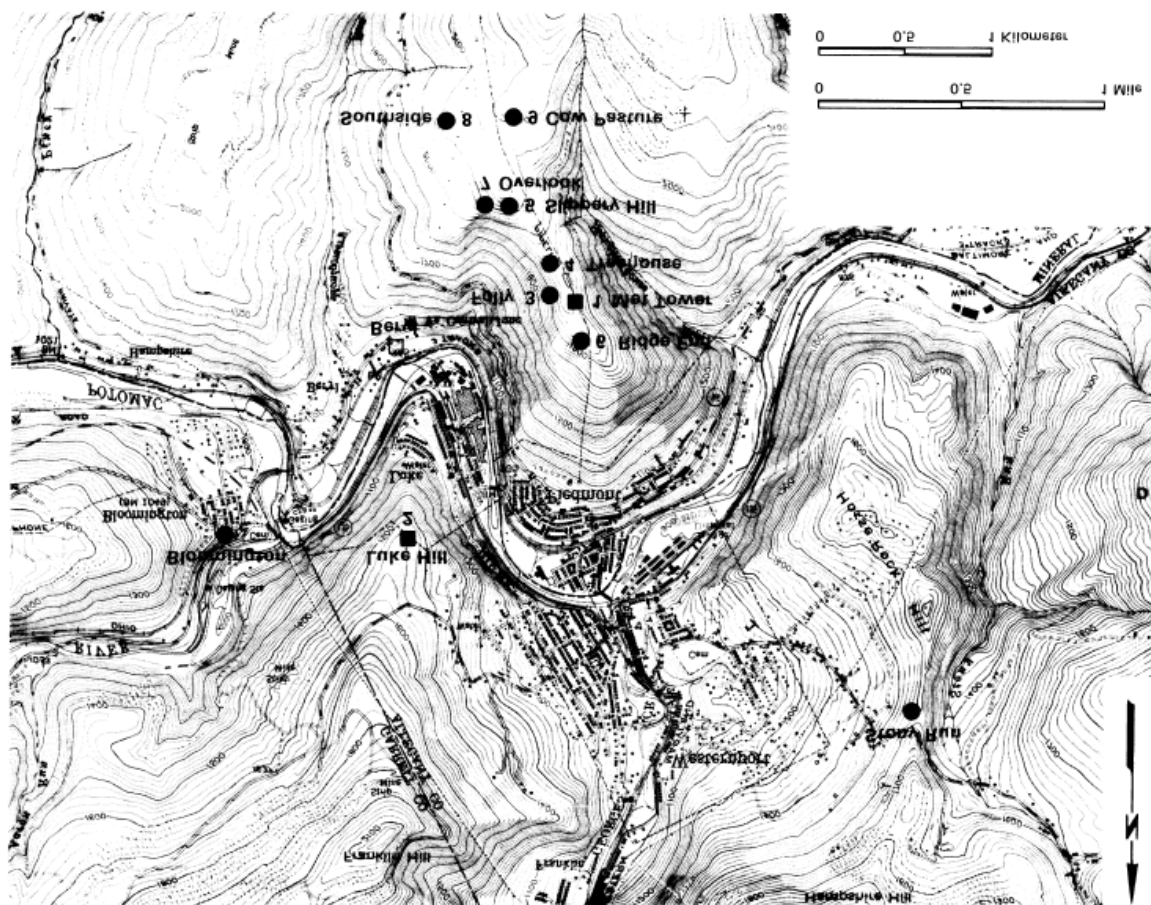


Figure B-4. Westvaco study area.

### B.2.5 DAEC

The Duane Arnold Energy Center (DAEC) is located in rural Iowa, located about 16 km northwest of Cedar Rapids. It is located in a river valley with some bluffs on the east side. Terrain varies by about 30 m across the receptor network with the eastern half of the semicircular receptor arcs being flat and the western half elevated. The tracer study<sup>35</sup> involved SF<sub>6</sub> releases from two rooftops (46-m and 24-m levels) and the ground (1-m level). Building tiers for the rooftop releases were 43 and 24 m high, respectively. The 1-m and 24-m releases were non-buoyant, non-momentum, while the 46-m release was close to ambient, but had about a 10 m/s exit velocity. The number of tracer release hours was 12, 16 and 11 from the release heights of 46 m, 24 m, and 1 m, respectively. There were two arcs of monitors at downwind distances of 300 and 1000 m (see Figure B-5). Meteorological data consisted of winds at 10, 24, and 50 m. The meteorological conditions were mostly convective (30 out of 39 hours), with fairly light wind speeds. Only one hour had a wind speed above 4 m/s (4.6) , and almost half of the hours were less than 2 m/s.

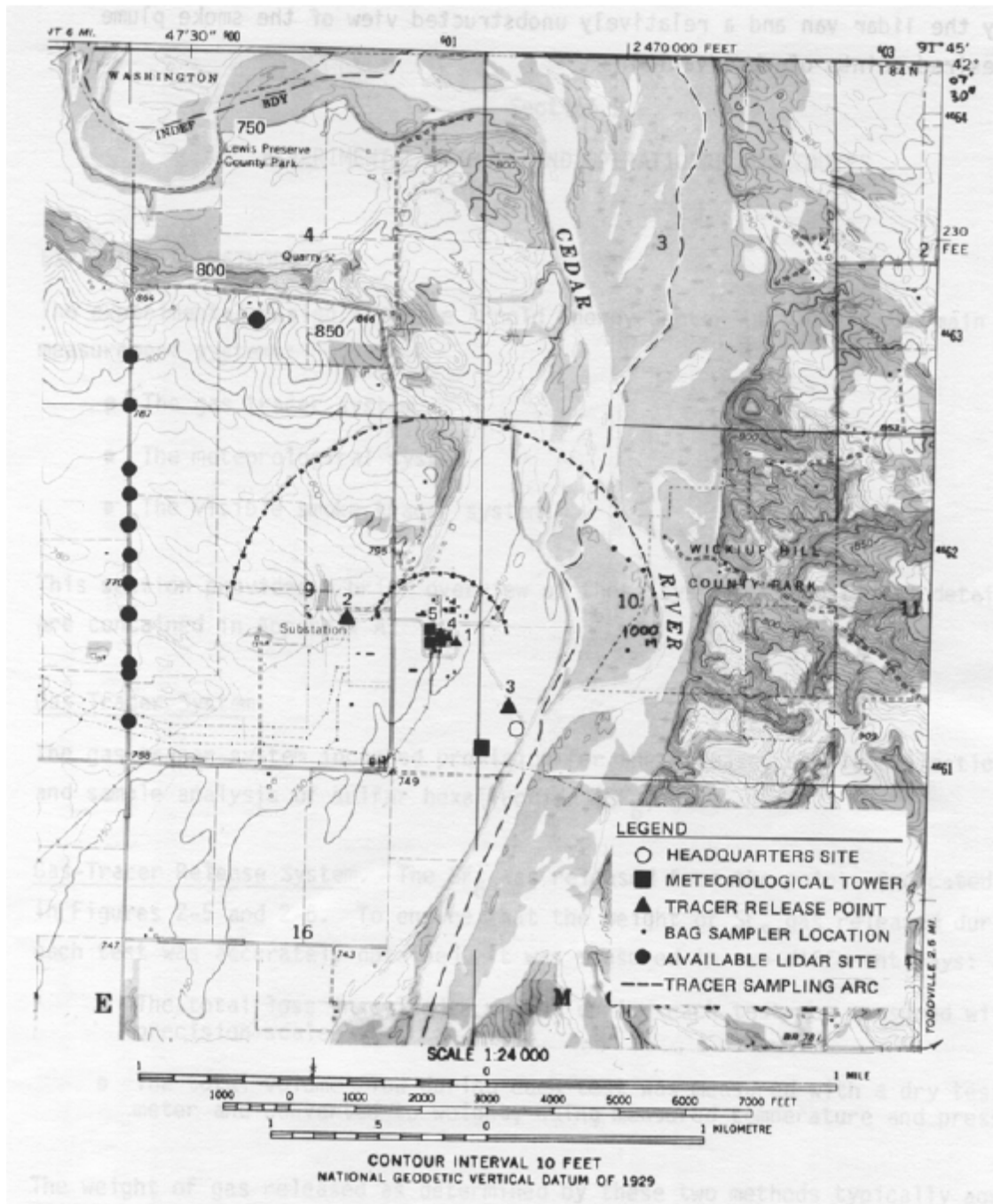


Figure B-5. DAEC study area (SF<sub>6</sub> releases).

### B.2.6 EOCR

The EOCR study involved the simultaneous release of three tracer gases (SF<sub>6</sub>, F<sub>12</sub>, and Freon-12B<sub>2</sub>) at three levels around the Experimental Organically Cooled Reactor (EOCR) test reactor building at the Idaho National Engineering Laboratory in Southeast Idaho. The terrain

was flat with low-lying shrubs. The main building was 25 m high with an effective width of 25 m. The tracer releases typically occurred simultaneously and were conducted during 22 separate time periods. Tracer sampler coverage was provided at eight concentric rings at distances of about 50, 100, 200, 400, 800, 1200, and 1600 m from the release points (see Figure B-6). The stability classes ranged from stable to unstable. The 10-m wind speeds for the cases selected ranged from 3 to 8 m/s.

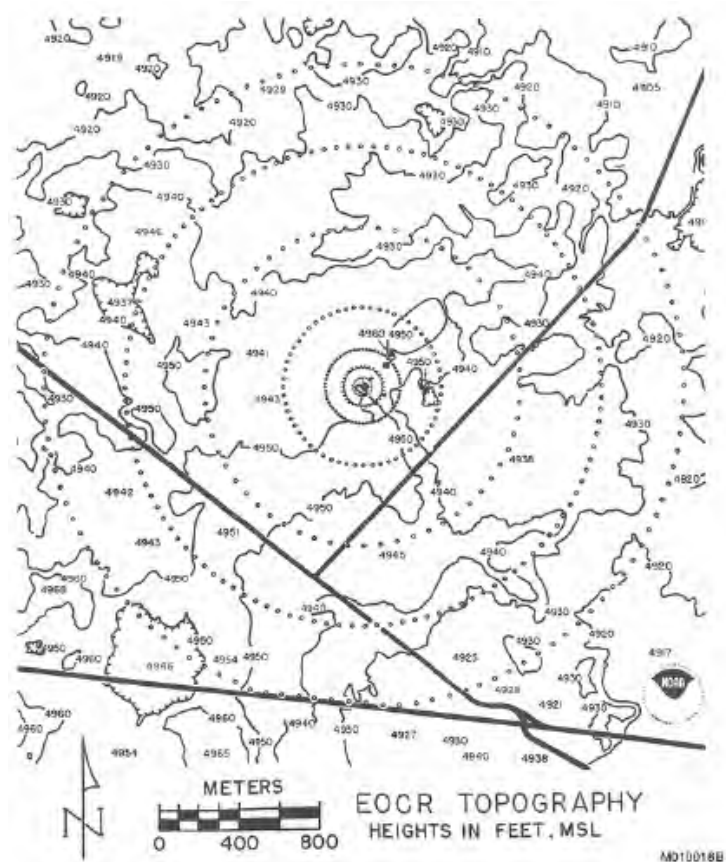


Figure B-6. Terrain map featuring the entire EOCR grid with the source at the grid center ( $\text{SF}_6$  releases). Arcs are at distances of about 40, 80, 200, 400, 800, 1200, and 1600 m.

### B.2.7 Alaska

The Alaska North Slope tracer study (see Figure B-7) involved 44 hours of buoyant  $\text{SF}_6$  releases from a 39-m high turbine stack. Tracer sampler coverage ranged over seven arcs from 50 to 3,000 m downwind. Meteorological data, including wind speed, wind direction, temperature, sigma-theta, and sigma-w, were available from an on-site tower at the 33-m level.

Atmospheric stability and wind speed profiles were influenced by the smooth snow-covered tundra surface with negligible levels of solar radiation in the autumn months. All experiments (44 usable hours) were conducted during the abbreviated day light hours (0900 – 1600). Wind speeds taken at the 33-m level during the tests were less than 6 m/s during one and part of another test, between 6 and 15 m/s during four tests, and in excess of 15 m/s during three tests. Stability conditions were generally neutral or slightly stable.

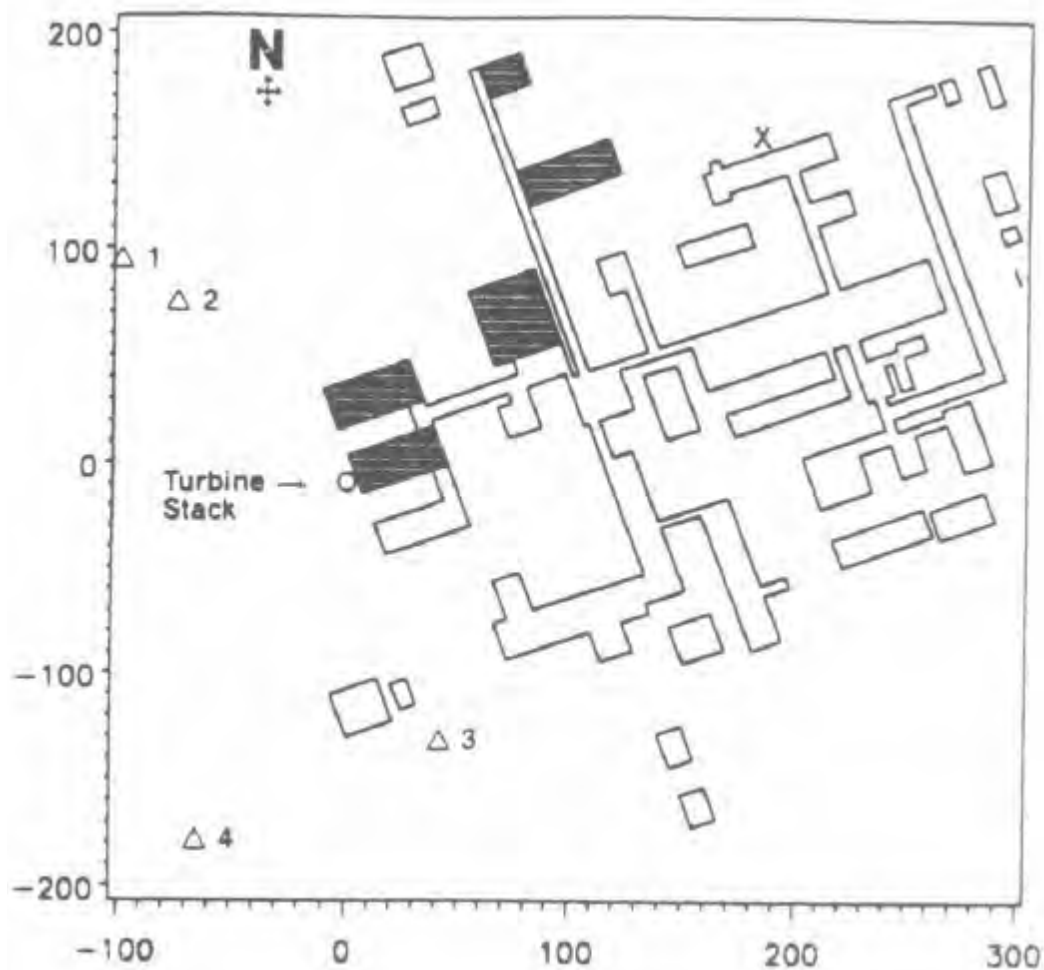


Figure B-7. Depiction of Alaska North Slope Oil Gathering Center turbine stack, meteorological tower (X), and camera locations used to visualize plume rise.

### B.2.8 Indianapolis

The Indianapolis study consisted of an elevated, buoyant tracer (SF<sub>6</sub>) released in a flat-terrain urban to suburban area from a single 84-m stack (Figure B-8). Data are available for approximately a four- to five-week period with 177 monitors providing 1-hour averaged samples along arcs from 250 m to 12 km downwind for a total of 1,297 arc-hours.

Meteorological data included wind speed and direction, sigma-theta on a 94-meter tower; and wind speed,  $\Delta T$  (2m - 10m) and other supporting surface data at three other 10-m towers (Figure B-9). Observed plume rise and estimates of plume sigma-y are also available from the database.



Figure B-8. Map showing the location of the Perry-K Station (A), the Hoosier Dome (B), and the central Indianapolis business district (C). The downtown surface meteorological site is located at (D) and the "bank tower" site was on top of the building at (E).

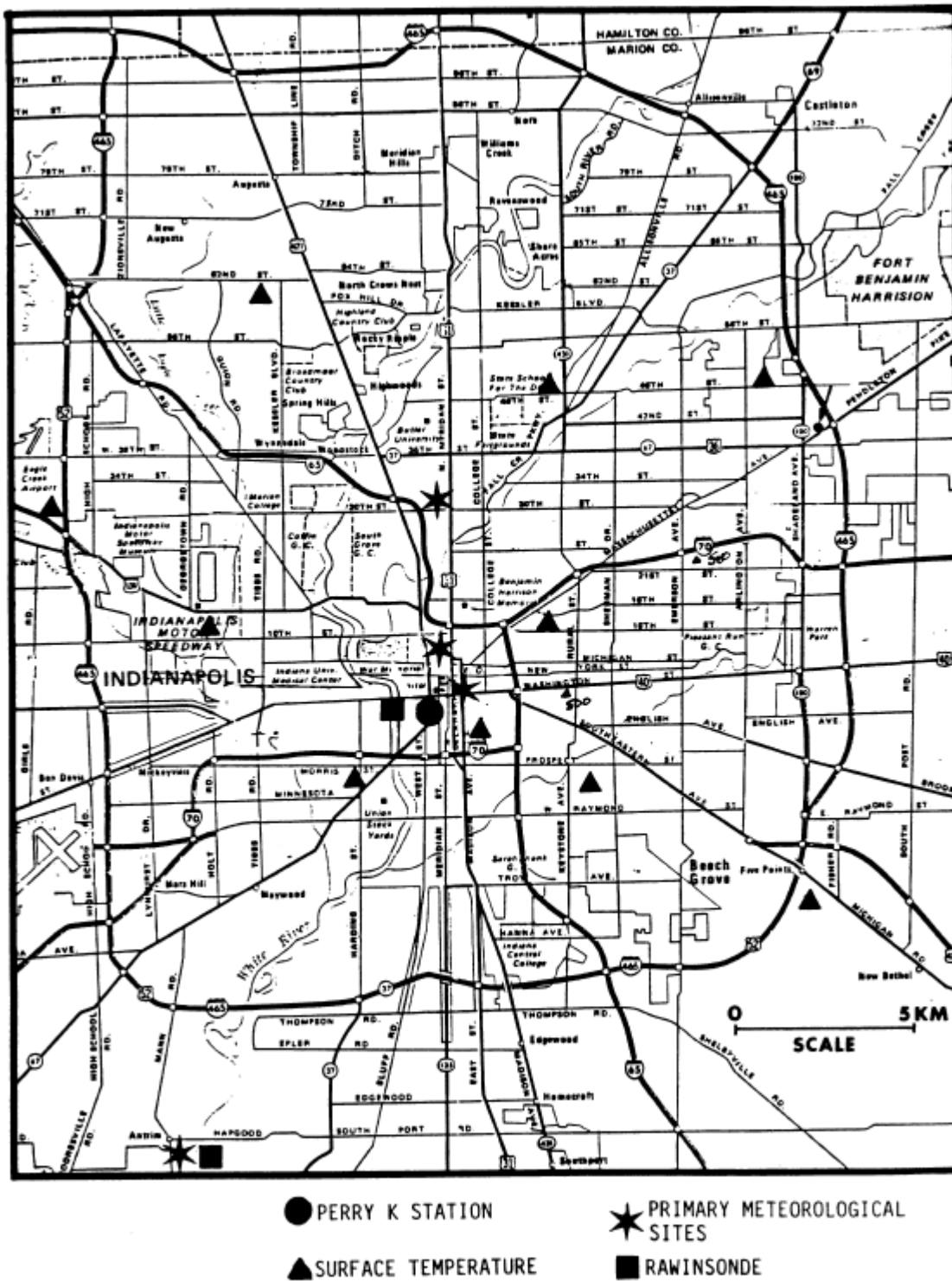


Figure B-9. Indianapolis meteorological sites and emissions site (Perry K Station).

### B.2.9 Kincaid

The Kincaid SO<sub>2</sub> study was conducted in a flat rural area of Illinois. It involved a buoyant, continuous release of SO<sub>2</sub> from a 187-m stack in rural flat terrain. The study included about six months of data between April 1980 and June 1981 (a total of 4,614 hours of samples). There were 30 SO<sub>2</sub> monitoring stations providing 1-hour averaged samples from about 2 km to 20 km downwind of the stack. Meteorological data included wind speed, direction, and temperature from a tower instrumented at 2, 10, 50, and 100 m levels, and nearby National Weather Service (NWS) data.

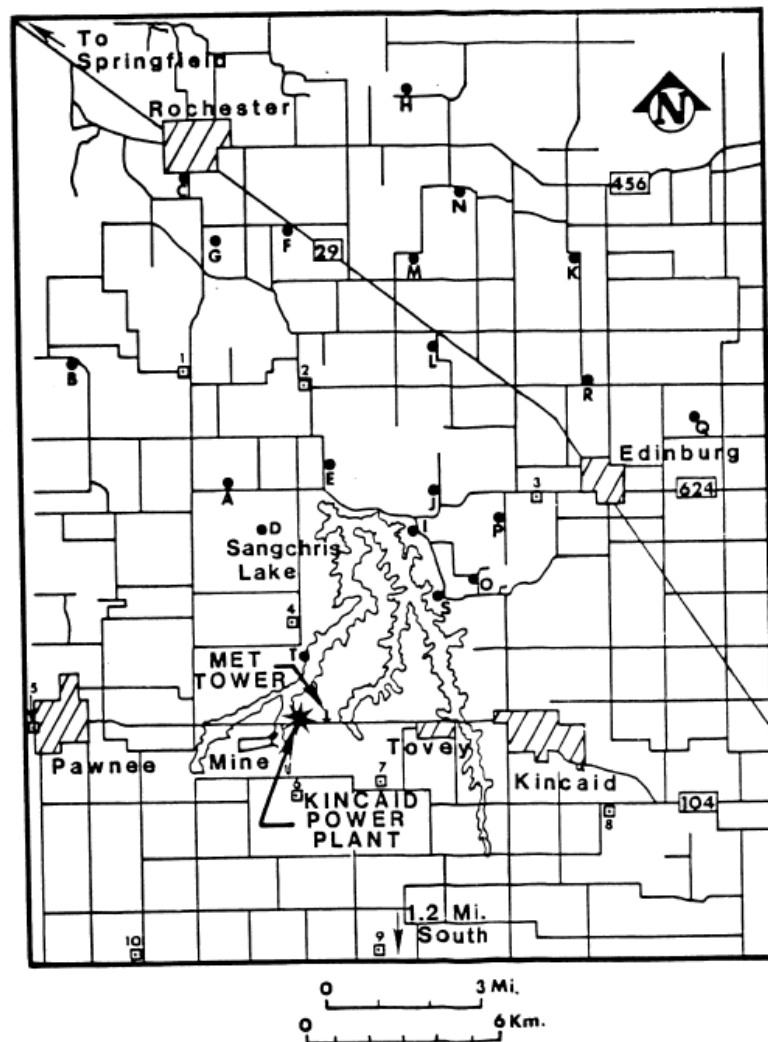


Figure B-10. Kincaid study area.

### B.2.10 AGA

The AGA experiments<sup>39</sup> occurred during spring and summer 1980 at gas compressor stations in Texas and Kansas. At each test facility, one of the gas compressor stacks was retrofitted to accommodate SF<sub>6</sub> tracer gas emissions. In addition, stack height extensions were provided for some of the experiments (with the normal stack height close to 10 m). The stack height to building height ratios for the tests ranged from 0.95 to 2.52. There were a total of 63 tracer releases over the course of the tests, and the tracer samplers were located between 50 and 200 m away from the release point (see Figure B-11). An instrumented 10-m tower was operated at both experimental sites. The tracer releases were generally restricted to daytime hours. Stability classes range from neutral to extremely unstable, except for three hours that were slightly stable. Wind speeds range from 2 to 11 m/s over the 63 hours.

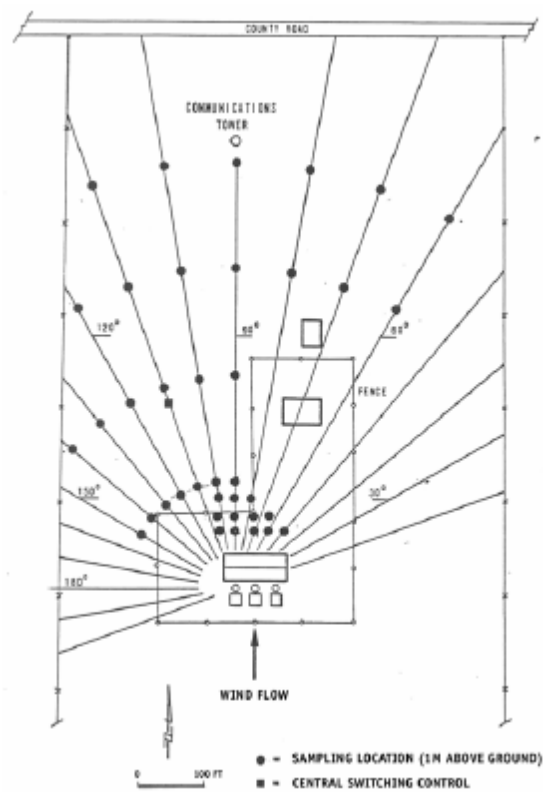


Figure B-11. Plan view of the locations of tracer samplers at Site 1, AGA field study (SF<sub>6</sub> releases)

### B.2.11 Millstone

The Millstone nuclear power plant is located on the Connecticut coast, near Niantic. The model evaluation database features 36 hours of SF<sub>6</sub> emissions from a 48-m reactor stack and 26 hours of Freon emissions from a 29-m turbine stack. Exit temperatures were close to ambient (about 295K) with exit velocities of about 10 m/s for both the reactor stack (48.3 m) and the three turbine stacks (29.1 m). These stacks were associated with 45-m and 28-m building tiers, respectively. The monitoring data consisted of three arcs at 350, 800 and 1,500 m. Meteorological data were available from an on-site tower at the 10-m and 43-m levels. There was about an even split between stable and unstable hours, with mostly on-shore winds and fairly high wind speeds. There were only 3 stable hours with wind speed less than 4 m/s, and the majority was above about 7 m/s and several above 10 m/s. Figure B-12 shows the layout of the study area.

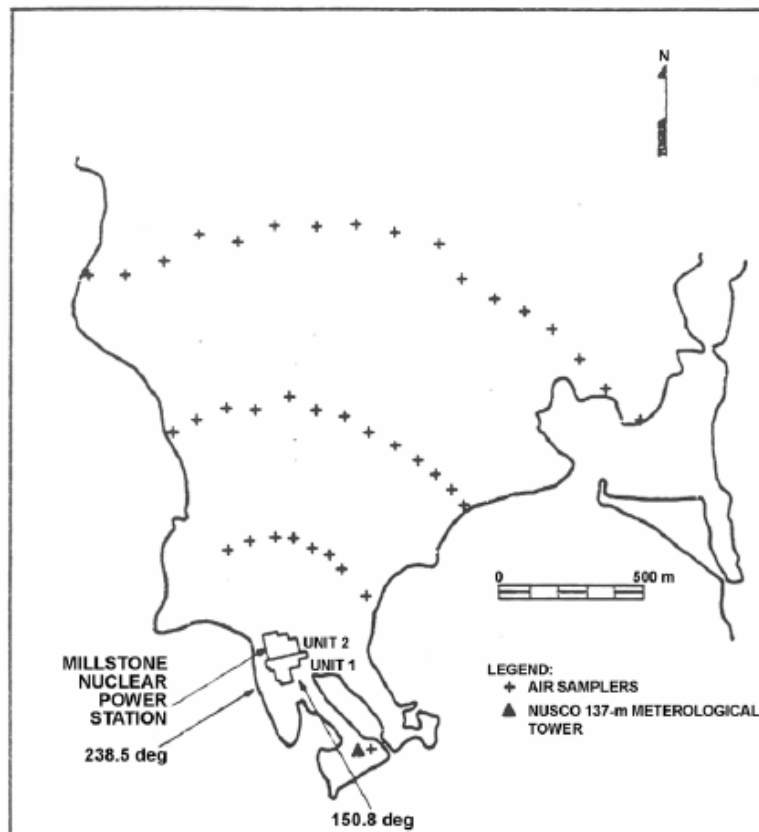


Figure B-12. Millstone study area (SF<sub>6</sub> and freon releases)

### B.2.12 Bowline

The Bowline Point site<sup>33</sup>, located in the Hudson River valley in New York State, is shown in Figure B-13 (topographic map). The electric utility site included two 600-MW units, each with an 86.9-m stack and a dominant roof tier with a height of 65.2 m high in a rural area. There were four monitoring sites as shown in Figure B-13 that ranged from about 250 to 850 m from the stacks. Hourly emissions data was determined from load data, coal analyses, and site-specific relationships between loads and fuel consumption. Meteorological data was obtained from a 100-m tower at the site. This site was also used as an independent evaluation database with the entire year included.



Figure B-13. Bowline Point study area (SO<sub>2</sub> releases)

### B.2.13 Baldwin

The Baldwin Power Plant is located in a rural, flat terrain setting of southwestern Illinois and has three identical 184-m stacks aligned approximately north-south with a horizontal spacing of about 100 m. There were 10 SO<sub>2</sub> monitors that surrounded the facility, ranging in distance from two to ten km. On-site meteorological data was available during the study period of 1 April 1982 through 31 March 1983 and consisted of hourly averaged wind speed, wind

direction, and temperature measurements taken at 10 m and wind speed and wind direction at 100 m.

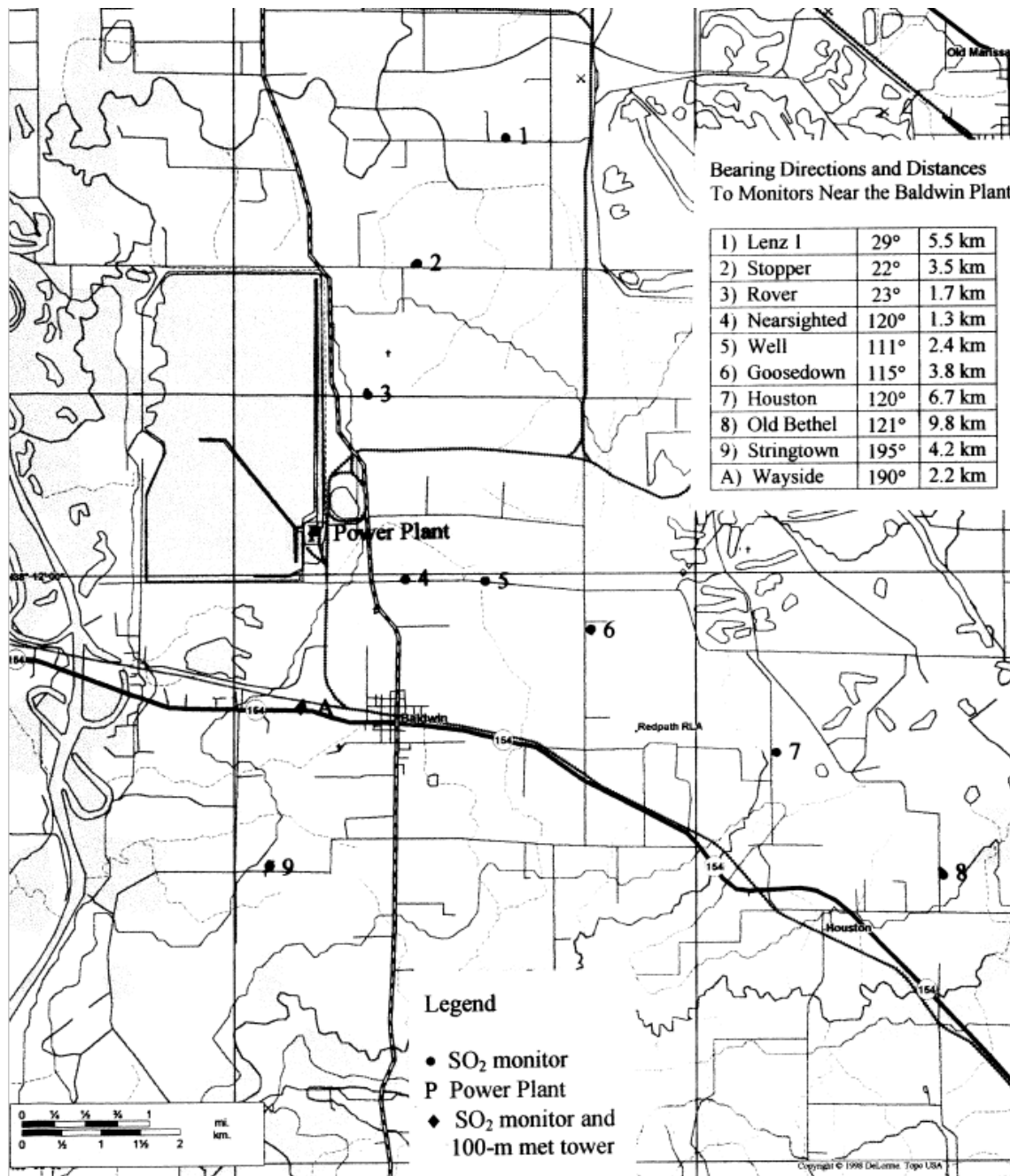


Figure B-14. Baldwin study area.

#### B.2.14 Clifty Creek

The Clifty Creek Power Plant is located in rural southern Indiana along the Ohio River with emissions from three 208-m stacks during this study (Figure B-15). The area immediately north of the facility is characterized by cliffs rising about 115 m above the river and intersected by creek valleys. Six nearby SO<sub>2</sub> monitors (out to 16 km from the stacks) provided hourly averaged concentration data. Meteorological data from a nearby 60-m tower covered the two-year period from 1 January 1975 through 31 December 1976, although only the data from 1975 were used in this evaluation. This database was also used in a major EPA-funded evaluation of rural air quality dispersion models in the early 1980s.

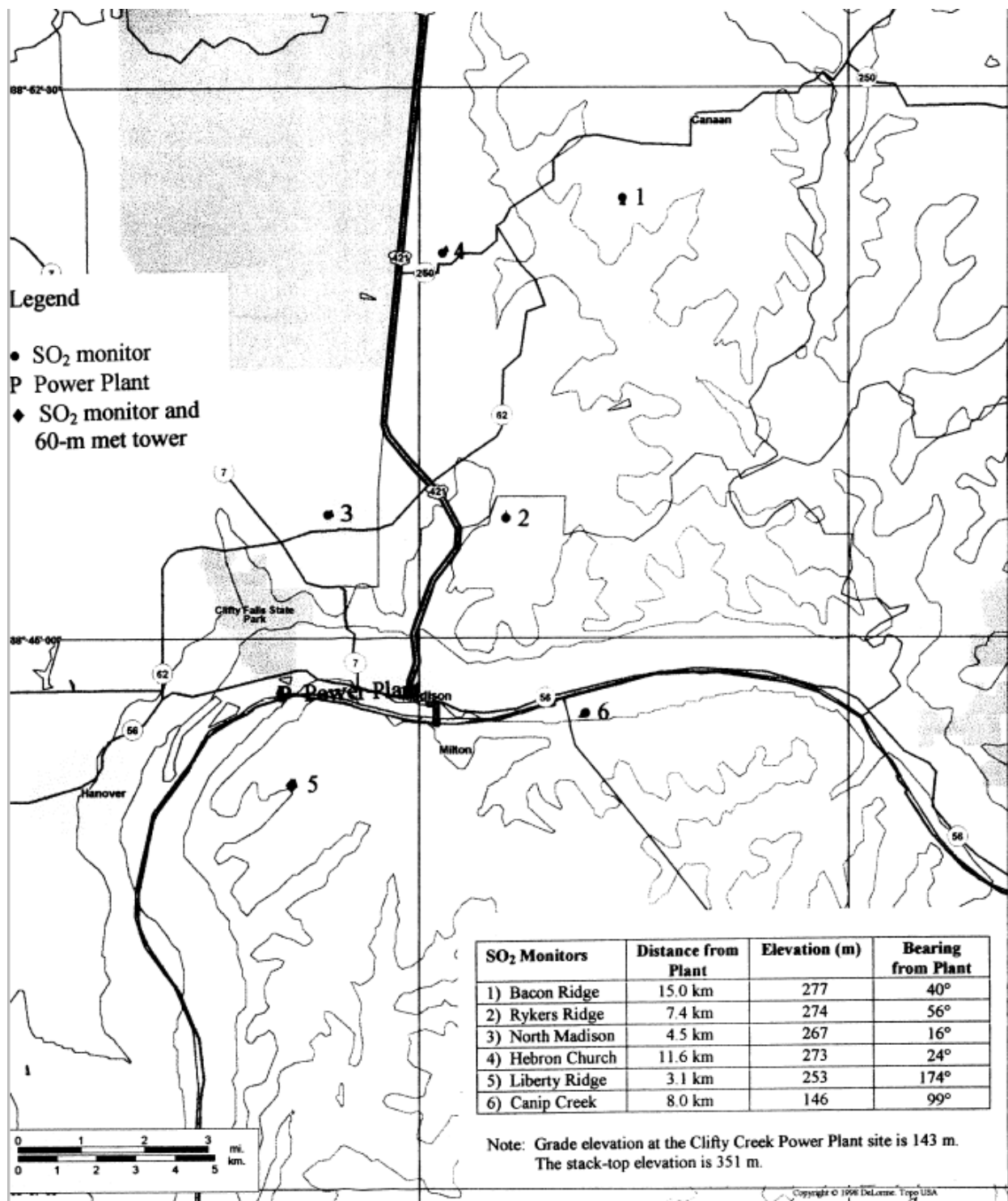


Figure B-15. Clifty Creek study area.

### B.3 Evaluation methodology

#### B.3.1 AERMET/AERMOD comparisons

Two versions of AERMET/AERMOD will be compared using Robust highest concentrations and the EPA Protocol for determining best performing model. AERMET 18081/AERMOD 18081 will be compared against AERMET 19191/AERMOD 19191 with various combinations of adjusted or non-adjusted surface friction velocity ( $u^*$ ) and inclusion/exclusion of turbulence parameters ( $s_v$  and  $s_w$ ). The modeled scenarios are:

- 18081\_no\_u\*\_with\_turb: AERMET/AERMOD 18081 with no  $u^*$  adjustment and turbulence included in the meteorological data
- 18081\_no\_u\*\_no\_turb: AERMET/AERMOD 18081 with no  $u^*$  adjustment and no turbulence included in the meteorological data
- 19191\_no\_u\*\_with\_turb: AERMET/AERMOD 19191 with no  $u^*$  adjustment and turbulence included in the meteorological data
- 19191\_with\_u\*\_no\_turb: AERMET/AERMOD 19191 with  $u^*$  adjustment and no turbulence included in the meteorological data.
- 19191\_no\_u\*\_no\_turb: AERMET/AERMOD 19191 with no  $u^*$  adjustment and no turbulence included in the meteorological data.

### B.4 Evaluation procedures

#### B.4.1 Robust highest concentrations

Robust highest concentrations (RHC) were calculated for each averaging period of each database. The RHC statistic is calculated as:

$$RHC = X(N) + [\bar{X} - X(N)] \times \ln \left[ \frac{3N - 1}{2} \right] \quad (119)$$

where  $X(N)$  is the Nth largest value,  $\bar{X}$  is the average of N-1 values, and N is the number of values exceeding the threshold value, usually 26.

For the 1-hour RHC, the RHC is calculated based on N=26 across all modeled and monitored values, i.e. not paired in time or space. For the 3-hour and 24-hour the RHC is calculated separately for each monitor within the network for observations and modeled values. The highest observed RHC is then compared to the highest modeled RHC.

#### B.4.2 EPA Protocol for determining best performing model

AERMOD output among the different meteorological datasets was evaluated using the EPA Protocol for determining the best performing model, or Cox-Tikvart method (U.S. EPA, 1992; Cox and Tikvart, 1990). The protocol uses a two-step process for determining the better performing model when comparing models. The first step is a screening test that fails to perform at a minimal operational level. The second test applies to those models that pass the screening test that uses bootstrapping to generate a probability distribution of feasible outcomes (U.S. EPA, 1992). This section will discuss the methodology using the evaluation cases as examples.

The first step is to perform a screening test based on fractional bias:

$$FB = 2 \left[ \frac{OB - PR}{OB + PR} \right] \quad (120)$$

where FB is the fractional bias, OB is the average of the highest 25 observed concentrations and PR is the average of the highest 25 predicted averages. The fractional bias is also calculated for the standard deviation where OB and PR refer to the standard deviation of the highest 25 observed and predicted concentrations respectively. This is done across all monitors and modeled receptors, unpaired in time and space for the 3-hour and 24-hour averaging periods. The fractional bias of the means is plotted against the fractional bias of the standard deviation. Biases that exceed a factor-of-two under-prediction or over-prediction are considered grounds for excluding a model for further evaluation (U.S. EPA, 1992).

Models that pass the screening test are subjected to a more comprehensive statistical comparison that involves both an operational and scientific component using the RHC (Eq. 1). For the evaluations presented here, the screening step was skipped. The operational component is to measure the model's ability to estimate concentration statistics most directly used for regulatory purposes and the scientific component evaluates the model's ability to perform

accurately throughout the range of meteorological conditions and the geographic area of concern (U.S. EPA, 1992).

The operational component of the evaluation compares performance in terms of the largest network-wide RHC test statistic. The RHC is calculated separately for each monitor within the network for observations and modeled values. The highest observed RHC is then compared to the highest modeled RHC using equation 2, where RHC now replaces the means of the top 25 values of observed or modeled concentrations. Absolute fractional bias (the absolute value of fractional bias), AFB is calculated for 3 and 24-hour averages.

The scientific component of the evaluation is also based on absolute fractional bias but the bias is calculated using the RHC for each meteorological condition and monitor. The meteorological conditions are a function of atmospheric stability and wind speed. For the purposes of these studies, six unique conditions were defined based on two wind speed categories (below and above 2.0 m/s) and three stability categories: unstable, neutral, and stable.

<sup>1</sup> In this evaluation, only 1-hour concentrations are used and the AFB is based on RHC values paired in space and stability/wind speed combination.

A composite performance measure (CPM) is calculated from the 1-hour, 3-hour, and 24-hour AFB's:

$$CPM = \frac{1}{3} \times (\overline{AFB_{i,j}}) + \frac{2}{3} \times \left[ \frac{AFB_3 - AFB_{24}}{2} \right] \quad (121)$$

where  $AFB_{i,j}$  is the absolute fractional bias for monitor  $i$  and meteorological condition  $j$ ,  $\overline{AFB_{i,j}}$  is the average absolute fractional bias across all monitors and meteorological conditions,  $AFB_3$  is the absolute fractional bias for the 3-hour average, and  $AFB_{24}$  is the absolute fractional bias for the 24-hour average. Once CPM values have been calculated for each model, a model

---

<sup>1</sup> In U.S. EPA (1992), the three stability categories are related to the Pasquill-Gifford categories, unstable being A, B, and C, neutral being D, and stable being E and F. Since AERMOD does not use the stability categories, the stability class was determined using Monin-Obukhov length and surface roughness using methodology from AERMOD subroutine LTOPG.

comparison measure is calculated to compare the models:

$$MCM_{A,B} = CPM_A - CPM_B \quad (122)$$

where  $CPM_A$  is the CPM for model A and  $CPM_B$  is the CPM for model B. When more than two models are being compared simultaneously, the number of MCM values is equal to the total of the number of unique combinations of two models. For Martins Creek, Lovett, Westvaco, and Kincaid, there are four scenarios each, so there were six MCM comparisons for each location. For Bowline, Baldwin, and Clifty Creek, there are three scenarios each, resulting in three MCM comparisons for each location.

In order to determine if the difference between models was statistically significant, the standard error was calculated. A bootstrapping technique was used to create 1000 sample years based on methodology outlined in U.S. EPA (1992). The original data is divided into 3-day blocks. Within each season, the 3-day blocks are sampled with replacement until a total season is created. The process is repeated until a 1000 boot-strap years are created<sup>2</sup>. The standard error is calculated as the standard deviation of the bootstrap generated outcomes for the MCM.

The magnitude and sign of the MCM are indicative of relative performance of each pair of models. The smaller the CPM the better the overall performance of the model. This means that for two models, A and B, a negative difference between the CPM for A and CPM for B implies that model A is performing better (Model A has a smaller CPM) while a positive difference indicates that Model B is performing better.

Since more than two scenarios are being evaluated in these studies, simultaneous confidence intervals of 90 and 95 percent were calculated. These were calculated by finding the 90<sup>th</sup> and 95<sup>th</sup> percentiles of the distribution across all MCM values from the bootstrapping procedure for all model comparisons. The confidence intervals were then found by:

---

<sup>2</sup> The bootstrapping was completed using the SAS® SURVEYSELECT procedure with resampling for 1000 replicates.

$$CI_{X,A,B} = MCM_{A,B} \pm c_X s_{A,B} \quad (123)$$

where  $CI_{X,A,B}$  is the confidence interval for X percent (90 or 95<sup>th</sup>) for models A and B,  $MCM_{A,B}$  is as defined in Equation 4,  $c_X$  is the X percentile of the MCM values from the bootstrap results and  $s_{A,B}$  is the standard deviation of the bootstrap MCM results for models A and B. Note that in Equation 5,  $MCM_{A,B}$  is the MCM value from the original data, not the bootstrap results.

For each pair of model comparisons, the significance of the model comparison measure depended on whether the confidence interval overlapped zero. If the confidence interval overlapped zero, then the two models were not performing at a level which was considered statistically different. Otherwise, if they did not overlap zero, then there was a statistically significant difference between the two models.

## B.5 Results

### B.5.1 Turbulence cases

Table 2 lists the hourly observed and modeled RHC, as well as 3-hour and 24-hour RHC for applicable database, for the databases that initially included turbulence. Table 3 lists the RHC values for those databases initially without turbulence. The modeled scenario(s) closest to the observed RHC are highlighted in gray for each database.

Results in Table 2 indicate that the 19191 and 21112 modeled RHC's are generally identical with the exception of Martins Creek 24-hour values, Westvaco 24-hour values (no  $u^*$  with turbulence and no  $u^*$  and no turbulence), EOOCR, and Kincaid 24-hour values (no  $u^*$  with turbulence). Results in Table 2 also indicate that for the most part for the databases with turbulence data, the 19191 or 21112 cases without the  $u^*$  adjustment and with turbulence data were the better performers against observations. For a few instances, depending on the averaging period, the cases with the  $u^*$  adjustment and no turbulence, or the cases with no  $u^*$  adjustment and no turbulence were the better performers.

Table 3 indicates that for the non-turbulence databases, the use of adjusted  $u^*$  increased modeled performance in some cases depending on the averaging period or stack height. while decreasing or not changing model performance in other cases, depending on averaging period or stack height. For the databases that had multiple averaging periods (Martins Creek, Lovett,

Westvaco, and Kincaid), there was not a consistent better performing model across the averaging periods. For example, for Martins Creek, 19191\_with\_u\*\_no\_turb and 21112\_with\_u\*\_no\_turb performed better for the 24-hour averaging period, while 19191\_no\_u\*\_with\_turb and 21112\_no\_u\*\_with\_turb performed better for the 1 and 3-hour period. For DAEC, which had observed concentrations for emissions from different stack heights, the better performing modeling appeared to be dependent on stack height. Overall, it appears that the use of adjusted u\* did not increase model performance for most of the cases and that the inclusion of turbulence is more important to model performance than the u\* adjustment.

Table 2. Hourly, 3-hour, and 24-hour RHC for turbulence cases. Best performing model compared to observed RHC are highlighted in gray.

Database	Avg. period (hr)	RHC						
		Observed	AERMOD version					
			19191			21112		
			No_u*_with turb	With_u*_no_ turb	No_u*_ no_turb	No_u*_ with turb	With_u*_ _no_tur b	No_u*_ no_turb
Martins Creek	1	1216	1133	1034	1427	1133	1034	1427
	3	461	497	505	655	497	505	655
	24	79	141	129	156	143	132	158
Tracy	1	15	13	18	25	13	18	25
Lovett	1	426	374	538	622	374	538	622
	3	187	169	239	254	169	239	254
	24	52	48	63	68	48	63	68
Westvaco	1	2757	2460	1252	2091	2460	1252	2091
	3	1575	1731	783	1654	1731	783	1654
	24	480	524	457	615	522	457	613
DAEC (h=1m)	1	346	240	188	222	240	188	222
DAEC (h=24m)	1	253	84	71	75	84	71	75
DAEC (h=46m)	1	140	91	59	99	91	59	99
EOCR	1	3763	5820	5752	8248	5822	5731	8250
Alaska	1	6	5	8	8	5	8	8
Indianapolis	1	6	4	4	5	4	4	5
Kincaid	1	1611	1312	717	717	1312	717	717
	3	618	635	470	470	635	470	470
	24	113	103	167	167	101	167	167

### B.5.2 Non-turbulence cases

Table 3 lists the RHC values for the non-turbulence databases for 19191 and 21112. In these databases, because of the lack of turbulence in the meteorological data, the effect of the  $u^*$  adjustment has more impact in improving model performance. Also, the results indicate the changes made to AERMOD between 19191 and 21112 did not impact these findings.

Table 3. Hourly, 3-hour, and 24-hour RHC for non-turbulence cases. Best performing model compared to observed RHC are highlighted in gray.

Database	Avg. period (hr)	RHC				
		Observed	AERMOD version			
			19191		21112	
			With_ $u^*$ _no_turb	No_ $u^*$ _no_turb	With_ $u^*$ _no_turb	No_ $u^*$ _no_turb
AGA	1	296	262	281	262	281
Millston (Freon)	1	76	96	101	96	101
Millston (SF6)	1	79	33	35	33	35
Bowline	1	763	552	547	552	547
	3	469	514	523	514	523
	24	204	307	290	307	290
Baldwin	1	2348	3531	3531	3531	3531
	3	920	1183	1184	1183	1184
	24	209	230	230	230	230
Clifty Creek	1	1451	1360	1360	1360	1360
	3	796	871	870	871	870
	24	243	170	165	170	165

### B.5.3 Statistical evaluations

While the review of RHC can indicate general model performance, the use of the EPA Protocol for Determining Best Model provides a statistical basis of determining the best performing model. Tables 4 and 5 show the composite performance measure (CPM) for the turbulence databases and non-turbulence databases respectively. For the databases with turbulence (Table 4), the best performing models for Martins Creek were the cases with adjusted

$u^*$  and no turbulence but for the remaining areas, the better performing models were the adjusted  $u^*$  and no turbulence scenarios. This means the use of adjusted  $u^*$  did not increase model performance and the use of turbulence was important to model performance. For the non-turbulence databases (Table 5), the use of adjusted  $u^*$  increased model performance for Baldwin and Clifty Creek, while for Bowline, the use of adjusted  $u^*$  slightly decreased model performance. For all cases, the CPM values were identical for the 19191 and 21112 model versions, suggesting the changes between 19191 and 21112 had minimal to no impact on model performance, which was expected based on the changes made to AERMET and AERMOD and no changes to the adjusted  $u^*$  equations.

Table 4. Composite Performance Measure (CPM) for turbulence cases. Scenarios with lowest CPM's for each study location are highlighted in gray.

Scenario	Database			
	Martins Creek	Lovett	Westvaco	Kincaid
19191_no_u*_with_turb	0.35	0.40	0.41	0.37
19191_with_u*_no_turb	0.31	0.52	0.60	0.56
19191_no_u*_no_turb	0.49	0.58	0.44	0.56
21112_no_u*_with_turb	0.35	0.40	0.41	0.37
21112_with_u*_no_turb	0.31	0.52	0.60	0.56
21112_no_u*_no_turb	0.49	0.58	0.44	0.56

Table 5. Composite Performance Measure (CPM) for non-turbulence databases. Scenarios with lowest CPM's for each study location are highlighted in gray.

Scenario	Database		
	Bowline	Baldwin	Clifty Creek
19191_no_u*_no_turb	0.47	0.46	0.51
19191_with_u*_no_turb	0.50	0.45	0.49
21112_no_u*_no_turb	0.47	0.46	0.51
21112_with_u*_no_turb	0.50	0.45	0.49

Tables 6 through 9 show the model comparison measure (MCM) for the turbulence databases while Tables 10 through 12 show the MCM for the non-turbulence databases. Also shown are the 90 and 95% confidence intervals of the MCM based on the bootstrapping results.

Confidence intervals highlighted in gray indicated statistical significance in the specific MCM cases. The original pairings of 19191 scenarios to other 19191 scenarios are shown for comparison to the analogous 21112 pairings. MCM pairings for the same  $u^*$ /turbulence pairings between 21112 and 19191 are also shown to show if model changes made differences to results. For all such cases, such comparisons are zero.

Martins Creek (Table 6): The better performing models were 19191 and 21112 with  $u^*$  and no turbulence. Also, the MCM results indicate that the use of adjusted  $u^*$  with no turbulence is not statistically significant when compared to no adjusted  $u^*$  with turbulence for both 19191 and 21112. There were three statistically significant MCM pairings that were statistically significant at the 90% confidence interval and these were the difference between no  $u^*$  adjustment and no turbulence and the cases (no adjusted  $u^*$  with turbulence or adjusted  $u^*$  with no turbulence) for both 19191 and 21112, indicating that not using adjusted  $u^*$  and not using turbulence noticeably decreases model performance. At the 95% confidence interval, the only statistically significant difference was between no adjusted  $u^*$ / no turbulence and adjusted  $u^*$ /no turbulence for both 18081 and 19191.

Lovett (Table 7): All cases of AERMET/AERMOD 19191 are statistically insignificant when compared AERMET/AERMOD 19191 at both the 90% and 95% CI. For 21112 all cases are statistically insignificant compared to each other at the 90% CI, with the exception of the 21112 no  $u^*$  and no turbulence case compared to the 21112 no  $u^*$  with turbulence case. However, the lower bound of the 90% CI is close to zero.

Westvaco (Table 8): The use of adjusted  $u^*$  decreases model performance significantly at both the 90% and 95% CI for both 19191 and 21112. The use of no adjusted  $u^*$  and no turbulence also decreases model performance at a statistically significant level for both 19191 and 21112.

Kincaid (Table 9): None of the MCM differences were statistically significant at 90% or 95% CI. The better performers were 19191 or 21112 with no  $u^*$  adjustment and inclusion of turbulence, but as previously stated, were not statistically different from the adjusted  $u^*$  case or the case with no adjusted  $u^*$  and no turbulence.

For the non-turbulence databases (Tables 10-12), the use of adjusted  $u^*$  was statistically insignificant compared to not using adjusted  $u^*$  and as expected, the MCM values indicated no difference between 19191 and 21112.

Table 6. Martins Creek Model Comparison Measure (MCM) results. Confidence intervals highlighted in gray are significant at that percent.

MCM Comparison	MCM	Confidence Intervals			
		90%		95%	
		Lower bound	Upper bound	Lower bound	Upper bound
19191_with_u*_no_turb - 19191_no_u*_with_turb	-0.04	-0.15	0.07	-0.17	0.10
19191_no_u*_no_turb - 19191_no_u*_with_turb	0.14	0.03	0.25	-0.01	0.28
19191_no_u*_no_turb - 19191_with_u*_no_turb	0.18	0.05	0.31	0.03	0.34
21112_no_u*_no_turb - 19191_no_u*_no_turb	0	-0.11	0.12	-0.14	0.15
21112_no_u*_with_turb - 19191_no_u*_with_turb	0	-0.08	0.09	-0.11	0.11
21112_with_u*_no_turb - 19191_with_u*_no_turb	0	-0.10	0.11	-0.12	0.13
21112_with_u*_no_turb - 19191_no_u*_with_turb	-0.03	-0.14	0.08	-0.17	0.10
21112_no_u*_no_turb - 19191_no_u*_with_turb	0.15	0.03	0.27	-0.002	0.30
21112_no_u*_no_turb - 19191_with_u*_no_turb	0.19	0.06	0.31	0.03	0.34

Table 7. Lovett Model Comparison Measure (MCM) results. Confidence intervals highlighted in gray are significant at that percent.

MCM Comparison	MCM	Confidence Intervals			
		90%		95%	
		Lower bound	Upper bound	Upper bound	Lower bound
19191_with_u*_no_turb - 19191_no_u*_with_turb	0.13	-0.05	0.30	-0.08	0.34
19191_no_u*_no_turb - 19191_no_u*_with_turb	0.18	-0.002	0.36	-0.04	0.40
19191_no_u*_no_turb - 19191_with_u*_no_turb	0.05	-0.07	0.17	-0.09	0.20
21112_no_u*_no_turb - 19191_no_u*_no_turb	0	-0.11	0.11	-0.13	0.13
21112_no_u*_with_turb - 19191_no_u*_with_turb	0	-0.13	0.12	-0.15	0.15
21112_with_u*_no_turb - 19191_with_u*_no_turb	0	-0.11	0.11	-0.13	0.13
21112_with_u*_no_turb - 21112_no_u*_with_turb	0.12	-0.04	0.30	-0.08	0.33
21112_no_u*_no_turb - 21112_no_u*_with_turb	0.18	0.003	0.36	-0.03	0.40
21112_no_u*_no_turb - 21112_with_u*_no_turb	0.05	-0.06	0.16	-0.08	0.19

Table 8. Westvaco Model Comparison Measure (MCM) results. Confidence intervals highlighted in gray are significant at that percent.

MCM Comparison	MCM	Confidence Intervals			
		90%		95%	
		Lower bound	Upper bound	Lower bound	Upper bound
19191_with_u*_no_turb - 19191_no_u*_with_turb	0.19	0.05	0.33	0.01	0.36
19191_no_u*_no_turb - 19191_no_u*_with_turb	0.03	-0.05	0.11	-0.07	0.12
19191_no_u*_no_turb - 19191_with_u*_no_turb	-0.16	-0.31	-0.01	-0.34	-0.02
21112_no_u*_no_turb - 19191_no_u*_no_turb	0	-0.09	0.09	-0.10	0.10
21112_no_u*_with_turb - 19191_no_u*_with_turb	0	-0.08	0.08	-0.10	0.08
21112_with_u*_no_turb - 19191_with_u*_no_turb	0	-0.07	0.07	-0.08	0.08
21112_with_u*_no_turb - 21112_no_u*_with_turb	0.19	0.03	0.35	-0.001	0.38
21112_no_u*_no_turb - 21112_no_u*_with_turb	0.03	-0.05	0.11	-0.07	0.13
21112_no_u*_no_turb - 21112_with_u*_no_turb	-0.16	-0.32	-0.001	-0.35	0.03

Table 9. Kincaid Model Comparison Measure (MCM) results. Confidence intervals highlighted in gray are significant at that percent.

MCM Comparison	MCM	Confidence Intervals			
		90%		95%	
		Lower bound	Upper bound	Lower bound	Upper bound
19191_with_u*_no_turb - 19191_no_u*_with_turb	0.19	-0.26	0.64	-0.32	0.70
19191_no_u*_no_turb - 19191_no_u*_with_turb	0.19	-0.27	0.66	-0.32	0.70
19191_no_u*_no_turb - 19191_with_u*_no_turb	-5.1x10 <sup>-4</sup>	-0.15	0.14	-0.16	0.16
21112_no_u*_no_turb - 19191_no_u*_no_turb	0	-0.14	0.14	-0.16	0.16
21112_no_u*_with_turb - 19191_no_u*_with_turb	0	-0.53	0.52	-0.59	0.59
21112_with_u*_no_turb - 19191_with_u*_no_turb	0	-0.14	0.14	-0.15	0.15
21112_with_u*_no_turb - 21112_no_u*_with_turb	0.19	-0.28	0.66	-0.33	0.71
21112_no_u*_no_turb - 21112_no_u*_with_turb	0.19	-0.28	0.66	-0.32	0.71
21112_no_u*_no_turb - 21112_with_u*_no_turb	-5.1x10 <sup>-4</sup>	-0.13	0.13	-0.15	0.15

Table 10. Bowline Model Comparison Measure (MCM) results. Confidence intervals highlighted in gray are significant at that percent.

MCM Comparison	MCM	Confidence Intervals			
		90%		95%	
		Lower bound	Upper bound	Lower bound	Upper bound
19191_no_u*_no_turb - 19191_with_u*_no_turb	-0.03	-0.11	0.05	-0.13	0.07
21112_no_u*_no_turb - 19191_no_u*_no_turb	0.0	-0.08	0.08	-0.10	0.10
21112_with_u*_no_turb - 19191_with_u*_no_turb	0.0	-0.07	0.07	-0.09	0.09
21112_no_u*_no_turb - 21112_with_u*_no_turb	-0.03	-0.19	0.03	-0.11	0.05

Table 11. Baldwin Model Comparison Measure (MCM) results. Confidence intervals highlighted in gray are significant at that percent.

MCM Comparison	MCM	Confidence Intervals			
		90%		95%	
		Lower bound	Upper bound	Lower bound	Upper bound
19191_no_u*_no_turb - 19191_with_u*_no_turb	0.002	-0.08	0.09	-0.10	0.11
21112_no_u*_no_turb - 19191_no_u*_no_turb	0	-0.08	0.08	-0.10	0.10
21112_with_u*_no_turb - 19191_with_u*_no_turb	0	-0.08	0.08	-0.10	0.10
21112_no_u*_no_turb - 21112_with_u*_no_turb	0.002	-0.06	0.06	-0.08	0.08

Table 12. Clifty Creek Model Comparison Measure (MCM) results. Confidence intervals highlighted in gray are significant at that percent.

MCM Comparison	MCM	Confidence Intervals			
		90%		95%	
		Lower bound	Upper bound	Lower bound	Upper bound
19191_no_u*_no_turb - 19191_with_u*_no_turb	0.02	-0.05	0.08	-0.06	0.09
21112_no_u*_no_turb - 19191_no_u*_no_turb	0.0	-0.05	0.05	-0.07	0.07
21112_with_u*_no_turb - 19191_with_u*_no_turb	0	-0.05	0.05	-0.07	0.07
21112_no_u*_no_turb - 21112_with_u*_no_turb	0.02	-0.03	0.06	-0.04	0.08

## **B.6 Summary/Conclusions**

Based on the results the RHC comparisons and the EPA protocol for determining best performing model, in situations involving turbulence, the use of turbulence without adjusting  $u^*$  usually led to better performance than using adjusted  $u^*$  without turbulence, especially in areas of complex terrain. In some instances, the differences between the adjusted  $u^*$  cases were statistically worse than non-adjusted  $u^*$  cases. For situations where turbulence is not in the meteorological data, the use of adjusted  $u^*$  often resulted in little change or some increase in model performance. However, the databases without turbulence were in flat terrain and had tall stacks, so model performance for non-turbulence cases with complex terrain cannot be determined from these results. The results of the RHC and EPA protocol also indicate that changes made to AERMOD 21112 had no unexpected changes from AERMOD 19191, which was expected.

## **Appendix C. Evaluation of modified urban option**

The urban option in AERMOD was modified, beginning with version 11059, to address potential issues associated with the transition from the nighttime urban boundary layer to the daytime convective boundary layer. Prior to version 11059, the enhanced dispersion associated with the urban nighttime heat island effect was ignored once the boundary layer turned convective. This could result in an unrealistic drop in the mixed layer height during early morning hours for urban applications, which could contribute to unrealistically high concentrations for low-level plumes. This effect was observed in the application of AERMOD for the Risk and Exposure Assessment (REA) in support of the NO<sub>2</sub> NAAQS review in association with mobile source emissions (EPA, 2008). Beginning with version 11059 the urban option in AERMOD continues application of the urban boundary layer approach for urban sources until the daytime convective mixing height exceeds the urban nighttime mixing height, based on the user-specified population (EPA, 2018a)). This revision to AERMOD will generally reduce concentrations during the early morning transition to convective conditions for low-level urban sources but may increase daytime concentrations for elevated urban sources.

The modified implementation of the urban option was evaluated using data from the 1985 Indianapolis SF<sub>6</sub> urban field study (Perry, et al, 2005), and model-to-monitor comparisons at four ambient monitors for 2002 from the Atlanta NO<sub>2</sub> REA (EPA, 2008). The Indianapolis study involved an elevated buoyant release and the Atlanta REA study involved mostly low-level mobile source emissions. Results from the Indianapolis study are presented in the form of Q-Q plots of ranked 1-hour modeled vs. observed concentrations, unpaired in time and space. Figure E-1 shows model performance for all stabilities and Figure E-2 shows model performance for convective conditions only. The revised urban option does not affect results under stable conditions. Results from the Atlanta NO<sub>2</sub> REA are also presented in the form of Q-Q plots of 1-hour ranked modeled vs. observed concentrations, unpaired in time, for each of the four ambient NO<sub>2</sub> monitors, shown in Figures E-3 through E-6. Both of these evaluations show improved model performance with the modified urban option in AERMOD.

INDIANAPOLIS SF<sub>6</sub> 1-HR Q-Q PLOT (CONC) - All Stabilities

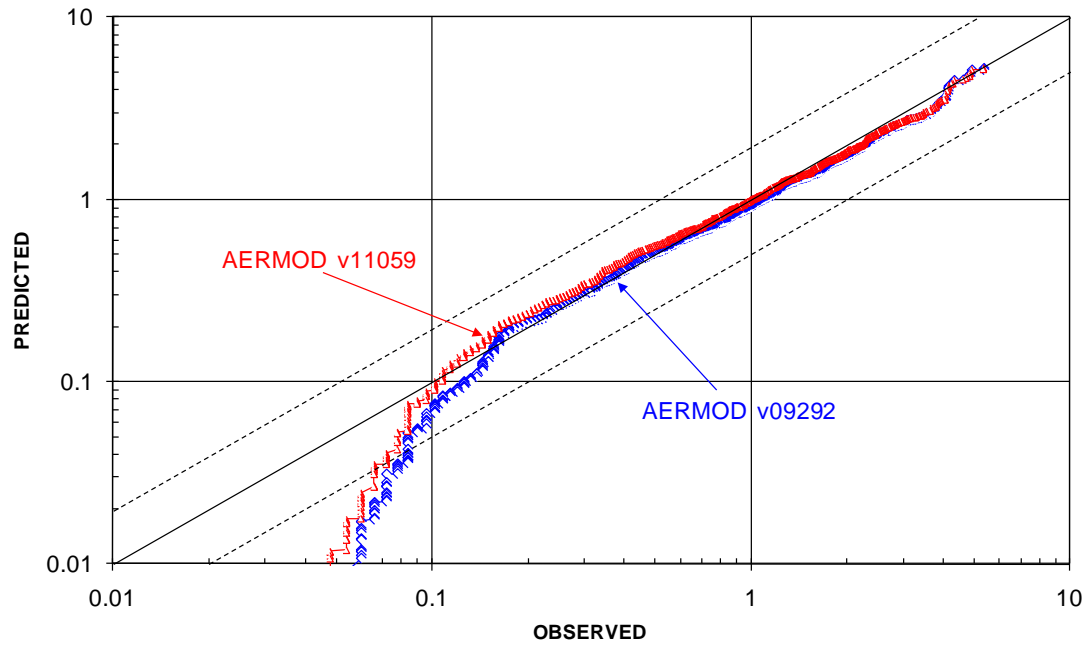


Figure E-1. 1-hour Q-Q Plot for Indianapolis SF<sub>6</sub> Study for All Stabilities

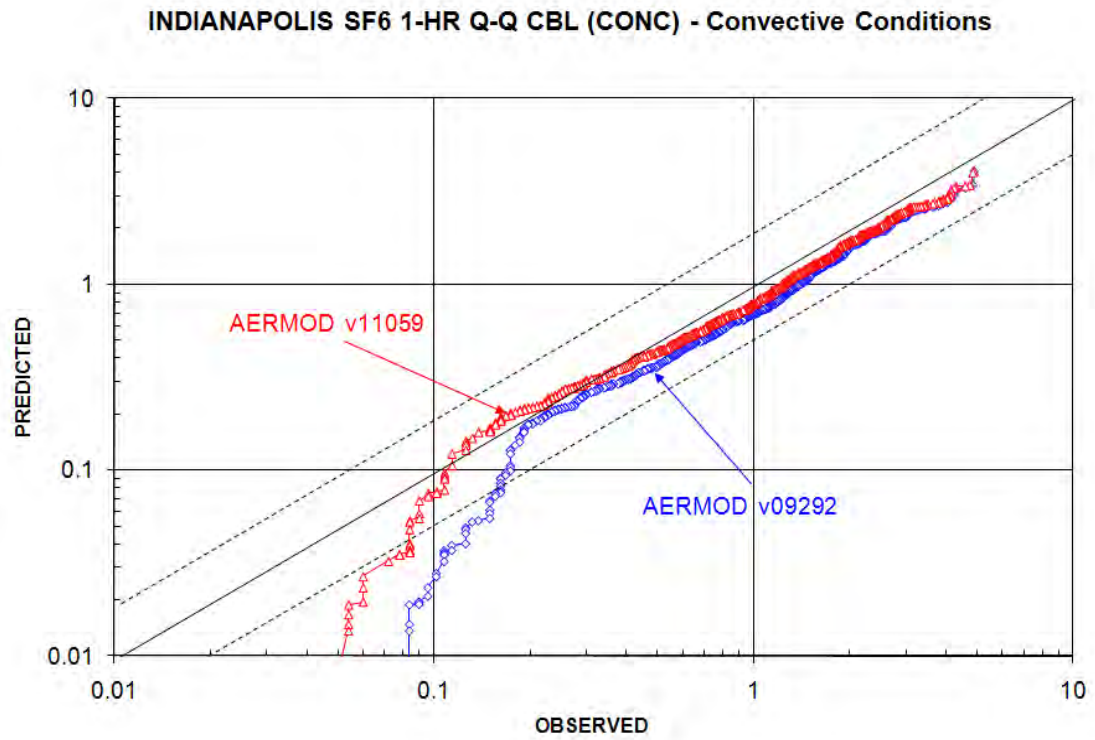


Figure E-2. 1-hour Q-Q Plot for Indianapolis SF<sub>6</sub> Study for Convective Conditions

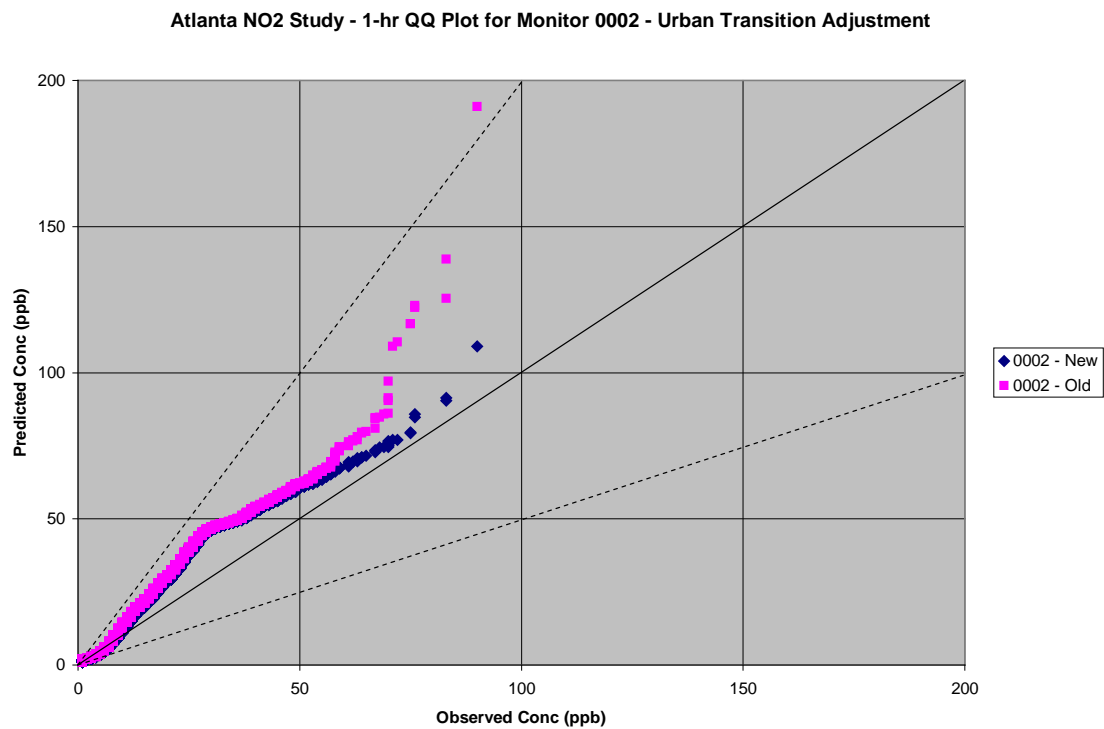


Figure E-3. 1-hour Q-Q Plot for Atlanta NO<sub>2</sub> Study for Monitor 0002

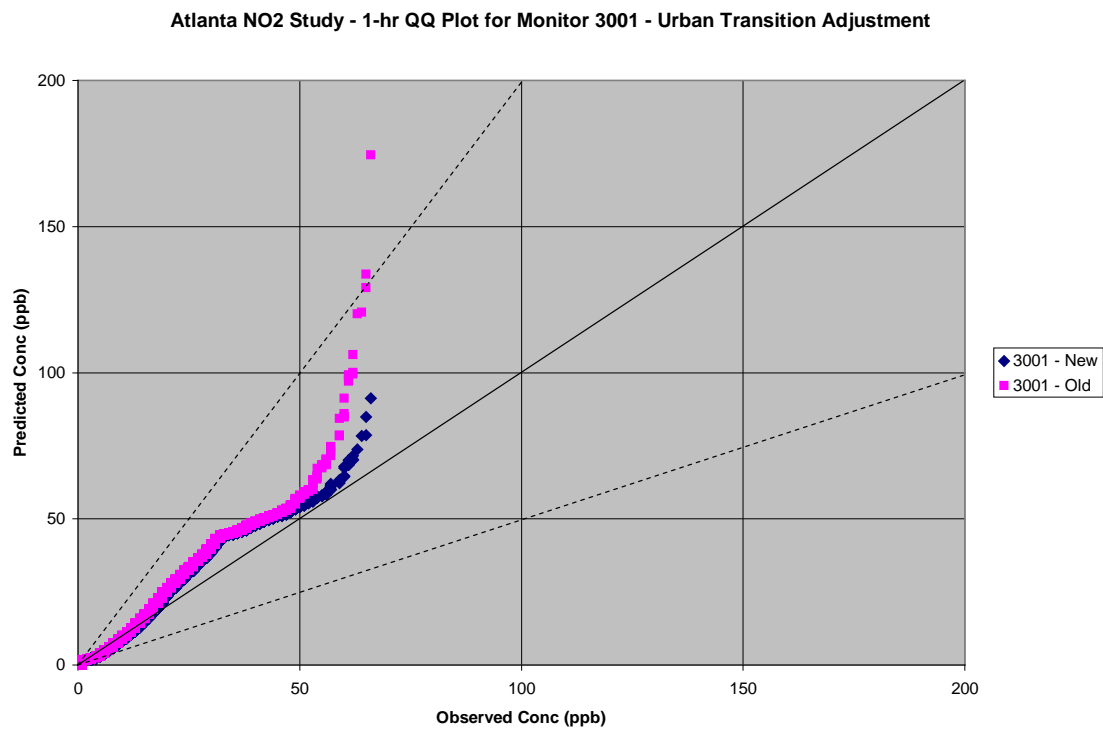


Figure E-4. 1-hour Q-Q Plot for Atlanta NO<sub>2</sub> Study for Monitor 3001

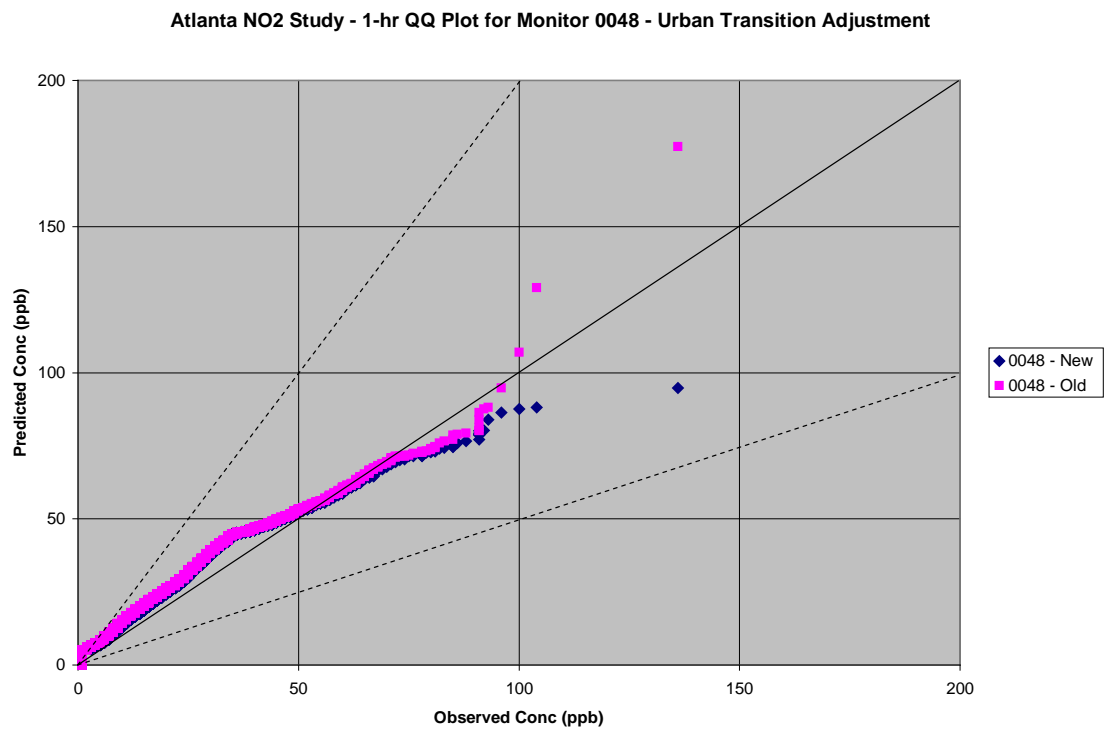


Figure E-5. 1-hour Q-Q Plot for Atlanta NO<sub>2</sub> Study for Monitor 0048

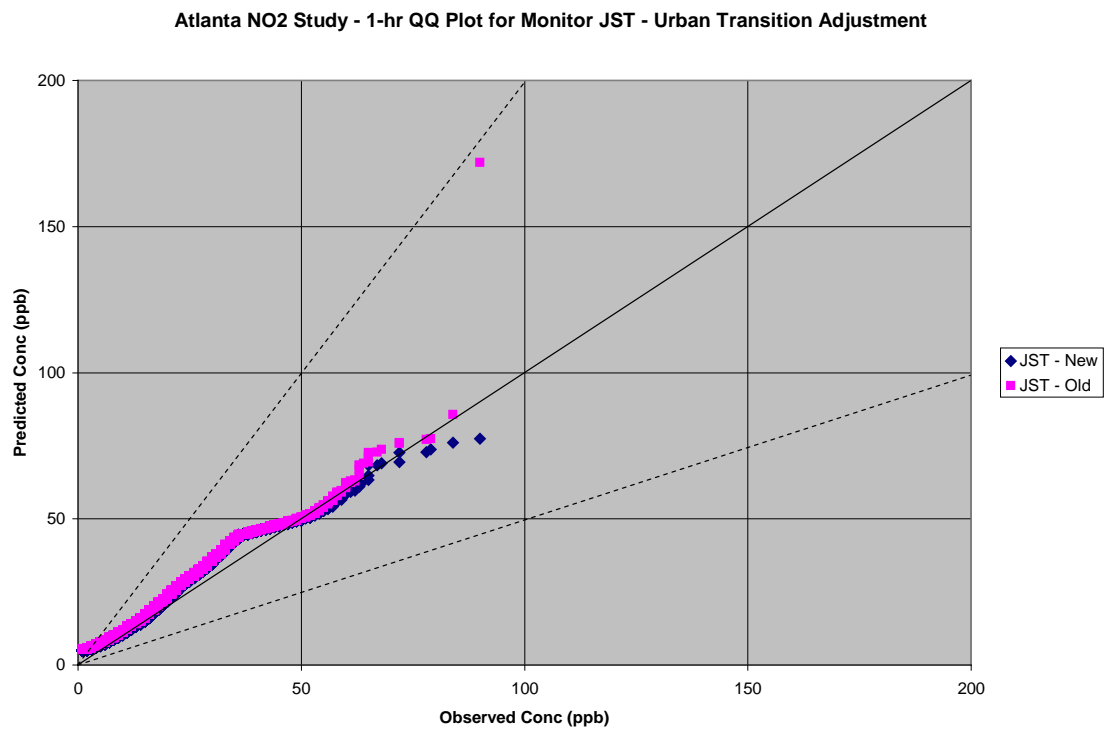


Figure E-6. 1-hour Q-Q Plot for Atlanta NO<sub>2</sub> Study for Monitor JST

## References

- AECOM, 2010: AERMOD Low Wind Speed Evaluation Study Results. Prepared for the American Petroleum Institute and Utility Air Regulatory Group. Prepared by AECOM, Westford, MA. March 22, 2010.
- Andre, J. C. and L. Mahrt, 1982: The nocturnal surface inversion and influence of clean-air radiative cooling. *J.Atmos.Sci.*, **39**, 864-878.
- Baerentsen, J. H. and R. Berkowicz, 1984: Monte Carlo simulation of plume dispersion in the convective boundary layer. *Atmos.Environ.*, **18**, 701-712.
- Bange, P., L. Jannsen, F. Nieuwstadt, H. Visser, and J. Erbrink, 1991. "Improvement of the modeling of daytime nitrogen oxidation in plumes by using instantaneous plume dispersion parameters," *Atmos. Environ.*, **25A** (10), 2321-2328.
- Barad, M. L., 1958: Project Prairie Grass, A Field Program in Diffusion. Geophysical Research Papers, No. 59, Vols. I and II, AFCRC-TR-58-235, Air Force Cambridge Research Center, 439pp.
- Berkowicz, R., Olesen, J. R., and Torp, U., 1986: The Danish Gaussian air pollution model (OLM): Description, test and sensitivity analysis, in view of regulatory applications. *Air Pollution Modeling and Its Application*. De Wispelaire, V. C., Schiermeier, F. A., and Grillani, N. V, Plemum, 453-481pp.
- Bornstein, R. D., 1968: Observations of urban heat island effects in New York City. *J.Appl.Meteor.*, **7**, 575-582.
- Bowne, N. E., R. J. Londergan, D. R. Murray, and H. S. Borenstein, 1983: Overview, Results, and Conclusions for the EPRI Plume Model Validation and Development Project: Plains Site. EPRI Report EA-3074, Project 1616-1, Electric Power Research Institute, Palo Alto, CA, 234 pp. 1983.
- Brett, A. C. and S. E. Tuller, 1991: Autocorrelation of hourly wind speed observations. *J.Appl.Meteor.*, **30**, 823-833.
- Briggs, G. A., 1969: Plume rise. USAEC Critical Review Series, TID-25075, NTIS, 81pp.
- Briggs, G. A., 1971: Some recent analyses of plume rise observations. *Proceedings of the Second International Clean Air Congress*. Englund, H. M. and Berry, W. T., Academic Press, 1029-1032.
- Briggs, G. A., 1973: Diffusion Estimation for Small Emissions. 1973 Annual Report, ATDL-106, Air Resources Atmospheric Turbulence and Diffusion Laboratory, Environmental Res. Lab., NOAA, Oak Ridge, TN.

- Briggs, G. A., 1975: Plume rise predictions. *Lectures on Air Pollution and Environmental Impact Analysis*. Haugen, D. A., American Meteorological Society, 59-111pp.
- Briggs, G. A., 1984: Plume rise and buoyancy effects. *Atmospheric Science and Power Production*. Randerson, D., U.S. Dept. of Energy, 327-366pp.
- Briggs, G. A., 1988: Analysis of diffusion field experiments. *Lectures on Air Pollution Modeling*. Venkatram, A. and Wyngaard, J. C., American Meteorological Society, 63-117.
- Briggs, G. A., 1993: Plume dispersion in the convective boundary layer. Part II: Analysis of CONDORS field experiment data. *J.Appl.Meteor.*, **32**, 1388-1425.
- Brode, R. W., 2002: Evaluation of the AERMOD Dispersion Model.
- Brost, R. A., J. C. Wyngaard, and D. H. Lenschow, 1982: Marine stratocumulus layers: Part II: Turbulence budgets. *J.Atmos.Sci.*, **39**, 818-836.
- Businger, J. A., 1973: Turbulent transfer in the atmospheric surface layer. *Workshop on Micrometeorology*. Haugen, D. A., American Meteorological Society.
- Businger, J. A., J. C. Wyngaard, Y. Izumi, and E. F. Bradley, 1971: Flux-profile relationships in the atmospheric surface layer. *J.Atmos.Sci.*, **28**, 181-189.
- Carruthers, D. J., and Coauthors, 1992: UK atmospheric dispersion modelling system. *Air Pollution Modeling and Its Application*. Plenum Press, New York.
- Carson, D. J., 1973: The development of a dry inversion-capped convectively unstable boundary layer. *Quart.J.Roy.Meteor.Soc.*, **99**, 450-467.
- Caughey, S. J. and S. G. Palmer, 1979: Some aspects of turbulence structure through the depth of the convective boundary layer. *Quart.J.Roy.Meteor.Soc.*, **105**, 811-827.
- Cimorelli, A. J., S. G. Perry, R. F. Lee, R. J. Paine, A. Venkatram, J. C. Weil, and R. B. Wilson, 1996: Current Progress in the AERMIC Model Development Program. Preprints, 89<sup>th</sup> Annual Meeting Air and Waste Management Association, Air and Waste Management Association, Pittsburgh, PA.
- Cimorelli, A. J., S. G. Perry, A. Venkatram, J. C. Weil, R. J. Paine, R. B. Wilson, R. F. Lee, W. D. Peters, R. W. Brode, and J. O. Paumier, 2002: AERMOD: Description of Model Formulation (Version 02222). EPA 454/R-02-002d. U. S. Environmental Protection Agency, Research Triangle Park, NC.
- Cimorelli, A. J., S. G. Perry, A. Venkatram, J. C. Weil, R. J. Paine, R. B. Wilson, R. F. Lee, W. D. Peters, and R. W. Brode, 2005: AERMOD: A dispersion model for industrial source applications Part I: General model formulation and boundary layer characterization. *J.Appl.Meteor.* **44**, 682-693

- Clarke, R. H., A. J. Dyer, R. R. Brook, D. G. Reid, and A. J. Troop, 1971: The Wangara experiment: boundary layer data. Technical Report No. 19, Division of Meteorological Physics CSIRO, Australia.
- Cole, H.S. and J.E. Summerhays, 1979. "A review of techniques available for estimating short-term NO<sub>2</sub> concentrations," *J. Air Pollut. Control Assoc.*, **29**(8), 812-817.
- Collier, L. R. and J. G. Lockwood, 1975: Reply to comment. *Quart.J.Roy.Meteor.Soc.*, **101**, 390-392.
- Cox, W.M. and J.A. Tikvart, 1990: A statistical Procedure for Determining the Best Performing Air Quality Simulation Model. *Atmos. Environ.*, 24A (9): 2387-2395.
- Deardorff, J. W., 1970: Convective velocity and temperature scales for the unstable boundary layer for Rayleigh convection. *J.Atmos.Sci.*, **27**, 1211-1213.
- Deardorff, J. W., 1972: Numerical investigation of neutral and unstable planetary boundary layers. *J.Atmos.Sci.*, **29**, 91-115.
- Deardorff, J. W., 1979: Prediction of convective mixed-layer entrainment for realistic capping inversion structure. *J.Atmos.Sci.*, **36**, 424-436.
- Deardorff, J. W., 1980: Progress in Understanding Entrainment at the Top of a Mixed Layer. Preprints, *Workshop on the Planetary Boundary Layer*, American Meteorological Society, Boston, MA.
- DiCristofaro, D. C. *et al.*, 1985: EPA Complex Terrain Model Development: Fifth Milestone Report - 1985. EPA-600/3-85-069, U. S. Environmental Protection Agency, Research Triangle Park, North Carolina.
- Dyer, A. J., 1974: A review of flux-profile relationships. *Bound.Layer Meteor.*, **7**, 363-372.
- Garratt, F. R., 1992: *The Atmospheric Boundary Layer*. Cambridge University Press, New York, New York, 334pp.
- Gifford, F. A., 1961: Uses of routine meteorological observations for estimating atmospheric dispersion. *Nuclear Safety*, **2**, 47-51.
- Hanna, S. R., 1983: Lateral turbulence intensity and plume meandering during stable conditions. *J.Appl.Meteor.*, **22**, 1424-1430.
- Hanna, S. R. and J. S. Chang, 1991: Modification of the Hybrid Plume Dispersion Model (HPDM) for urban conditions and its evaluation using the Indianapolis data set, Volume III: Analysis of urban boundary layer data. EPRI Project No. RP-02736-1, Electric Power Research Institute, Palo Alto, CA.
- Hanna, S. R. and J. S. Chang, 1993: Hybrid Plume Dispersion Model (HPDM), improvements and testing at three field sites. *Atmos.Environ.*, **27A**, 1491-1508.

- Hanna, S. R. and R. J. Paine, 1989: Hybrid Plume Dispersion Model (HPDM) development and evaluation. *J.Appl.Meteor.*, **28**, 206-224.
- Hanna, S. R., J. C. Weil, and R. J. Paine, 1986: Plume Model Development and Evaluation - Hybrid Approach. EPRI Contract No. RP-1616-27, Electric Power Research Institute, Palo Alto, CA.
- Hanrahan, P.L., 1999a. "The plume volume molar ratio method for determining NO<sub>2</sub>/NO<sub>x</sub> ratios in modeling. Part I: Methodology," *J. Air & Waste Manage. Assoc.*, **49**, 1324-1331.
- Haugen, D. A. (Editor), 1959: Project Prairie Grass, A field program in diffusion. Geophysical Research Paper, No. 59, Vol. III. Report AFCRC-TR-58-235, Air Force Cambridge Research Center, 439 pp.
- Hayes, S. R. and G. E. Moore, 1986: Air quality model performance: a comparative analysis of 15 model evaluation studies. *Atmos.Environ.*, **20**, 1897-1911.
- Hicks, B. B., 1985: Behavior of turbulent statistics in the convective boundary layer. *J.Appl.Meteor.*, **24**, 607-614.
- Holtslag, A. A. M., 1984: Estimates of diabatic wind speed profiles from near-surface weather observations. *Bound.Layer Meteor.*, **29**, 225-250.
- Holtslag, A. A. M. and A. P. van Ulden, 1983: A simple scheme for daytime estimates for the surface fluxes from routine weather data. *J.Climate Appl.Meteor.*, **22**, 517-529.
- Irwin, J. S., J. O. Paumier, and R. W. Brode, 1988: Meteorological Processor for Regulatory Models (MPRM) User's Guide. EPA-600/3-88-043, U.S. Environmental Protection Agency, RTP, NC.
- Izumi, Y., 1971: Kansas 1968 Field Program Data Report. No. 379, AFCRL-72-0041, Air Force Cambridge Research Laboratory, Bedford, MA, 79pp.
- Kaimal, J. C., J. C. Wyngaard, D. A. Haugen, O. R. Cote', Y. Izumi, S. J. Caughey, and C. J. Readings, 1976: Turbulence structure in the convective boundary layer. *J.Atmos.Sci.*, **33**, 2152-2169.
- Kasten, F. and G. Czeplak, 1980: Solar and terrestrial radiation dependent on the amount and type of cloud. *Solar Energy*, **24**, 177-189.
- Lamb, R. G., 1982: Diffusion in the convective boundary layer. *Atmospheric Turbulence and Air Pollution Modelling*. Nieuwstadt, F. T. M. and van Dop, H., Reidel, 159-229pp.
- Lee, R. F., R. J. Paine, S. G. Perry, A. J. Cimorelli, J. C. Weil, A. Venkatram, and R. B. Wilson, 1998: Developmental Evaluation of the AERMOD Dispersion Model. Preprints, *10th Joint AMS/AWMA Conference on Application of Air Pollution Meteorology*, American Meteorological Society, Boston.

- Lee, R. F., S. G. Perry, A. J. Cimorelli, R. J. Paine, A. Venkatram, J. C. Weil, and R. B. Wilson, 1995: AERMOD - the developmental evaluation. Preprints, *Tewnty-First NATO/CCMS International Technical Meeting on Air Pollution Modeling and Its Application*, Baltimore, MD, U.S.A.
- Liu, M. K., and G. E. Moore: 1984: Diagnostic validation of plume models at a plains site. EPRI Report No. EA-3077, Research Project 1616-9, Electric Power Research Institute, Palo Alto, CA. (1984)
- Luhar, A.K., and K. N. Rayner, 2009: “Methods to Estimate Surface Fluxes of Momentum and Heat from Routine Weather Observations for Dispersion Applications under Stable Stratification”, *Boundary-Layer Meteorology*, **132**, 437–454.
- Misra, P. K., 1982: Dispersion of non-buoyant particles inside a convective boundary layer. *Atmos. Environ.*, **16**, 239-243.
- Morton, B. R., G. I. Taylor, and J. S. Turner, 1956: Turbulent gravitational convection from maintained and instantaneous sources. *Proc.Roy.Soc.London*, **A234**, 1-23.
- Nieuwstadt, F. T. M. and H. van Dop, 1982: *Atmospheric Turbulence and Air Pollution Modelling*. Reidel, 358pp.
- NOAA, 1974: Technical Memorandum ERL ARL-52, 1974. “Diffusion under Low Wind Speed, Inversion Conditions.” Sagendorf, J. F., C. Dickson. Air Resources Laboratory, Idaho Falls, Idaho.
- NOAA, 1976: Technical Memorandum ERL ARL-61, 1976. “Diffusion under Low Wind Speed Conditions near Oak Ridge, Tennessee.” Wilson, R. B., G. Start, C. Dickson, N. Ricks. Air Resources Laboratory, Idaho Falls, Idaho.
- Oke, T. R., 1973: City size and the urban heat island. *Atmos. Environ.*, **7**, 769-779.
- Oke, T. R., 1978: *Boundary Layer Climates*. John Wiley and Sons, New York, New York, 372pp.
- Oke, T. R., 1982: The energetic basis of the urban heat island. *Quart.J.Roy.Meteor.Soc.*, **108**, 1-24.
- Oke, T. R., 1998: An algorithmic scheme to estimate hourly heat island magnitude. Preprints, *2nd Urban Environment Symposium*, American Meteorological Society, Boston, MA, 80-83.
- Paine, R. J. and B. A. Egan, 1987: User's guide to the Rough Terrain Diffusion Model (RTDM) - Rev. 3.20. ERT Document PD-535-585, ENSR, Acton, MA, 260pp.

- Paine, R. J. and S. B. Kendall, 1993: Comparison of observed profiles of winds, temperature, and turbulence with theoretical results. Preprints, *Joint conference of the American Meteorological Society and Air & Waste Management Association Specialty Conference: The Role of Meteorology in Managing the Environment in the 90s*, Scottsdale, AZ. Publication VIP-29, Air & Waste Management Association, Pittsburgh, PA.
- Panofsky, H. A. and J. A. Dutton, 1984: *Atmospheric Turbulence: Models and Methods for Engineering Applications*. John Wiley and Sons, New York, 417pp.
- Panofsky, H. A., H. Tennekes, D. H. Lenschow, and J. C. Wyngaard, 1977: The characteristics of turbulent velocity components in the surface layer under convective conditions. *Bound. Layer Meteor.*, **11**, 355-361.
- Pasquill, F., 1961: The estimation of the dispersion of windborne material. *Meteorol. Mag.*, **90**, 33-49.
- Pasquill, F., 1976: Atmospheric dispersion parameters in Gaussian plume modeling - Part III: possible requirements for change in the Turner's Workbook values. EPA-600/4-76-030B, U. S. Environmental Protection Agency, Research Triangle Park, NC.
- Pasquill, F. and F. R. Smith, 1983: *Atmospheric Diffusion*. John Wiley and Sons Inc., New York, 440pp.
- Paumier, J. O., S. G. Perry, and D. J. Burns, 1992: CTDMPLUS: A dispersion model for sources near complex topography. Part II: Performance characteristics. *J. Appl. Meteor.*, **31**, 646-660.
- Perry, S. G., 1992: CTDMPLUS: A dispersion model for sources in complex topography. Part I: Technical formulations. *J. Appl. Meteor.*, **31**, 633-645.
- Perry, S. G., D. J. Burns, R. J. Adams, R. J. Paine, M. G. Dennis, M. T. Mills, D. G. Strimaitis, R. J. Yamartino, and E. M. Insley, 1989: User's Guide to the Complex Terrain Dispersion Model Plus Algorithms for Unstable Situations (CTDMPLUS) Volume 1: Model Description and User Instructions. EPA/600/8-89/041, U.S. Environmental Protection Agency, RTP, NC, 196pp.
- Perry, S. G., A. J. Cimorelli, R. F. Lee, R. J. Paine, A. Venkatram, J. C. Weil, and R. B. Wilson, 1994: AERMOD: A dispersion model for industrial source applications. Preprints, *87<sup>th</sup> Annual Meeting Air and Waste Management Association*, Air and Waste Management Association, Pittsburgh, PA.
- Perry, S. G., A. J. Cimorelli, R. J. Paine, R. W. Brode, J. C. Weil, A. Venkatram, R. B. Wilson, R. F. Lee, and W. D. Peters, 2005: AERMOD: A dispersion model for industrial source applications Part II: Model performance against seventeen field-study databases. *J. Appl. Meteor.* **44**, 694-708.

- Qian, W., and A. Venkatram, 2011: "Performance of Steady-State Dispersion Models Under Low Wind-Speed Conditions", *Boundary Layer Meteorology*, **138**, 475-491.
- Readings, C. J., D. A. Haugen, and J. C. Kaimal, 1974: The 1973 Minnesota atmospheric boundary layer experiment. *Weather*, **29**, 309-312.
- Schulman, L.L., and J.S. Scire, 1980: Boyant Line and Point Source (BLP) Dispersion Model User's Guide. Final Report. Environmental Research & Technology, Inc. P-7304B. July 1980.
- Schulman, L. L., D. G. Strimaitis, and J. S. Scire, 2000: Development and evaluation of the PRIME plume rise and building downwash model. *Journal of the Air & Waste Management Association*, **50**, 378-390.
- Sheppard, P. A., 1956: Airflow over mountains. *Quart.J.Roy.Meteor.Soc.*, **82**, 528-529.
- Smith, M. E., 1984: Review of the attributes and performance of 10 rural diffusion models. *Bull.Amer.Meteor.Soc.*, **65**, 554-558.
- Snyder, W. H., R. S. Thompson, R. E. Eskridge, R. E. Lawson, I. P. Castro, J. T. Lee, J. C. R. Hunt, and Y. Ogawa, 1985: The structure of the strongly stratified flow over hills: Dividing streamline concept. *J.Fluid Mech.*, **152**, 249-288.
- Snyder, M. G., A. Venkatram, D. K. Heist, S. G. Perry, W. B. Petersen, V. Isakov, 2013: RLINE: A Line source dispersion model for near-surface releases. *Atmos.Environ.*, **77(0)**, 748-756.
- Stull, R. B., 1983: A heat flux history length scale for the nocturnal boundary layer. *Tuller*, **35A**, 219-230.
- Sykes, R. I., D. S. Henn, and S. F. Parker, 1996: SCIPUFF - A generalized hazard dispersion model. Preprints, *9th Joint Conference on Applications of Air Pollution Meteorology with AWMA, Amer. Meteor. Soc.*, American Meteorological Society, Boston, 184-188.
- Taylor, G. I., 1921: Diffusion by continuous movements. *Proc.London Math.Soc.*, **Ser. 2(20)**, 196-211.
- Turner, D. B., T. Chico, and J. Catalano, 1986: TUPOS - A Multiple Source Gaussian Dispersion Algorithm Using On-site Turbulence Data. EPA/600/8-86/010, U.S. Environmental Protection Agency, RTP, NC, 39pp.
- U.S. Environmental Protection Agency, 1992: Protocol for Determining the Best Performing Model. EPA-454/R-92-025, U.S. Environmental Protection Agency, RTP, NC.
- U.S. Environmental Protection Agency, 1995a: User's Guide for the Industrial Source Complex (ISC3) Dispersion Models (revised) Volume I - User Instructions. EPA-454/b-95-003a, U.S. Environmental Protection Agency, Research Triangle Park, NC.

- U.S. Environmental Protection Agency, 1995b: *Modeling Fugitive Dust Impacts from Surface Coal Mining Operations – Phase III*. U.S. Environmental Protection Agency, Office of Air Quality Planning and Standards, EPA-454/R-96-002. December 1995.
- U.S. Environmental Protection Agency, 2003: AERMOD: Latest Features and Evaluation Results. EPA-454/R-03-003, U.S. Environmental Protection Agency, RTP, NC.
- U.S. Environmental Protection Agency, 2002: Compendium of Reports from the Peer Review Process for AERMOD. U.S. Environmental Protection Agency, RTP, NC.  
<http://www.epa.gov/scram001/7thconf/aermod/dockrpt.pdf>.
- U.S. Environmental Protection Agency, 2015: Technical Support Document (TSD) for NO<sub>2</sub>-related AERMOD modifications. EPA-454/B-15-004. July 2015.
- U.S. Environmental Protection Agency, 2020: User's Guide for AERSURFACE Tool. EPA-454/B-20-008. February 2020.
- U.S. Environmental Protection Agency, 2021a: User's Guide for the AERMOD Meteorological Preprocessor (AERMET). EPA-454/B-21-004. April 2021.
- U.S. Environmental Protection Agency, 2021b: User's Guide for the AMS/EPA Regulatory Model (AERMOD). EPA-454/B-21-001. April 2021.
- USGS, 1994: The 1994 plan for the National Spatial Data Infrastructure - Building the foundation of an information based society. Federal Geographic Data Committee Report. U.S. Geological Survey, Reston, VA. <https://www.fgdc.gov/policyandplanning/NSDI Strategy 1994.pdf>.
- van Ulden, A. P. and A. A. M. Holtslag, 1983: The stability of the atmospheric surface layer during nighttime. Preprints, *Sixth Symposium on Turbulence and Diffusion*, American Meteorological Society, Boston, 257-260.
- van Ulden, A. P. and A. A. M. Holtslag, 1985: Estimation of atmospheric boundary layer parameters for diffusion applications. *J.Climate Appl.Meteor.*, **24**, 1196-1207.
- Venkatram, A., 1978: Estimating the convective velocity scale for diffusion applications. *Bound.Layer Meteor.*, **15**, 447-452.
- Venkatram, A., 1980: Estimating the Monin-Obukhov length in the stable boundary layer for dispersion calculations. *Bound.Layer Meteor.*, **19**, 481-485.
- Venkatram, A., 1982: A semi-empirical method to compute concentration associated with surface releases in the stable boundary layer. *Atmos.Environ.*, **16**, 245-248.
- Venkatram, A., 1983: On dispersion in the convective boundary layer. *Atmos.Environ.*, 529-533.
- Venkatram, A., 1988: Dispersion in the stable boundary layer. *Lectures on Air Pollution Modeling*. Venkatram, A. and Wyngaard, J. C., American Meteorological Society, 229-265pp.

- Venkatram, A., 1992: Vertical dispersion of ground-level releases in the surface boundary layer. *Atmos. Environ.*, **26A**, 947-949.
- Venkatram, A., R. Brode, A. Cimorelli, R. Lee, R. Paine, S. Perry, W. Peters, J. Weil, and R. Wilson, 2001: A complex terrain dispersion model for regulatory applications. *Atmospheric Environment*, **35**, 4211-4221.
- Venkatram, A., D. G. Strimaitis, and D. Dicristofaro, 1984: A semiempirical model to estimate vertical dispersion of elevated releases in the stable boundary layer. *Atmos. Environ.*, **18**, 923-928.
- Venkatram, A. and J. C. Wyngaard, 1988: *Lectures on Air Pollution Modeling*. American Meteorological Society, Boston, 390pp.
- Weil, J. C., 1985: Updating applied diffusion models. *J. Climate Appl. Meteor.*, **24(11)**, 1111-1130.
- Weil, J. C., 1988a: Dispersion in the convective boundary layer. *Lectures on Air Pollution Modeling*. Venkatram, A. and Wyngaard, J. C., American Meteorological Society, 167-227pp.
- Weil, J. C., 1988b: Plume rise. *Lectures in Air Pollution Modeling*. Venkatram, A. and Wyngaard, J. C., American Meteorological Society, 119-162pp.
- Weil, J. C., 1992: Updating the ISC model through AERMIC. Preprints, *85<sup>th</sup> Annual Meeting of Air and Waste Management Association*, Air and Waste Management Association, Pittsburgh, PA.
- Weil, J. C., 1996: A new dispersion model for stack sources in building wakes. Preprints, *Ninth Joint Conference on Applications of Air Pollution Meteorology with the Air & Waste Management Association*, American Meteorological Society, Boston, MA, 333-337.
- Weil, J.C., 1998. The SERDP Open Burn/Open Detonation Dispersion Model (SOBODM), Volume IIa – Technical Description, and Volume IIb – Meteorological Inputs (DRAFT), CIRES, University of Colorado, Boulder, CO.
- Weil, J. C. and R. P. Brower, 1983: Estimating convective boundary layer parameters for diffusion applications. PPSP-MD-48, Maryland Power Plant Siting Program, Maryland Department of Natural Resources, Baltimore, MD, 45pp.
- Weil, J. C. and R. P. Brower, 1984: An updated Gaussian plume model for tall stacks. *J. Air Poll. Control Assoc.*, **34**, 818-827.
- Weil, J.C., B. Templeman, R. Banta, R. Weber, and W. Mitchell, 1996. "Dispersion model development for open burn/open detonation sources," *Preprints 9<sup>th</sup> Joint Conference on Applications of Air Pollution Meteorology*, American Meteorological Society, Boston, MA, 610-616.

- Weil, J. C., L. A. Corio, and R. P. Brower, 1997: A PDF dispersion model for buoyant plumes in the convective boundary layer. *J.Appl.Meteor.*, **36**, 982-1003.
- Willis, G. E. and J. W. Deardorff, 1981: A laboratory study of dispersion in the middle of the convectively mixed layer. *Atmos.Environ.*, **15**, 109-117.
- Wyngaard, J. C., 1988: Structure of the PBL. *Lectures on Air Pollution Modeling*. Venkatram, A., and Wyngaard, J. C., eds., American Meteorological Society, 9-57pp.
- Zilitinkevich, S. S., 1972: On the determination of the height of the Ekman boundary layer. *Bound.Layer Meteor.*, **3**, 141-145.

---

United States  
Environmental Protection  
Agency

Office of Air Quality Planning and Standards  
Air Quality Assessment Division  
Research Triangle Park, NC

Publication No. EPA-454/B-21-003  
April 2021

---